Oxidation Chemistry of n-Heptane, Selected Alkyl-Esters and Biodiesels in the Low to Intermediate-Temperature Regime

A Dissertation

Presented in Partial Fulfillment of the Requirements for the

Degree of Doctor of Philosophy

with a

Major in Mechanical Engineering

in the

College of Graduate Studies

University of Idaho

by

Elyasa Al-Gharibeh

Major Professor: Kamal Kumar, Ph.D.

Committee Members: Steven W. Beyerlein, Ph.D.; John C. Crepeau, Ph.D.;

Dev Shrestha, Ph.D.

Department Administrator: Gabriel Potirniche, Ph.D.

December 2020

Authorization to Submit Dissertation

This dissertation of Elyasa Al-Gharibeh, submitted for the degree of Doctor of Philosophy with a Major in Mechanical Engineering and titled "Oxidation Chemistry of n-Heptane, Selected Alkyl-Esters and Biodiesels in the Low to Intermediate-Temperature Regime," has been reviewed in final form. Permission, as indicated by the signatures and dates below, is now granted to submit final copies to the College of Graduate Studies for approval.

Major Professor: _____ Date: _____
         Kamal Kumar, Ph.D.

Committee Members: _____ Date: _____
         Steven W. Beyerlein, Ph.D.

         _____ Date: _____
         John C. Crepeau, Ph.D.

         _____ Date: _____
         Dev Shrestha, Ph.D.

Department
Administrator: _____Date: _____
         Gabriel Potirniche, Ph.D.

Abstract

This work examines the low-to-intermediate temperature combustion chemistry of long-chain alkyl esters through detailed speciation and heat release analysis in a motored engine. The data include in-cylinder pressure measurements and GC-MS analysis of the reaction end products. The fuels investigated include methyl decanoate, coconut, and canola oil methyl esters. In addition, n-heptane, known for its pronounced low-temperature oxidation features, is studied to establish a general understanding of the combustion process. For each of the fuels tested, the reaction was initiated and sustained by a gradual increase of the engine compression ratio to traverse the low-to-intermediate-temperature range.

All the fuels revealed a low-temperature heat release feature. n-Heptane has the most pronounced low-temperature heat release in terms of amount and rate among the tested fuels. This was followed by methyl decanoate, coconut oil biodiesel, and canola oil biodiesel. The heat release during coconut and canola derived biodiesel combustion correlate with their saturated methyl ester content. Coconut biodiesel oxidation showed a considerable low-temperature heat release as its composition is dominated by saturated methyl esters. On the other hand, canola oil biodiesel had negligible, largely suppressed, low-temperature heat release as it consists mainly of unsaturated methyl esters. Moreover, canola biodiesel exhibited oxidation characteristics similar to unsaturated methyl esters with a centered carbon double bond.

The speciation studies identified multiple oxidation end-products in the exhaust gases of the tested fuels. The concentrations of these products correlate with the extent of the low-temperature heat release of the fuel. Sixty-four intermediate species were identified in the case of coconut and canola biodiesels. It was found that the oxidation products of biodiesel are similar to that of the saturated surrogate methyl decanoate. This suggests that the saturated methyl esters content may be primarily responsible for the low-temperature heat release. The unsaturated constituents in biodiesel, do not seem to participate and may suppress the low-temperature heat generation under the current test conditions. The present work verifies the approach of modeling the biodiesel oxidation as a combination of saturated and unsaturated simple methyl esters. Unsaturated methyl ester with a centered $C = C$ double bond exhibit similar characteristics to canola oil biodiesel and are well suited as its surrogate fuels.

Furthermore, the combustion of four decanoic acid-derived alkyl esters, namely methyl, ethyl, propyl, and butyl decanoate, were investigated in a Fuel Ignition Tester (FIT) using global measurements, to infer the influence of carbon number variation for the alkyl moiety within the alkoxy group on the autoignition delay times. It was observed that increasing the alcohol chain length increased fuel reactivity. However, this enhancement diminishes as the carbon number exceeds a certain value, eventually leading to a negative impact on the ester reactivity.

Acknowledgments

I would like to express the deepest appreciation to my committee chair, Professor Kamal Kumar, who has provided the guidance and expertise to have this dissertation possible. He generously provided his expertise in experiments design, computational analysis, and technical writing throughout the various stages of the work. He continually and convincingly conveyed a spirit of adventure regarding research and teaching. He has made sure that the projects meet deadlines while providing a flexible and encouraging atmosphere.

I would like to thank my committee members, Professor Steven Beyerlein, Professor John Crepeau, Professor Dev Shrestha, for dedicating the time and effort to review the progress and provide their expertise throughout the various stages of my degree.

I acknowledge the assistantship support from the department of mechanical engineering at the University of Idaho.

I appreciate the support provided by Prof. Dev Shrestha and his student Chad Dunkel in the production of the biodiesel fuels used in the experiments reported in chapter 4 of this dissertation.

Dedication

To Mohammed, Fatima, Jafar, Elyas, Abeer, Shatha, and Raja'a.

Table of Contents

List of Tables

List of Figures

Statement of Contribution

Elyasa Al-Gharibeh is the lead author of the collaborative work included as chapter 5 of this dissertation. The authorship contribution as follows:

Elyasa Al-Gharibeh: Conceptualization, Investigation, Writing original draft.

Richard Leathers: Investigation.

Kamal Kumar: Supervision, Resources, Writing - original draft, Project administration.

Chih-Jen Sung: Resources, Writing - review & editing.

Chapter 1: Introduction

1.1 Energy use in the transportation sector

According to the U.S. Energy Information Administration (EIA), the country's total energy consumption is projected, under a reference scenario, to increase from 100–110 quadrillion British thermal units between the years 2019–2050 [1]. Despite the projected growth of on-road travel and the freight movement increasing across all the transportation modes, the transportation sector's share of the energy consumption will decrease from 28.2–24.42 % during the same period. This reduction is attributable to new technologies and more fuel-efficient vehicles entering the market. Electric cars will be the fastest-growing technology in the transportation sector. However, electricity will account for less than 2.0 % of transportation fuel consumption in 2050. The proportion of biofuels blended into fossil fuel is estimated to increase from 7.3 % in 2019 to 9.0 % in 2040 [1]. That leaves conventional fuel-powered engines as the dominant type through 2050.

Fossil-fuel burning vehicles are subject to uncertain oil prices, availability, and stringent emission regulations related to environmental concerns. Emissions have begun to dictate the future of the transportation sector. Detailed exhaust gas analysis of diesel and gasoline engines reveals the presence of several volatile organic compounds (VOCs), some of which are known to be toxic for human health [2-4]. As far as climate change is concerned, the estimated CO_2 emission in 2019 was 1890 million metric tons (MMmt), and the largest share came from petroleum usage. The scenario projects 1729 MMmt CO_2 emissions in 2050 [1]. This projection, however, is subject to the evolution of more efficient engines and increased contribution from alternative fuels. Advanced concepts such as low-temperature combustion engines offer a more efficient and less polluting alternative to conventional spark-ignited and diesel engines. Biofuels, especially ethanol and biodiesel, have been used as an alternative to petroleum-derived fuels in internal combustion engines [5].

1.2 Homogenous Charge Compression Ignition (HCCI) engine

Homogenous Charge Compression Ignition (HCCI) combustion is a promising technology that combines the advantages of spark and compression ignition engines while reducing their undesirable features. Diesel engines provide higher fuel efficiency as they utilize high compression ratios and globally fuel-lean operation. Also, the absence of throttling and

lower operational speed reduce operational losses. However, these conditions yield high temperatures (higher than 2200 K), which is the perfect environment to generate a significant amount of oxides of nitrogen (NOx) and particulate matter [7, 8]. On the other hand, gasoline engines operate under near-stoichiometric conditions, produce lesser NOx and soot, but are constrained to operate under lower compression ratios to avoid knock. Lower compression ratios imply a reduced thermodynamic efficiency. HCCI engines attempt to realize the controlled autoignition of a lean, premixed fuel-air charge within a more moderate temperature regime. Under these conditions, diesel engine efficiencies can be achieved while maintaining gasoline engine-like emissions [6].

The HCCI implementation uses a well-mixed charge of lean fuel-air and recycled combustion products that is burned in a diesel-like operating range. Compression induced reactions initiate the combustion. Simultaneous heat release occurs at multiple sites within the combustion chamber at the lean global equivalence ratio [7]. This method offers advantages over diesel engine combustion, which is limited by the mixing rate following the injection, and over a spark-ignition engine in which a flame front controls the combustion characteristics [7]. The HCCI approach limits combustion to the low-temperature regime, thereby avoiding excessive NOx formation. Indeed, the homogeneity of the charge and the in-cylinder temperature field plays a vital role in ensuring simultaneous volumetric heat release [8].

Several technical challenges impede the commercialization of the HCCI technology, such as combustion phasing control, energy release rate, operating range, homogeneous charge preparation, cold start, and emissions of unburned hydrocarbon (UHC) and carbon monoxide (CO) [8]. Therefore, it is suggested that future engines should be optimized to function on dual-mode, where it operates in an HCCI mode at part-load, and switch to the conventional spark-ignition mode at start-up and high loads. Such engines result in high thermal efficiency and low emissions at a wide operating range [7]. Controlled autoignition in the low-temperature regime remains the crucial factor if the HCCI engine is to be commercialized. Low-temperature oxidation of hydrocarbons has been researched extensively [9-22]. The approximate pressure-temperature regimes of hydrocarbon oxidation chemistry are described in the work of Morley and Pilling [23]. The current work introduces low- temperature oxidation studies of alternative fuels under HCCI combustion mode.

1.3 Low to intermediate-temperature chemistry of hydrocarbon oxidation

The oxidation process is a branched-chain reaction that involves four categories of elementary reactions referred to as initiation, propagation, termination, and branching. The initiation step starts with H-atom abstraction from the fuel molecules. It is initially a slow process and is driven by reactions involving oxygen molecules; these elementary reactions are characterized by high activation energy and selectivity [18]. Subsequently, the OH radicals become the dominant species that participate in the H-atom abstraction. Regardless of the specie participating in the abstraction process, alkyl radicals (R•) are formed. At low temperature, the alkyl radicals favor the pathway of reactions with oxygen to form alkyl peroxy radicals (ROO•) as shown by reaction (1) in Figure 1.1 [24], rather than other pathways such as decomposition (reaction (2) favored at high temperature), recombination or isomerization. A detailed discussion of the formation and fate of alkyl peroxy radicals can be found in the work by Villano et al. [18].
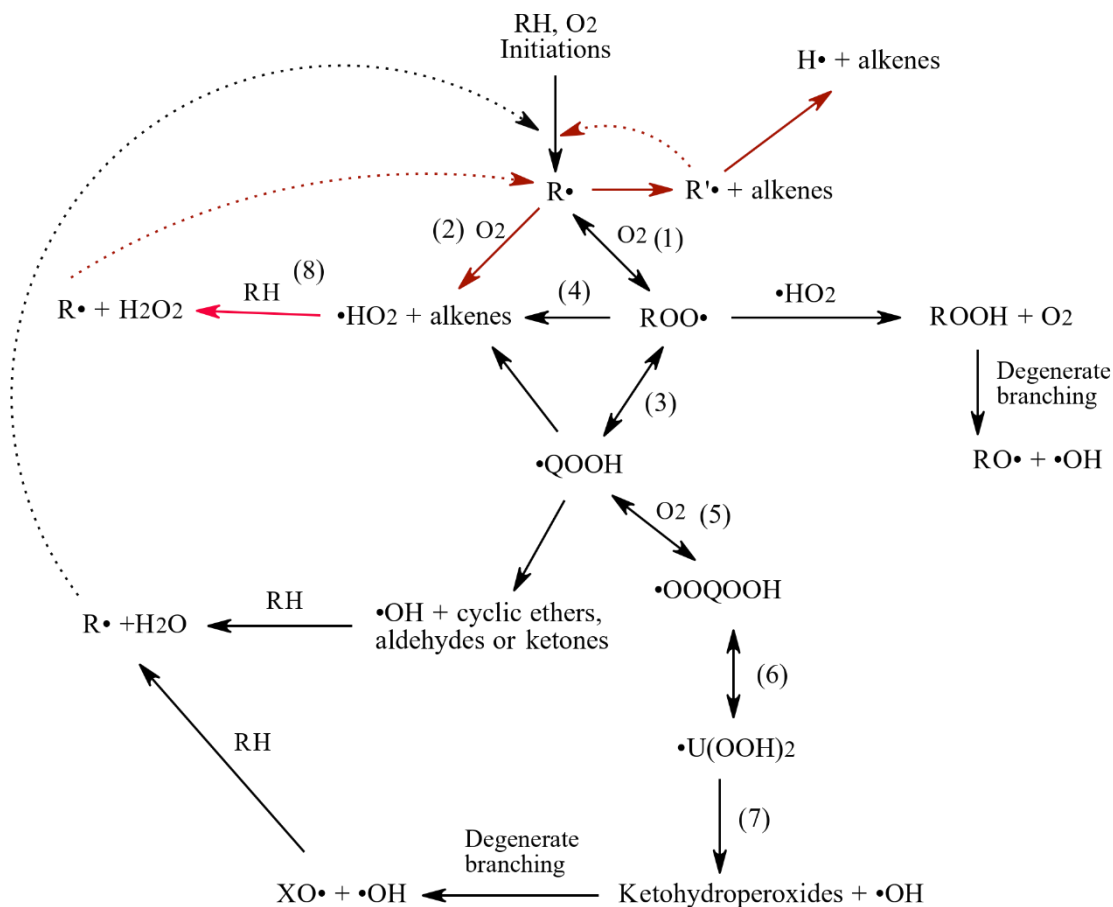
Figure 1.1. General oxidation scheme for alkyl radicals at low and high temperatures [24]. Red arrows stand for high-temperature pathways.

At low temperatures, the bimolecular reactions lead to the formation of stable alkyl peroxy radicals. As the temperature increases, alkyl peroxy adducts (ROO*•) isomerize to form hydroperxy alkyl radicals (QOOH•) as in reaction (3). An equally important pathway is the fast decomposition into alkene and hydroperoxy radicals (HOO•) as in reaction (4) [18]. These pathways (1,3 and 2,4) compete against each other to characterize the hydrocarbon oxidation chemistry in the low-to-intermediate-temperature regime. The former creates a pool of radicals through subsequent branching reactions, which tells the story of low-temperature heat release, in one sense known as first-stage ignition or cool flame. The latter pathway, on the other side, also known as concerted elimination of alkyl peroxy radicals, leads to oxidation inhibition through the production of the less reactive hydroperoxy radicals. At certain conditions of pressures and temperatures, the concerted elimination becomes more favorable, leading to longer ignition delay time, less heat release, and reduction of stable intermediates generation. As this behavior is observed at temperatures higher than those of cool flame temperatures, it is conventionally called negative temperature coefficients or NTC.

Hydroperoxy alkyl adducts (QOOH*•) are destined to a similar fate as discussed previously for alkyl peroxy adducts, where the adducts undergo a second oxygen addition, or through several unimolecular reactions include, reverse isomerization to alkyl peroxy, cyclic ether formation or, β-scission reactions. Their fate depends upon the conditions of the oxidation and the type of QOOH*• isomer, which includes isomers such as β-, γ-, or δ- QOOH*•. The various pathways these adducts favor under various conditions are discussed in a work by Villano et al. [19].

The second oxygen addition to QOOH• radical leads to the formation of •OOQOOH radical (reaction 5), which is an easy target for isomerization (reaction 6), followed by decomposition reactions into ketohydroperoxides and hydroxy radicals (reaction 7) [20]. Another easy decomposition would take place for the ketohydroperoxides as they contain a very weak O-O bond. Consequently, the low-temperature chain branching continues through the generation of alkoxy and hydroxy radicals. Equally important is the production of diones and several oxygenated species. An alternative pathway was recently proposed for the •OOQOOH radicals, which is through isomerization, followed by a third oxygen addition and subsequent reactions, leading to the formation of molecules such as olefinic dihydroperoxide, dihydroperoxy cyclic ether, and keto-dihydroperoxide [10, 20].

The competition between the isomerization pathway of alkyl peroxy adducts and their decomposition into alkene and HOO• is controlled chemically by the equilibrium R• + O2 = ROO•. When the equilibrium is placed toward the products, branching takes place, leading to a pool of radicals resulting in enhanced reactivity, simply first-stage ignition. As the temperature increases, the equilibrium shifts toward the reactants. Thus, the concerted elimination is favored, leading to the formation of the less reactive HOO• radical, resulting in a reduced reactivity, or NTC regime. This very same pathway is responsible for the second-sage ignition phenomena or hot ignition. As the temperature further progresses into the intermediate-temperature regime, the concentration of HOO• radicals will increase substantially. This excess production of HOO• radicals opens a new pathway for increased reactivity, this time through the generation of hydrogen peroxides (reaction 8), which branch into two hydroxy radicals. This pathway starts secondary initiations for the stable intermediates, which accumulate throughout the first-stage ignition and advance the reacting system to its final destination, complete combustion.

1.4   Biodiesel

Biodiesel has been used and studied in internal combustion engines as a replacement for fossil fuels. It is the product of a triglyceride-alcohol transesterification reaction in the presence of a catalyst. Vegetable oils, animal fats, and algal lipids are among the feedstocks used to extract triglycerides. The composition and characteristics of the resulting biodiesel fuel depend on the starting triglyceride and alcohol reactants.

The complexities of biodiesel impose several experimental and modeling challenges. Researchers have mainly targeted several neat methyl esters as surrogates for commercial biodiesel [25-32], and real biodiesel has rarely been studied. Among the few studies on biodiesel fuels are those in a jet-stirred reactor by Dagaut et al. [33, 34]. The use of surrogates in combustion kinetic research enabled a fundamental understanding of the nature of ignition, combustion, and emissions while building models of reasonable computational requirements compared to the complex multi-component biodiesel fuels. However, these models have rarely been validated against real biodiesel data due to the lack of related experiments.

1.5   Objectives of the dissertation

The objective of this dissertation is to advance the fundamental understanding of low-to-intermediate-temperature oxidation chemistry of biodiesel and to provide a database for establishing and validating predictive combustion chemistry models. This work follows an established hierarchical approach in studying hydrocarbon oxidation, which assumes that the individual compounds with a specific functional group share similar fundamental oxidation characteristics. Moreover, it is hypothesized that the ester moiety in saturated esters remain intact while the carbon chain undergoes usual paraffin-like oxidation steps [35]. The oxidation kinetics of biodiesel and its surrogate is elucidated through a set of well-designed motored engine experiments on:

- n-Heptane: A fuel used to confirm characteristics of paraffinic fuel oxidation chemistry, and validate the method used in this work. (Chapter 2)

- Methyl decanoate: A biodiesel surrogate examined to develop a fundamental understanding of ester oxidation chemistry, investigate the effect of ester group on the oxidation process, and provide insights into the differences between ester and paraffin oxidation kinetics. (Chapter 3)

- Coconut oil methyl ester: A biodiesel composed primarily of saturated fatty acids, which makes it a suitable transitory candidate between studying simple, saturated biodiesel surrogates, such as methyl decanoate and complex real fuels such as soybean and canola oil methyl esters. (Chapter 4)

- Canola oil methyl ester: Real biodiesel composed primarily of unsaturated long-chain fatty acids. (Chapter 4)

Additionally, autoignition experiments are conducted on methyl decanoate, a commonly used biodiesel surrogate, and three other decanoic acid-derived alkyl esters (ethyl-, propyl-, and butyl decanoate). A fuel ignition tester to investigate the effect of varying alcohol moiety on the biodiesel ignition and combustion.. (Chapter 5)

Chapter 2: Speciation and Heat Release Studies during n-Heptane Oxidation in a Motored Engine

Submitted to Fuel

2.1   Abstract

The low-to-intermediate temperature oxidation of *n*-heptane was investigated by means of speciation and heat release analysis using a motored single-cylinder engine. The experiments were conducted under a fixed engine speed and variable compression ratios in the range of $5.0 - 7.75$. A premixed fuel-air mixture corresponding to an equivalence ratio of $\phi = 0.25$ was examined for stable intermediate product evolution with varying compression ratios. The experiments focus on pre-ignition species evolution and avoid explosive autoignition. The progress of reactions was followed from the onset of the low-temperature heat release (LTHR) through the negative temperature coefficient (NTC) region. A Fourier transform infrared spectrometer (FTIR) was used to detect and quantitate carbon monoxide, carbon dioxide, and *n*-heptane, while a gas chromatograph-mass spectrometer (GC-MS) was used to identify species that evolve between the first and second stages of ignition. A total of fifty-six stable intermediates were identified. In-cylinder pressure measurements were used to carry out a heat release analysis and correlate the global markers such as the first and second stage pressure rise to species evolution. Quantitative concentration measurements were carried out for selected alkenes, aldehydes, ketones, ethers, and alcohols. The relative experimental trend for the production of compounds within each of these chemical classes was obtained. The experimental results for speciation and heat release were compared to numerical results obtained using a detailed chemical kinetic mechanism in the literature.

2.2   Introduction

The desire to improve efficiencies and reduce pollutant formation continues to motivate research into hydrocarbon combustion chemistry. A comprehensive understanding of combustion processes requires an interdisciplinary research effort. There is a need for multiple well-designed experimental approaches capable of elucidating the low-temperature oxidation chemistry of fuels through speciation studies. The results of such detailed experiments also yield additional global data needed to construct and validate chemical kinetic mechanisms.

Low-temperature oxidation kinetics can be studied experimentally by tracking the evolution of intermediate species preceding the autoignition process [36-39]. There has been much progress in developing detailed reaction mechanisms for long-chain hydrocarbons [40, 41] aided by experiments and computing advancements. However, there is still a need for improvement in the low-temperature sub-models for reaction mechanisms.

Researchers have used laboratory apparatus such as jet-stirred reactor [42-46], rapid compression machine [47-51], and shock tube [52-56] to study hydrocarbon oxidation. These devices offer a high degree of control over the experimental variables but are not entirely representative of conditions under which fuel combustion occurs in real-life applications. On the other hand, practical devices such as furnaces, gas-turbine combustors, and spark and diesel engines are designed for specific end-use and hence are not well-suited for fundamental studies. There exist only a limited set of experimental tools that are genuinely representative of practical device operating conditions, and also lend themselves to experiments designed to extract kinetic information on the oxidation of fuels. One such apparatus is the motored single-cylinder Co-operative Fuel Research (CFR) engine. This engine is a single-cylinder device that permits continuous adjustment of the compression ratio while in operation. It also allows independent control over the air-to-fuel ratio, engine speed, intake temperature, and can be fueled with a single component or a precise blend of chemically pure substances. These features make it exceptionally well-suited for speciation studies under elevated pressure and low-to-intermediate-temperature conditions, which are scarce in the literature. Such experiments, while intrinsically useful, also enable the validation of kinetic models for real-world problems that they intend to solve. Model comparisons to experimental data, especially engine data, guide additional model refinements that may be necessary for improved predictions [9].

The primary reference fuels for gasoline consists of a mixture of *n*-heptane and *iso*-octane. There have been extensive studies on the combustion characteristics of *n*-heptane. Its straight-chain structure and a reasonably large carbon number enable it to capture some of the critical features of the oxidation chemistry observed in real fuel blends. Existing detailed kinetic models of *n*-heptane oxidation in the literature can predict its global combustion characteristics fairly-well. There is also a large volume of research related to fundamental experimental data on *n*-heptane [44, 53, 57-64]. These include studies by Dagaut et al. [57]

and Herbinet et al. [59] who studied *n*-heptane oxidation in jet-stirred reactors. The work of Herbinet et al. [59] followed the intermediate species evolution over a wide range of temperatures and pressures via gas chromatography and synchrotron vacuum ultra-violet photo-ionization mass spectrometry (SVUV-PIMS). Their analysis confirmed the formation of unstable ketohydroperoxides during the low-temperature oxidation. Another study by Minetti et al. [60] examined the oxidation of *n*-heptane using a rapid compression machine. They investigated cyclic ether formation and the selectivity of lower alkenes in the resulting products of combustion. The oxidation of *n*-heptane has also been studied in internal combustion engine environments [65-71]. Szybist et al. [68] used gas chromatography-mass spectrometry (GC-MS) and Fourier transform infrared spectroscopy (FTIR) to study the extent of *n*-heptane oxidation under various compression ratios in a motored engine. They identified eleven intermediate species belonging to chemical classes such as aldehyde, ketone, acid, and di-ketone in their GC-MS analysis. A recent study by Wang et al. [69] on *n*-heptane oxidation using a stirred reactor and the motored engine was able to detect over 45 intermediate species. They used (SVUV-PI) MBMS and an atmospheric pressure chemical ionization (APCI) orbitrap mass spectrometer for analysis of the stirred reactor products. The products of oxidation from the motored engine were analyzed using an (APCI) orbitrap mass spectrometer. A majority of the detected species were of carbon chain length longer than five atoms. Furthermore, there are additional modeling studies that have investigated *n*-heptane oxidation and developed detailed mechanisms capable of predicting its main oxidation features [11, 44, 61, 72-74].

This work examines the oxidation kinetics of *n*-heptane using analysis of stable intermediate species formed during motored engine operation as well as global metrics for combustion heat release. The experiments were carried out over a range of compression ratios that spanned the low-to-intermediate-temperature region (660 – 808 K) at pressures between 8.0 – 15.0 bar. A total of fifty-six stable intermediate species were identified. The diagnostic instruments used in the detection process consist of a GC-MS system and an FTIR. Additional combustion relevant markers such as the pressure-time traces, heat release rate, accumulated heat release, parent fuel consumption, and production of end-products such as carbon monoxide and carbon dioxide were also examined. The experimental results were compared to computed values using an existing detailed mechanism for the combustion of *n*-heptane [11,

75, 76]. This research provides fundamental insights into the oxidation chemistry of *n*-heptane under high pressure and low-to-intermediate-temperature conditions with an emphasis on the negative temperature coefficient (NTC) region. The quantitative results obtained in this work provide benchmark data for a comprehensive validation of detailed kinetic models using speciation and heat release trends.

2.3 Experimental approach

2.3.1 The CFR engine setup

The experimental results reported in this study were obtained using a modified Waukesha Cooperative Fuel Research (CFR) engine. Modifications to the engine include the addition of fuel injectors into the air intake system to generate a premixed charge. The engine has a single-cylinder and is capable of variable compression ratios (CR) in the range of 4.0 – 9.0. Engine speed can be varied between 500 – 900 rpm. The premixed fuel-air mixture passes through a heated intake manifold section, which raises the gas temperature to the desired value. The temperature of the fuel-air mixture entering the cylinder is measured at a location just before the intake valve. Figure 2.1 shows a schematic of the engine and its associated auxiliary systems.
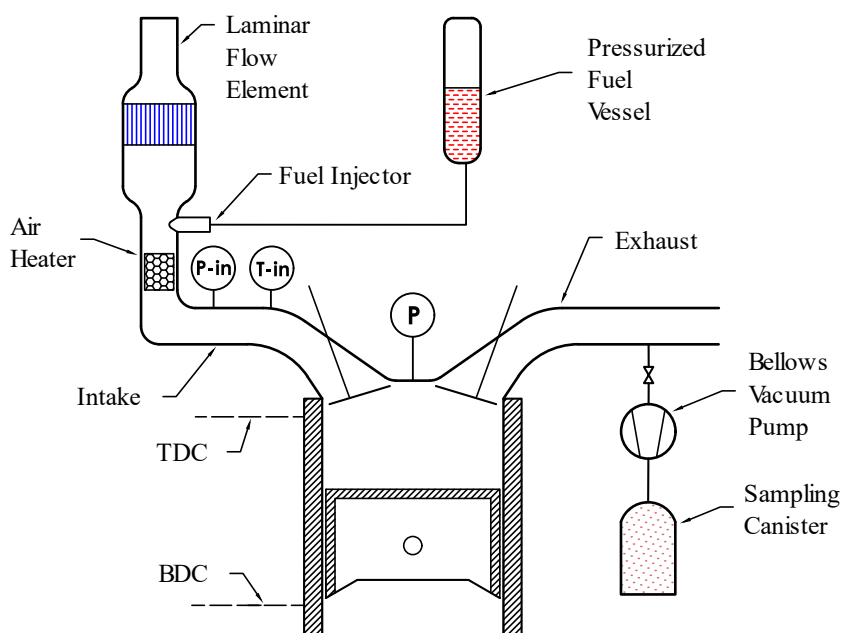
Figure 2.1. Experimental setup.

A pre-calibrated fuel injector controls the fuel flow and is attached mid-way in the intake port. A laminar flow element measures the airflow rate. An external heater is used to raise the oil temperature, as this reduces the time needed for reaching steady operating conditions. The cooling system consists of a radiator and a fan to maintain the desired coolant temperature. An electronic feedback control system regulates all the temperature setpoints for the auxiliaries. The engine is driven by an electric motor with the spark plug deactivated. Following the compression of the gases within the cylinder, the undiluted exhaust gas is sampled for analysis. The gas sampling system consists of an oil-free metal bellows vacuum pump that discharges to a pre-vacuumed silonite coated stainless-steel sampling canister.

2.3.2 Test conditions and experimental procedures

The tests were started by operating the engine in a motored mode for approximately thirty minutes without fuel injection until desired steady operating temperatures for the coolant, oil, and the intake air were achieved. The engine speed was held constant at 700 rpm, and the oil and coolant temperatures were both set to a value of $38 \pm 2°C$. The air intake temperature was maintained at $110 \pm 4°C$. Rapid evaporation of the injected liquid fuel is guaranteed for these conditions. High purity n-heptane (>99.0%) from OmniSolv® was used in these experiments. The fuel, pressurized at 50 psi, was injected at a frequency of 20 Hz and at an appropriate injection period to generate a fuel-lean mixture corresponding to an equivalence ratio of $\phi = 0.25$. This equivalence ratio was verified via an FTIR quantitation of the mix going through a complete engine cycle under the lowest compression ratio conditions (CR = 4.0) without any reaction.

Tests were performed for compression ratios in the range of $5.0 - 7.75$, with an increment of 0.5. This corresponds to compressed pressure and temperature ranges of $8.0 - 15.0$ bar and $660 - 808$ K, respectively. The estimates for the compressed temperature assume isentropic compression with no reactions. Smaller increments in compression ratios were used when relatively rapid changes in combustion responses with compression ratios occurred. The upper bound of the compression ratio was constrained to be 7.75 to prevent the rapid autoignition of the charge. At a given compression ratio, baseline pressure data consisting of one-hundred consecutive motored-cycles with air—without fuel injection—were recorded. Fuel injection was then initiated, and the fuelled engine cycle data were acquired after waiting for 90 seconds. This time interval was sufficient to ensure repeatable combustion events. Three

hundred fuelled-cycles were used in the data analysis for this study. A piezoelectric pressure sensor (PCB 112M275) was used for the in-cylinder pressure measurements with a resolution of 1.0 crank angle degrees (CAD).

An averaged pressure versus crank angle trace was used to understand the heat release characteristics based on the observed pressure rise. It provides an accurate representative trace for these experiments. The use of the averaged pressure trace can be justified based on the excellent repeatability among the successive individual pressure traces for both the unfuelled and fuelled experiments, as illustrated in Figure 2.2.
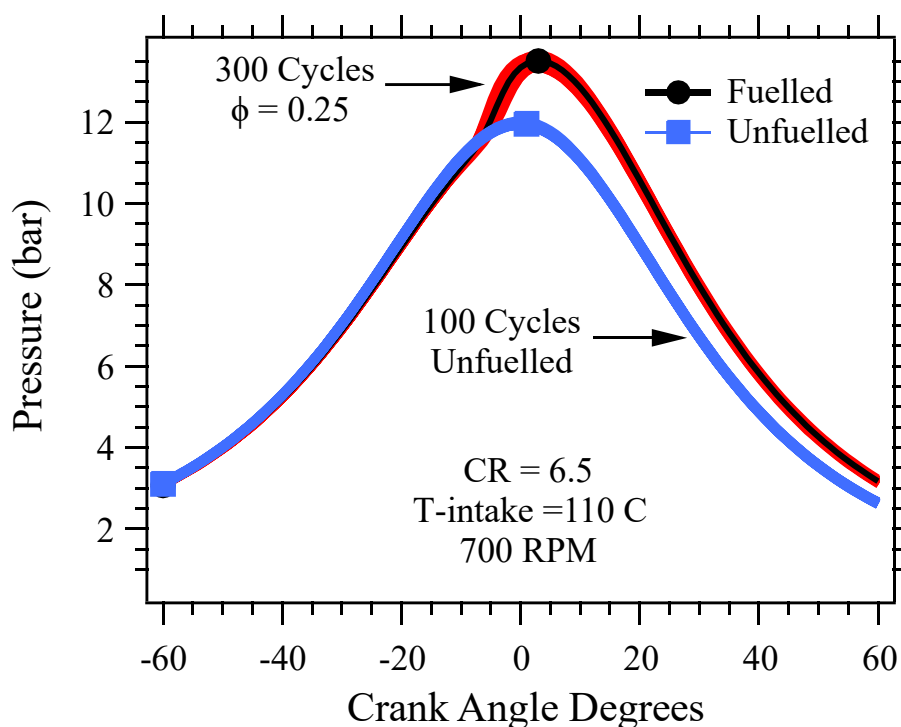
Figure 2.2. Repeatability of the pressure measurements at a compression ratio of 6.5.

2.3.3   Gas sampling and product analysis

The products of low-temperature oxidation were sampled in the gas-phase from the engine exhaust. An oil-free metal bellows vacuum pump was used to draw the sample into a silonite coated pre-cleaned and vacuumed canister with a volume of 2.7 liters. Silonite coating provides an inert environment for long-term sample storage, even for extremely low concentrations of volatile organic compounds. The canister was cleaned for reuse by evacuating and purging with atmospheric air. After cleaning, the canister was vacuumed and leak-tested before collecting the test gas samples.

The gaseous exhaust samples were analyzed using two spectrometric apparatuses, namely FTIR and a GC-MS. An FTIR (Nicolet® iS5) with a spectral resolution of 0.8 cm-1 and equipped with short path length gas cell was used to measure the carbon monoxide, carbon dioxide, and n-heptane concentrations. The detection of more complex constituents was accomplished using a GC-MS system. The GC-MS system consists of a Trace GC Ultra and a Trace Dual-stage Quadrupole Mass Spectrometer. The sampled gases were loaded into a 1.0-ml gas sampling loop on the gas chromatograph. Both the gas sample loop and the GC are equipped with heated ovens. A 50-meter fused silica capillary column having a 0.2 mm ID (Restek Rtx-DHA) was used for the separation of the compounds. This column is suitable for light hydrocarbons as well as polar oxygenates. The split injection method, with a split ratio of 75:1, was used. The helium carrier gas flow rate was 1.5 ml/min. The column temperature was held at 30 °C for 20 minutes after injection, followed by a ramp of 2 °C/min to a final temperature of 100 °C. The NIST spectral database was used to identify the compounds present in the sampled gases. Spectral database for organic compounds (SDBS) [44] was also used to identify a few species. The identification of a compound by the MS detector relies on the fact that a given compound has a unique fragmentation pattern when it is subjected to electron ionization.

2.4   Computational specifications

Numerical modeling for the CFR engine experiments is based on the general equations for a zero-dimensional closed system with time-varying volume and finite-rate kinetics. The modeling approach uses the single-zone internal combustion engine simulator (HCCI) present in the Chemkin-Pro® software package [77]. The time variation of the cylinder volume is derived from the formulation presented in the work of Heywood [78]. The simulations assume adiabatic conditions with the engine parameters listed in Appendix B.

The chemical kinetic model of Mehl et al. [75, 76] is used in these simulations. The reaction mechanism consists of 654 species and 2827 reactions. This mechanism is based on the previously developed mechanism of Curran et al. [11] and has been validated against experiments in both the low and high-temperature regions. The global validation targets included ignition delay data from shock tubes and rapid compression machines. The mechanism was also validated against speciation results obtained from a variable pressure flow reactor (VPFR) (O_2, CO), and a jet stirred reactor (JSR) for a total of ten species. The

speciation studies used in the validation for both the VPFR and the JSR were conducted with a high nitrogen dilution (99%). Furthermore, the validation targets were carefully chosen to cover the temperature range over which the negative temperature coefficient (NTC) behavior was readily apparent.

The current work identifies a significantly larger number of stable gaseous intermediates under realistic fuel loading conditions. It also provides both speciation data as well as global combustion markers to enable a more robust comparison between experiments and simulations drawn from the same set of experiments.

2.5   Results and discussion

2.5.1   Pressure traces

The experimental in-cylinder pressure profiles as a function of crank angle for various compression ratios are shown in Figure 2.3(a). The pressure traces are averaged over 300 fuelled-cycles. A noticeable difference in the shape and peak values between the fuelled and the 14nfueled traces begin to appear at compression ratios greater than 5.5. The heat release is readily apparent in the fuelled-traces (CR > 5.5). The location of the peak pressure is shifted to a position slightly after the top dead center with an increase in the compression ratio.
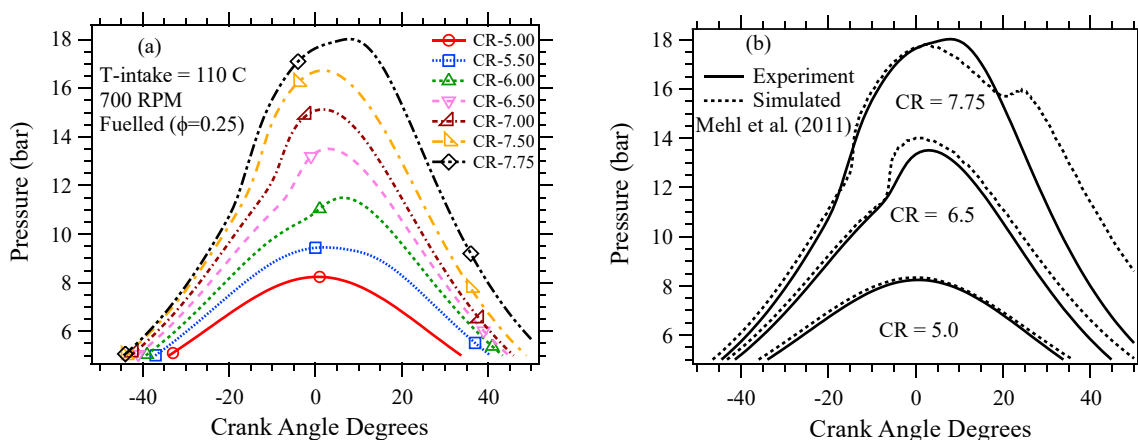
Figure 2.3. (a) Average of 300 fuelled experimental pressure traces and (b) comparison of simulated and experimental traces at various compression ratios at an equivalence ratio of $\phi = 0.25$.

A comparison of the experimental and simulated pressure traces, shown in Figure 2.3(b), using the mechanism of Mehl et al. [11, 75, 76], reveals that while there is a reasonable agreement with the experiments at lower compression ratios, a significant deviation occurs at higher values. The differences relate to the earlier onset of heat release and the location of peak

pressure being shifted to earlier times in the simulations. Additionally, the simulated pressure during the expansion stroke is much higher compared to the experiments.

2.5.2 Apparent heat release

The experimental heat release profiles at different compression ratios are shown in Figure 2.4(a) and (b), the traces were averaged over 300 fuelled-cycles. The heat release rates were calculated based on the methodology described in the text by Heywood [78], and account for the variation of specific heat ratio of the mixture with temperature. An increase in the compression ratio leads to a change in the temperature-time history of the premixed charge, with higher temperatures occurring earlier during the compression stroke. Consequently, the reactions are initiated relatively quickly, and the location of the peak heat release shifts to earlier crank angles before TDC, as shown in Figure 2.4(a).
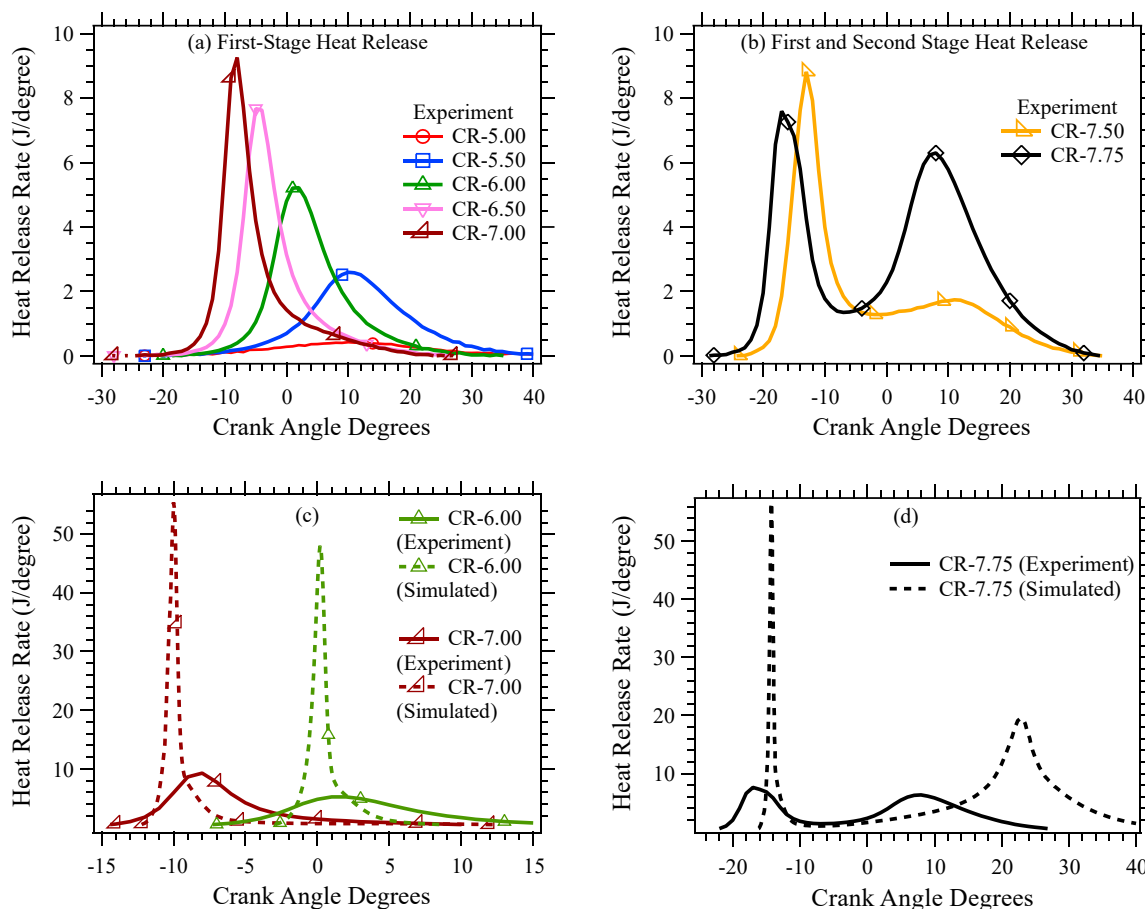
Figure 2.4. Experimental heat release rate profiles at various compression ratios with (a) single first-stage peak (b) dual first and second-stage peaks (c-d) comparison of experimental and simulated heat release rates.

Furthermore, there is only a single-stage low-temperature heat release (LTHR) peak at low temperatures (CR < 7.50), and its magnitude is enhanced with increasing compression ratio. A further rise in the compression ratio (7.50 – 7.75) leads to heat release with twin peaks, as shown in Fig. 4(b). Dual heat release peaks are a characteristic feature of large carbon number hydrocarbon oxidation in the low-to-intermediate temperature range. For cases with a two-stage heat release, the first-stage LTHR takes place before the TDC, while the bulk of second-stage heat release occurs after the TDC. The existence of a strong first-stage LTHR means that the fuel will also likely exhibit a negative temperature coefficient trend for the reaction rate. Based on Figure 2.4(a) and (b), we can conclude that the current experiments span the region associated with typical low-to-intermediate temperature combustion for this pressure range. Another noticeable feature is that both the first and second-stage heat release profiles are symmetric about their peaks within their respective full widths at half maximum, except for the second-stage heat release at a compression ratio of 7.5.

An NTC trend is observed in the experimental results for the maximum heat release rates (HRR) for the first-stage LTHR when plotted as a function of compression ratio in Figure 2.5(a). It first increases with the compression ratio in the range of 5.0 – 6.5, followed by a reduction for compression ratios between 6.50 – 6.75. This reduction is attributable to the NTC effect. Recovery from the NTC behavior occurs for compression ratios between 6.75 – 7.0. Increasing the compression ratio beyond 7.0 inhibits the peak value of the first-stage LTHR while enhancing the same for the second-stage, as can be seen for the experimental results in Figure 2.5.
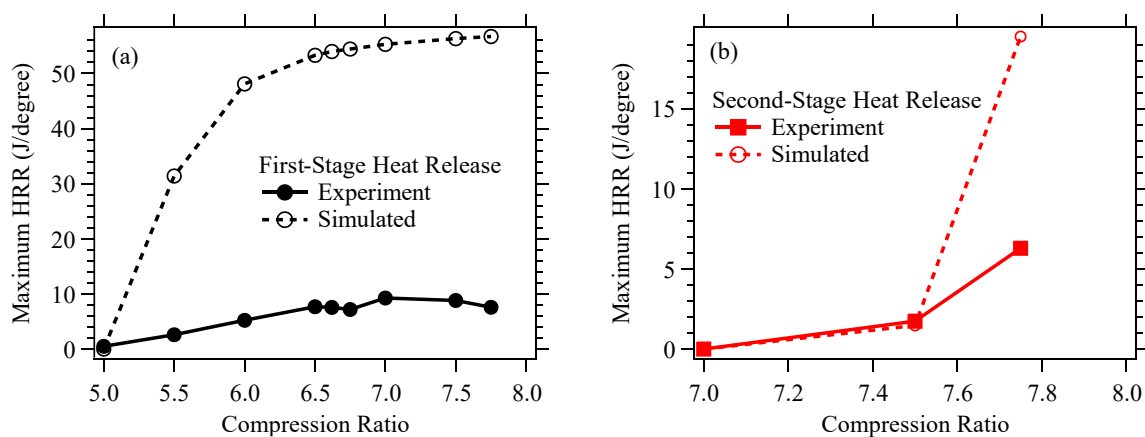
Figure 2.5. Comparison of maximum experimental and simulated values for (a) the first stage and (b) second stage heat release as a function of compression ratio.

The simulations overpredict the peak heat release rates during both the first and second stages, with a reasonable agreement only for the second-stage for compression ratios lesser than 7.5, as shown in Figure 2.5(b). A comparison of the experimental and simulated results plotted in Figure 2.4(c) shows that the simulated heat release for the first-stage LTHR occurs within a much shorter time interval but has a higher magnitude compared to the experimental results. The experimentally observed heat release is lower in magnitude and spread out over a longer time duration. Therefore, it is of significant interest to compare the accumulated heat release in the experiments to the mechanism predictions. The accumulated heat release measures the area under the HRR curve and accounts for both the magnitude and spread of the profiles.

The accumulated heat release for both the experiments, as well as the computations are shown in Figure 2.6. It was calculated by integrating the area under the heat release profile. There is an excellent agreement between the experimental and computed accumulated heat release values over the whole range, except for the highest compression ratio of 7.75. Both the experimental and computed profiles show an NTC like apparent reduction in reactivity in the compression ratio range of $6.0 - 7.0$. Note that this compression ratio range is also associated with a single low-temperature heat release. There is a sharp increase in the accumulated heat release once the second-stage heat release sets in at compression ratios higher than 7.0. There is a disagreement between the experimental and computed values in this region (CR > 7.0), with the simulated value being significantly higher at the highest compression ratio.

(b)
Reactions contributing to first-stage heat release
$CH_3+O_2(+M)<=>CH_3O_2(+M)$
$HCO+O_2<=>CO+HO_2$
$CH_3O_2+OH<=>CH_3OH+O_2$
$CH_2CHO+O_2<=>CH_2O+CO+OH$

Reactions contributing to second-stage heat release
$H+O_2(+M)<=>HO_2(+M)$
$HCO+O_2<=>CO+HO_2$
$HO_2+OH<=>H_2O+O_2$
$CH_2O+OH<=>HCO+H_2O$
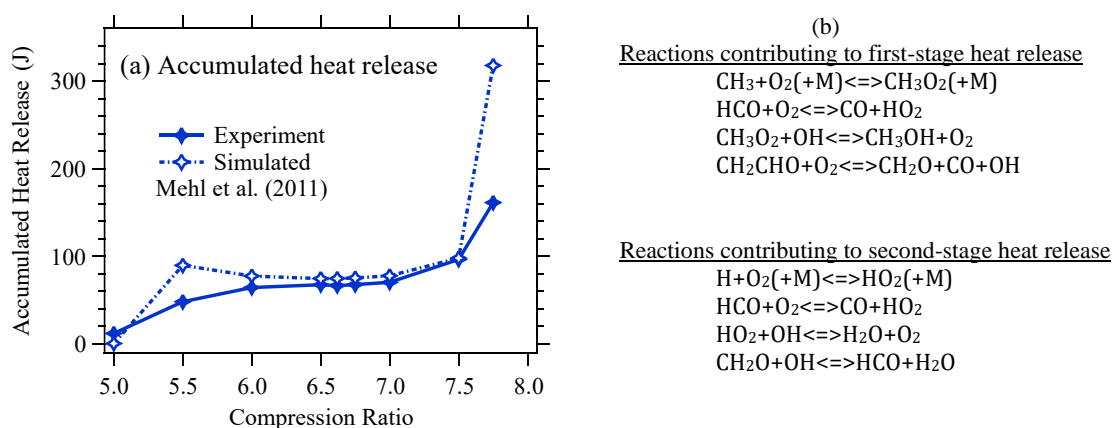
Figure 2.6. (a) Experimental and simulated values for accumulated heat release and (b) major reactions contributing to volumetric heat release in the simulations.

The important exothermic reactions responsible for both the first and second stage heat release, based on the computations, are also shown in Figure 2.6. It is found that the oxidation

of the formyl radical is an important reaction common to both the first and second stage heat release. The two other important reactions contributing to the second-stage heat release come from termination reactions involving the hydrogen-oxygen system. The chemical reactions responsible for the energy release, are primarily three-body and radical chain termination in nature.

In addition to identifying the reactions contributing to the heat release, it is also of interest to determine the sensitivity of the temperature to the model parameters (Ai) in the simulations. The peak value for such sensitivity coefficients is shown in Figure 2.7(a) and (b) for the first and the second stages of heat release, respectively. The plots show the normalized sensitivity coefficient given by $S_i = \frac{A_i}{T}\frac{\partial T}{\partial A_i}$, where A_i is the pre-exponential factor for the ith reaction in the model.

The temperature during the first-stage heat release (LTHR) is most sensitive to heptylperoxy radical isomerization to hydroperoxy-heptyl radical ($R\dot{O}_2 \rightarrow \dot{Q}OOH$). The 2-heptylperoxy isomerization exhibits the highest positive sensitivity. The other important class of reaction that shows a positive sensitivity is of the type $\dot{O}_2QOOH \rightarrow Ketohydroperoxide + OH$. These two types of reactions either directly yield an OH radical or subsequently undergo reactions that provides one. This is the likely reason for their positive sensitivity. On the other hand, the $R\dot{O}_2 \rightarrow Olefin + HO_2$ shows a negative sensitivity likely due to the resulting less reactive HO_2 radical.
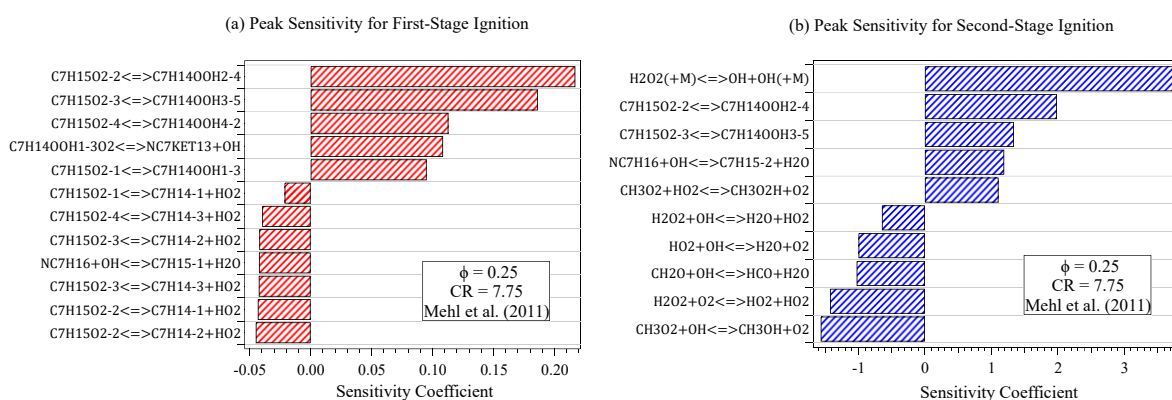
Figure 2.7. Normalized sensitivity coefficients for temperature with respect to pre-exponential factors. Peak values at (a) first-stage and (b) second-stage of heat release.

The results of this sensitivity analysis for the system temperature indicates that fuel-specific reactions are essential for the first-stage heat release. Moreover, the hydrogen peroxide decomposition reaction dominates the temperature sensitivity during the second-stage heat release. The heptylperoxy radical isomerization to hydroperoxyl-heptyl radical ($R\dot{O}_2 \rightarrow \dot{Q}OOH$) also shows a considerable positive sensitivity, as was observed for the first-stage ignition. Further work is needed to quantify the extent of individual contributions of these sensitive reactions to the differences observed between the experimental and computed results for the heat release rate profiles as well as the accumulated heat release.

2.5.3 Fuel consumption, carbon monoxide, and carbon dioxide formation

Fuel consumption and end-product formation provide valuable insights into the overall combustion rates and are the most commonly measured quantities in combustion experiments. In this work, we track the parent fuel consumption alongside carbon monoxide and carbon dioxide production as a function of the compression ratio. The carbon monoxide (CO) formation shown in Figure 2.8(a), obtained by FTIR analysis, highlights some essential aspects of the oxidation process. The CO and CO2 concentrations, shown in Figure 2.8(a) and (b) are negligible for the lowest compression ratio of 5.0, despite a 30% conversion of the parent fuel, as shown in Fig. 8(c). A further increase in the compression ratio ($5.0 < CR < 6.0$) leads to an increase in the CO concentration with relatively slower growth in CO2 production. Note that the rate of fuel consumption with respect to the compression ratio shows a decrease in this range.
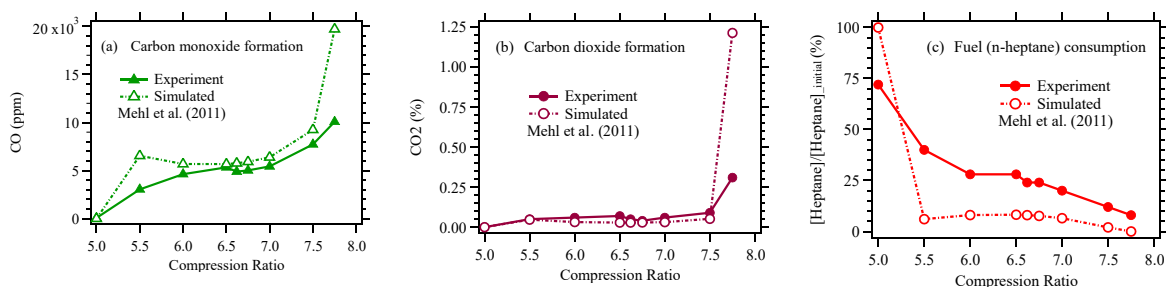
Figure 2.8. Experimental and simulated values for (a) carbon monoxide production, (b) carbon dioxide production, and (c) fuel consumption with varying compression ratios.

A small drop in both the CO and CO2 production is observed for the next set of increments in compression ratios ($6.0 < CR < 6.5$). This drop is an indication of the NTC of the reaction rate. A relatively slower rate of fuel consumption is also apparent in Figure 2.8(c).

Beyond a compression ratio of 7.0, the qualitative nature of the heat release begins to change with an emergent second-stage heat release. This is manifested by a rapid increase in the CO and CO2 production, as well as an increased rate of fuel consumption with respect to the compression ratio. A gradual transition to dual heat release peaks also occurs in this region (c.f. Figure 2.4(b)).

The qualitative trends observed in the experiments agree reasonably well with the simulations. The trend for carbon monoxide formation is very well reproduced by the simulations, with the maximum deviation being within a factor of two as compared to the experiment. Furthermore, the carbon monoxide formation trend observed in Figure 2.8(a) correlates surprisingly well with the accumulated heat release trends shown in Figure 2.6. The fuel conversion is found to be slightly higher for the simulations over the entire compression ratio range except for the lowest value of 5.0. Most of the fuel is consumed during the first-stage ignition and before the onset of the second-stage heat release. The highest fuel conversions occur in the compression ratio range of $5.0 - 6.0$ for both the experiments and simulations.

2.5.4 Speciation results for stable intermediates

The evolution of stable intermediate species was followed by GC-MS analysis of the sampled exhaust products. The species generated during *n*-heptane oxidation can be seen by plotting the total ion chromatogram (TIC) signal intensity from the mass spectrometer, as shown in Figure 2.9. The chromatogram is split into three separate plots for clarity. The first plot in Figure 2.9(a) shows the retention time from $2.7 - 4.0$ minutes for light species with strong peaks. Figure 2.9(b) and (c) contain relatively heavier compounds at longer retention times and lower peak intensities. The species were matched against the NIST mass spectra library [79]. The Spectral Database for Organic Compounds (SDBS) [80] was also used for identifying a few compounds. The major classes of compounds detected include olefins, aldehydes, alcohols, ethers, and ketones.

The area under a given peak relates to the specie concentration in the gas mixture. The variation of peak area for a given specie with the compression ratio shows a similar trend across all the species with few exceptions. The peak area for a specific specie initially increases as the compression ratio increases $(5.0 < CR < 6.5)$. The onset of NTC in the compression ratio range of $6.5 - 6.75$ leads to a slight decrease in concentrations for nearly all the components.

A slight increase occurs in the compression ratio range ($6.75 < CR < 7.0$). Lastly, a significant reduction in the concentrations for most species occurs at the highest compression ratio of 7.75, where the second-stage heat release takes place. The plots in Figure 2.9 show the peak areas in increments of 0.5 compression ratio units and skip the chromatograms in the range ($6.5 < CR < 6.75$) for clarity. This region is later included when reporting quantitative data in subsequent sections.
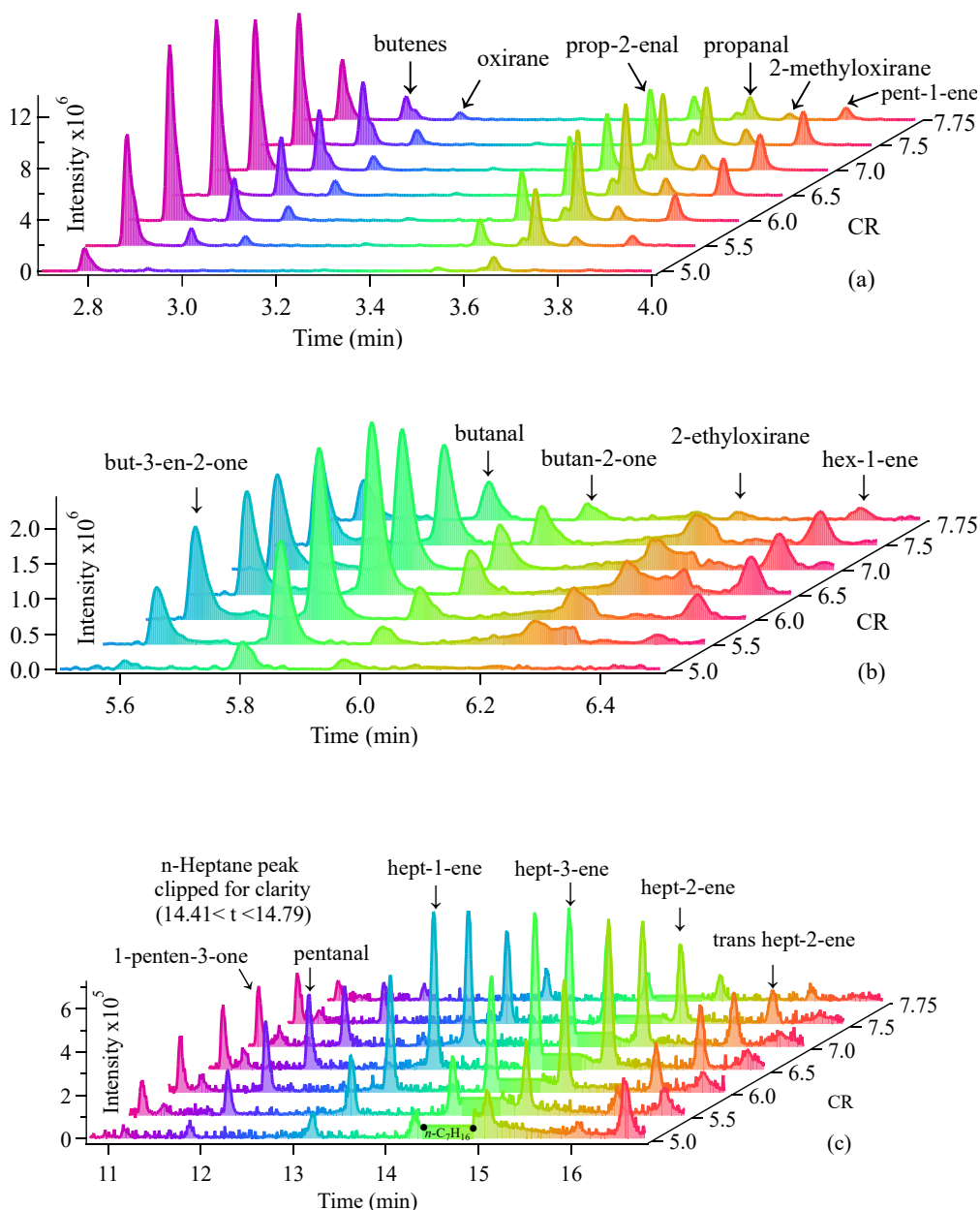
Figure 2.9. Total ion chromatograms at retention times of (a) $2.7 - 4.0$ min (b) $5.0 - 6.5$ min, and (c) $10.7 - 17.0$ min for various compression ratios.

Among the early eluting lighter compounds are the two epoxides which form in small but detectable quantities. The relative peak for ethylene oxide (oxirane) and propylene oxide (2-methyloxirane) is much lower compared to the other species in Figure 2.9(a). It can also be seen from Figure 2.9(a) that all the early eluting small carbon number compounds are present over the entire compression ratio range $5.5 - 7.75$. Their presence, even at the highest compression ratios, shows that these species participate in the low- as well as the high-temperature oxidation chemistry.

A total of fifty-six species were identified in the current study. All intermediate species identified in this work are included in the Appendix A, which groups the species in terms of their respective chemical classes. It also contains information about the degree of certainty in their identification. Among the identified species, about a fifth of them are olefins, including C7 compounds, and isomeric forms for butene and heptene. Carbonyl compounds comprise about a third of the species and include small carbon number aldehydes and ketones, except for hexanal and hexanone. The remaining portion of the intermediates consists of alcohols, ethers, carboxylic acids, and dienes. Three-, five-, and six-membered O-heterocycles were also detected. The cyclic ethers formed include including 2-methyloxirane (propylene oxide), oxolane (tetrahydrofuran), and 2-methyloxane.

2.5.5 Quantitation of selected stable intermediates

The speciation effort in this work is advanced further by carrying out quantitative measurements of selected species belonging to various chemical classes. The concentrations for selected alkenes, aldehydes, ketones, cyclic ethers, and alcohols were measured as a function of compression ratio and compared to simulations. The area under the curve in the total ion chromatogram in conjunction with a corresponding calibration curve was used to determine individual species concentrations. The calibration curve for each quantitated specie was obtained separately using a single pure component. The following sections discuss the evolution of stable intermediate species as a function of compression ratios.

2.5.5.1 Alkenes

Alkenes of carbon chain length of two to seven $(C_2 - C_7)$ were detected, including isomeric forms for butene, pentene, and heptene. Butene isomers eluted at the same retention time as multiple overlapping peaks. The concentrations of butene isomers, pent-1-ene, and

hex-1-ene in the motored engine exhaust for various compression ratios are shown in Figure 2.10(a – c).

A minimal olefinic species production (< 5ppm) is observed for the lowest compression ratio of 5.0, although more than 25% of the fuel had been consumed. There is a sharp increase in the olefin production between $5.5 < CR < 6.5$, followed by a slight reduction as the compression ratio is increased further ($6.5 < CR < 6.75$) due to the onset of NTC. An additional increase in the compression ratio ($7.0 < CR < 7.5$) initiates the second-stage heat release, and the $C_4 – C_7$ olefins concentrations begin to drop. There is a steep drop in the $C_4 – C_7$ olefins concentration at the compression ratio of 7.75, where the bulk of the energy release is associated with the second-stage ignition.
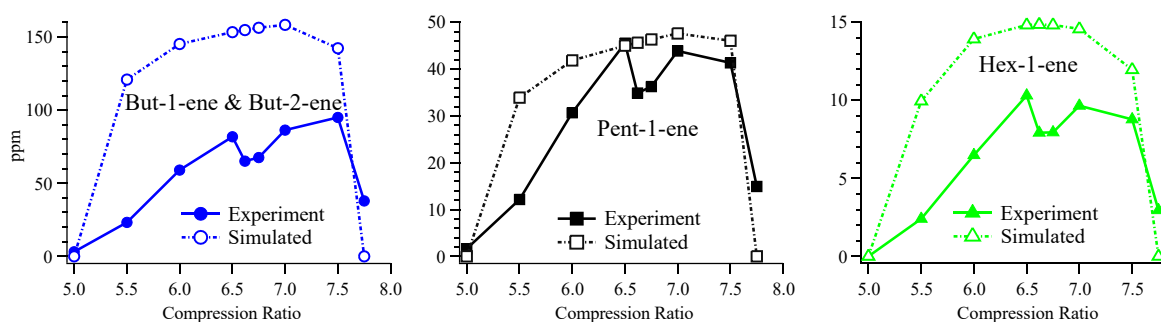
Figure 2.10. Experimental and simulated concentrations for selected olefinic species.

Among the alkenes quantified in this work, the combined butene concentration is found to exceed those of pentene and hexene over the entire range of compression ratios. Furthermore, the amount of butenes in the system continues to increase even for compression ratios where the second-stage heat-release begins to set in ($7.0 < CR < 7.5$). This behavior is contrary to what is observed for the larger alkenes, which exhibit a reduction. There is a preference for small carbon number alkene generation during the early phase of the second-stage heat release. This notable increase in the concentration of the butene isomers near the onset of the second-stage ignition may be attributed to the decomposition of the alkylperoxy radicals into small alkenes at relatively higher temperatures compared to the first-stage ignition.

The simulated results are in good agreement with the experiments for the alkene formation, especially for pent-1-ene and hex-1-ene. The initial rising trends ($5.0 < CR < 6.5$) are captured in the simulated data, but the simulations are unable to reproduce the subsequent decrease in alkene formation ($6.5 < CR < 7.0$) near the onset of the NTC region. However, the

model does show a reduced reactivity in this region. Additionally, the sharp drop in all the alkene concentrations at the highest compression ratio is also very well replicated by the model.

2.5.5.2   Aldehydes and ketones

Carbonyl compounds, especially aldehydes and ketones, were produced in abundance during these low-to-intermediate temperature oxidation experiments. Saturated straight-chain aldehydes in the carbon number range of two to seven were detected, except for hexanal ($C_2 -$ C_5, C_7). Similarly, saturated ketones with carbon numbers of three to seven were identified with the exception of hexanone ($C_3 - C_5, C_7$). The lack of formation of carbonyl compounds with six carbon atoms is in line with the relatively lower concentration of hex-1-ene observed for the alkenes.
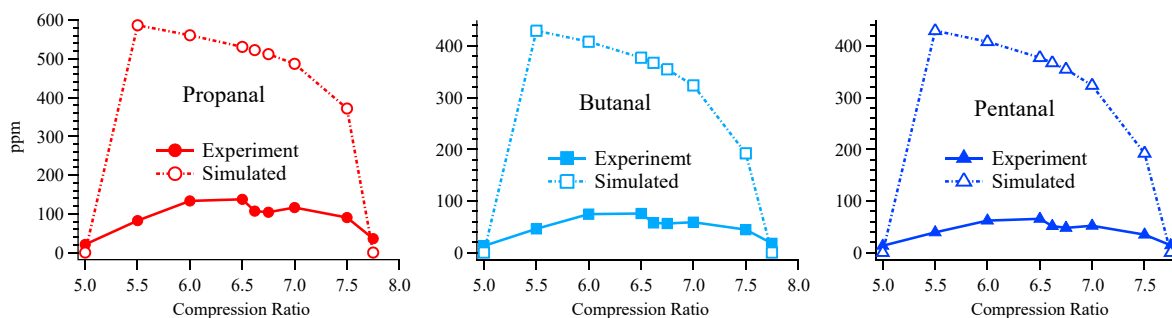
Figure 2.11. Experimental and simulated concentrations for propanal, butanal, and pentanal.

Propanal has the highest concentration among the aldehydes quantitated under all test conditions, followed by butanal and pentanal, as can be seen from Figure 2.11. Aldehydes and ketones are the precursors to the onset of the first-stage ignition (CR = 5.0). The simulated trends for the aldehydes correctly predict propanal to be the most abundant among the three aldehydes. Similar amounts of butanal and pentanal are formed in the simulations, which is concordant with the experimental data. The absolute magnitude for each of the three aldehyde concentrations is overpredicted in the simulated results except for the lowest and highest compression ratio. The simulated values are two to six times higher than the experimental results. This implies that the temperatures for the onset and cessation of aldehyde production are accurately reflected in the model, but the reactivity related to aldehyde formation between those limits is not.
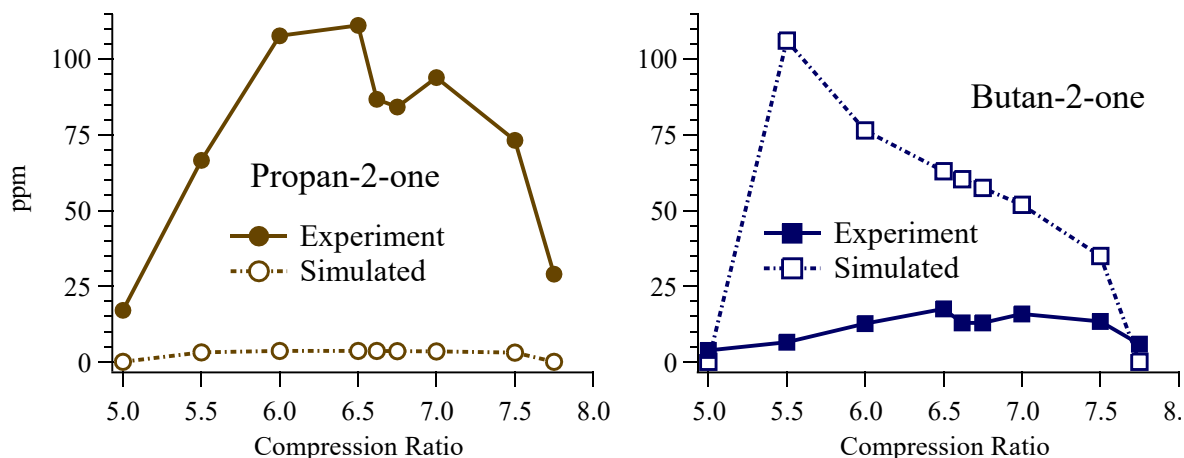
Figure 2.12. Experimental and simulated concentrations for propan-2-one and butan-2-one.

Propan-2-one (acetone) and butan-2-one were the two saturated ketones whose concentrations were quantified in this study. The acetone production was significantly higher than that of butan-2-one over the entire compression ratio range of the experiments, as shown in Figure 2.12. The qualitative trend for their concentration variation with respect to temperature/compression ratio was similar to the other intermediates, including the display of the NTC characteristic. However, the magnitudes for propan-2-one and butan-2-one production are not in agreement between the experiment and simulations. Butan-2-one production is overestimated, while the acetone concentration is underpredicted by the model. A reaction path analysis for the production of acetone and butan-2-one from n-heptane shows that the most important pathways originate from the 2-heptyl and 3-heptyl radicals, respectively.

2.5.5.3 Small carbon number cyclic ethers and alcohols

The production of cyclic ethers during the oxidation of n-heptane is due to the chain propagation reactions proceeding via the hydroperoxyalkyl radicals ($\dot{Q}OOH$). This route becomes important as the system temperature increases [11]. The quantitation of most cyclic ether species except propylene oxide was not done due to low signal-to-noise ratio and limited availability of calibration standards. The experimental and predicted concentrations for 2-methyloxirane (propylene oxide) at various compression ratios are shown in Figure 2.13. The trend of the experimental results is in line with that observed for other species. The simulated results, however, show a very distinct pattern where the formation of 2-methyloxirane

gradually increases until it reaches its peak at a compression ratio of 7.5. The model results show a good agreement (with a slight underprediction) with experimental data at lower temperatures ($5.0 < CR < 6.5$). The simulated values are higher in the compression ratio range $6.62 – 7.50$, with the most significant mismatch at the peak simulated value. Other straight-chain ethers such as methoxymethane and methoxyethene were also detected at much lower concentrations.
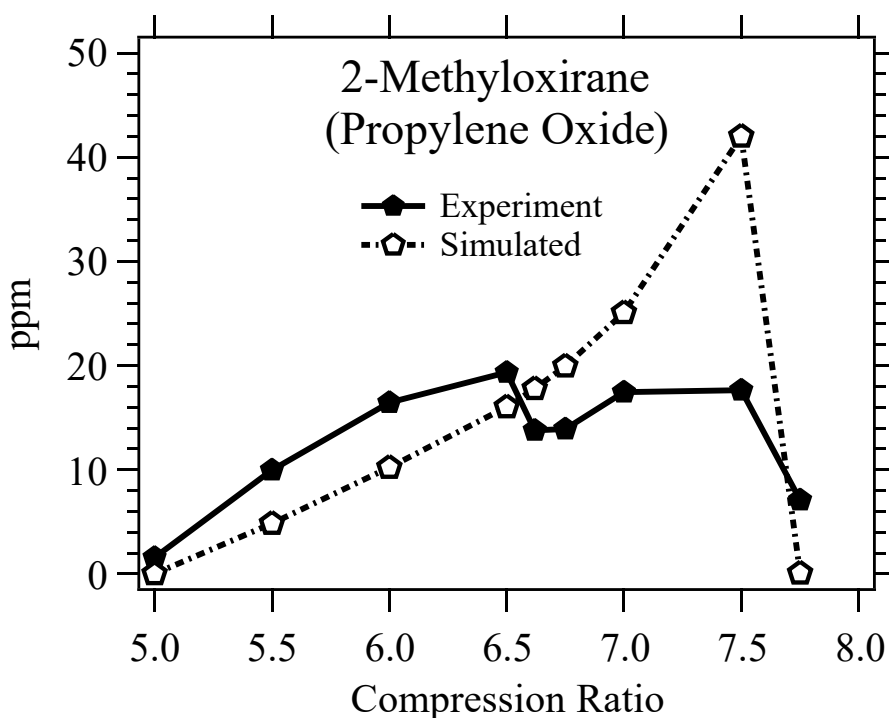
Figure 2.13. Experimental and simulated concentrations for 2-methyloxirane.

The low-temperature oxidation also led to the production of saturated lower alcohols, especially methanol, in significant amounts. Among the two main pathways for the production of methanol are reactions of methyl peroxy radicals with OH and, more interestingly, the hydrogen abstraction reactions from n-heptane at the primary, secondary, and tertiary sites by the methoxy radical. The concentration of methanol in the exhaust products is nearly two orders of magnitude higher compared to ethanol at moderate compression ratios. The simulated results for both these alcohols are in excellent agreement with the experiments, as seen in Figure 2.14(a) and (b). In particular, the model accurately predicts the substantial differences in their relative concentrations.
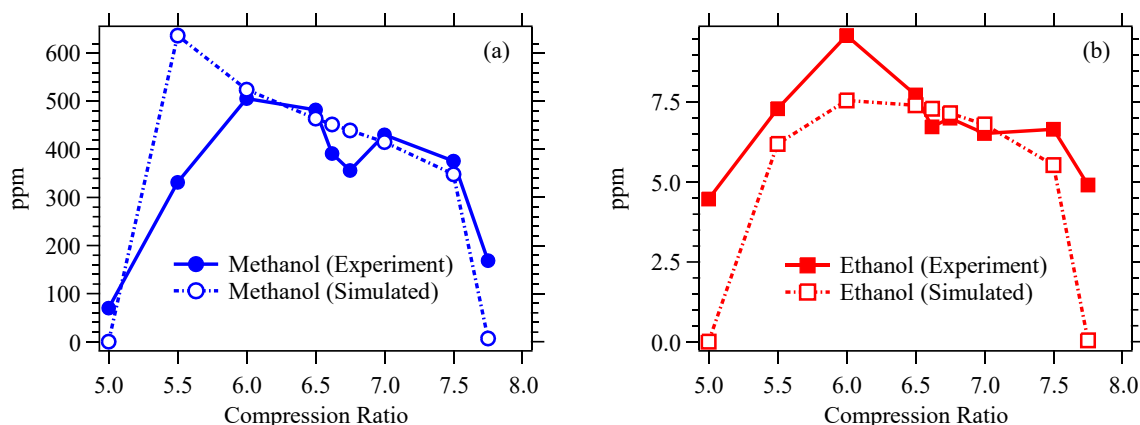
Figure 2.14. Experimental and simulated concentrations for (a) methanol and (b) ethanol.

2.5.5.4 Oxygen heterocycles with five- and six-membered rings

Oxygen-containing heterocycles have been the subject of renewed interest [20, 69, 81] in combustion chemistry. These species provide information related to the earlier stages in the oxidation sequence [82]. Although this work focused on quantitation of stable intermediates with straight-chain oxygenated structures, various five and six-membered heterocyclic intermediates were also detected. The chemical structures of these compounds are provided in Figure 2.15. It is important to note that the identification of this class of compounds occurred with a relatively lower certainty compared to the other species listed in Appendix A.

(a) Five-membered O heterocycles
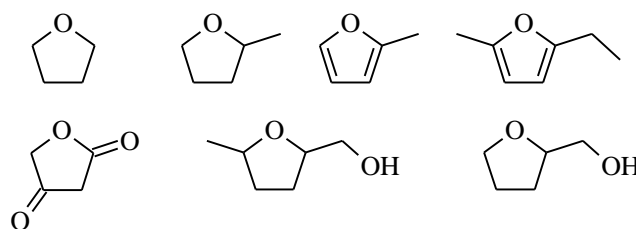
(b) Six-membered O heterocycles
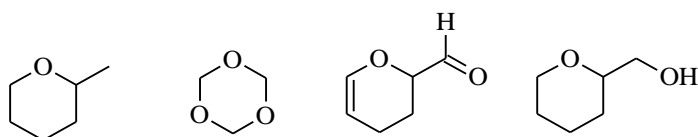
Figure 2.15. Structures for O heterocycles detected in this study.

2.6   Conclusions

A variable compression ratio single-cylinder motored engine was used to study the oxidation of *n*-heptane in the low-to-intermediate temperature range. The oxidation chemistry was followed by means of detailed speciation analysis of the undiluted exhaust. Heat release trends were obtained using the experimentally obtained pressure profiles, and this global marker was related to changes in the gaseous exhaust product composition.

The onset of heat release occurred at a compression ratio of 5.5, and the NTC of the reaction rate was noted in the compression ratio range of 6.5 - 6.75. The lower temperature oxidation exhibited a single heat release peak, while a two-stage heat release was present at relatively higher temperature conditions. A comparison between the experimental and computed results showed an excellent agreement for the accumulated heat release, although the profiles for the heat release themselves were not in agreement. The results for the temperature sensitivity of the system indicate that parent-fuel specific reactions are important for the first-stage heat release. The onset of the second-stage heat release was accompanied by a rapid increase in CO and CO_2 concentrations in the gaseous exhaust, with the bulk of the fuel being consumed during the first-stage heat release. The accumulated heat release and the carbon monoxide formation trends were very similar.

The speciation analysis in this research detected fifty-six stable intermediate species across a wide range of chemical classes such as alkenes, aldehydes, ketones, ethers, alcohols, and acids. This work also provides quantitative measurements for eleven intermediate species and compares them to results from an existing detailed chemical kinetic mechanism in the literature. Species of the same chemical group show similar trends for variation with compression ratios, although there were differences in their relative concentrations. The NTC effect was apparent in nearly all species detected in this work. This NTC effect was not as strong in the computed results, which, however, did show a diminished reactivity, but not a reduction in the region of interest ($6.5 < CR < 6.75$). The model predictions were found to be in good agreement with the experiments for alkene and alcohol production but were unable to account for the generation of acetone. A noticeable feature in the experimental results was the relative lack of straight-chain carbonyl compounds with six carbon atoms in the oxidation products. The incipient second stage heat release was associated with a preference for the formation of small carbon number alkenes, especially the butene isomers. This work provides

benchmark data for the validation of chemical kinetic mechanisms using both global and detailed responses. It fills in the gap for speciation studies existing in the literature, especially under high-pressure condition.

Chapter 3: Low to Intermediate-Temperature Oxidation of a Biodiesel Surrogate in a Motored Engine

3.1 Introduction

Fatty acid methyl esters are among an essential class of compounds that constitute non-petroleum derived diesel fuel. Their use for transportation applications has nearly quadrupled during the last decade. Much attention has been devoted to properties such as energy density and cold weather behavior of such fuels to ensure compatibility with existing assets and infrastructure, and there is a need to advance fundamental understanding related to their combustion kinetics. In this work, we study the low-to-intermediate temperature oxidation chemistry of methyl decanoate at elevated pressures in an engine environment. Both global and detailed combustion responses are investigated. Developing an understanding of long-chain saturated FAME's is an essential step in closing the gap between the rapidly growing scientific knowledge for low carbon number esters and real biodiesel. While small carbon number methyl esters help develop an understanding of FAME oxidation, they are inadequate surrogates for biodiesel. Previous experimental research efforts at understanding the combustion chemistry of fatty acid methyl esters have focused primarily on small carbon number neat components [32, 48, 52, 83-88]. A typical example of such a compound is methyl butanoate. Its autoignition has been studied in the low-to-intermediate and high-temperature ranges. Dooley et al.[83] conducted one such study where they used a shock tube and a rapid compression machine to obtain the ignition delay times for methyl butanoate in the high (1250-1760 K) and low-to-intermediate (640-949 K) temperature conditions, respectively.

Methyl decanoate is the most common large carbon number single component surrogate for biodiesel and has proven to be very useful in replicating the combustion properties of commercial biodiesel [30, 89, 90]. The low-temperature oxidation similarity between Jet A-1 and an 80/20 molar blend of kerosene/rapeseed oil methyl ester (biokerosene) was examined in a study by Dagaut and Gail [34]. They reported no significant variation in the product distribution except for the presence of mono-unsaturated methyl esters such as methyl-2-propenoate, methyl-3-butenoate, methyl-4-pentenoate and methyl-5-hexenoate for biokerosene. Similar products, except methyl-4-pentanoate, were identified via gas chromatogram-mass spectrometer (GC-MS) analysis by Pedersen et al. [27] during the

oxidation of rapeseed methyl ester under low-temperature conditions in a reactor. The combustion chemistry of methyl decanoate has been investigated in droplet ignition experiments [90], jet stirred reactors [31], shock tubes [91, 92], rapid compression machines [93], constant volume spray ignition [94, 95], and laminar flames [96]. The experimental efforts have been accompanied by modeling studies aimed at capturing the unique features of methyl ester oxidation [28, 31, 97-101]. This includes a detailed chemical kinetic mechanism for methyl decanoate oxidation recently developed by Herbinet et al. [100].

There are very limited fundamental combustion studies on methyl decanoate, a biodiesel surrogate, under engine relevant conditions. Often times laboratory experiments strive to be engine relevant while true engine data is deemed device-specific and difficult to interpret. This limitation can be carefully overcome by well-planned and systematic experiments in specific engine environments. Such experiments provide kinetic data under operating conditions and timescales, which are closer to end-use applications. The single-cylinder engine configuration has been successfully used by researchers to conduct fundamental oxidation studies on various fuels. In particular, the single-cylinder cooperative fuel research engine (CFR) provides an ideal platform for such studies due to its variable compression ratio and other controllable experimental parameters. Prior experimental studies using methyl decanoate as a fuel in a single-cylinder CFR engine include the work of Szybist et al. [68]. The work of Szybist et al. [68] studied three diesel relevant fuels and reported significant carbon dioxide production during the low-temperature heat release of methyl decanoate, unlike the other two diesel surrogates. All three fuels were found to exhibit a two-stage ignition. They also confirmed the formation of other methyl esters and oxo-methyl ester compounds during methyl decanoate oxidation. The work of Szybist et al. [68] conducted exhaust analysis using an FTIR to quantify CO, CO2, formaldehyde, and acetaldehyde concentration. They also carried out a GC-MS analysis of condensable species collected in a dry ice bath and extracted using methylene chloride. Their GC-MS analysis was designed for species identification and did not quantify the condensable intermediates. Another study by Cheng et al. [102] used an optically accessible diesel engine to explore the influence of methyl decanoate on combustion and emissions performance. The planar laser-induced fluorescence and incandescence techniques were used to develop a fundamental understanding of the spatial and temporal development of the high-temperature reaction zone and the sort distribution in a

study by Le et al. [103]. Their study used a small-bore optical diesel engine, which was fueled by methyl decanoate. A review of the past work related to methyl decanoate combustion shows that systematic quantitative speciation studies in the low to intermediate temperature and high-pressure conditions have received little attention.

This work examines the low-to-intermediate temperature combustion characteristics of lean premixed methyl decanoate air mixtures in a CFR engine over a compression ratio range of $5.5 - 9.0$. Detailed species evolution profiles with varying compression ratios, as well as global heat release trends inferred from in-cylinder pressure traces, were obtained to address these gaps in the existing literature. The experimental results obtained in this work are compared to numerical results obtained using an existing detailed mechanism in conjunction with an appropriate physical model. The current work also seeks to understand the differences between the oxidation chemistry of large carbon number esters and straight-chain alkanes by comparing previously obtained results for and heptane with the current methyl decanoate experiments.

3.2   Experimental setup

3.2.1   Engine test cell

A Co-Operative Fuel Research (CFR) engine was used to study the pre-ignition LTHR and speciation characteristics of methyl decanoate. This CFR engine is a variable compression ratio single-cylinder engine (4:1 to 13:1), which consists of a standard crankcase and a cylinder with separate head and associated accessories. The cylinder head has a variable compression plug hand-wheel assembly that permits continuous adjustment of compression ratio while the engine is in operation. The engine is connected to an electric motor that assists in starting up the engine and absorbs power once the engine is fueled and running. The engine was operated at a fixed speed, with fuel being injected into the intake port of the engine and the spark plug deactivated. A fixed speed ensures a similar variation in volume as a function of time. The fuel-air equivalence ratios were obtained from a direct measurement of fuel and airflow rates using a pre-calibrated injector fuel and a laminar flow element for the air. Crank angle resolved $(0.1°)$ cylinder pressure was acquired by means of a piezoelectric pressure transducer.

The in-cylinder thermodynamic conditions were varied by adjusting the compression ratio between $5.5 - 9.0$ in increments of 0.5 units. Additional data points were obtained at the

compression ratio of 7.25. The air inlet temperature was set to 125 °C to ensure complete evaporation. The air-to-fuel ratio corresponded to an equivalence ratio of $\phi = 0.25$. The engine speed was held constant at 700 rpm for all the tests, and the coolant and oil temperatures were maintained at 38 °C. The methyl decanoate test fuel had a minimum purity of 98% and was sourced from Tokyo Chemical Industries (TCI). Further details of the engine setup and the operating procedure are discussed in prior work [104].

3.2.2   Speciation diagnostics

A gas chromatograph-mass spectrometer and an FTIR system were separately used for the detection and quantitation of the stable intermediate species formed during the motored engine experiments. Undiluted gaseous products of oxidation were collected from the engine exhaust and transferred to a clean and vacuumed silonite coated stainless steel canister. An oil-free metal bellows pump was used to transfer the gases. A Trace GC Ultra gas chromatograph and a Trace Dual-stage Quadrupole Mass Spectrometer were used for off-line product analysis. The gas chromatograph was equipped with a 50-meter fused silica capillary column having a 0.2 mm ID (Restek Rtx-DHA). This column is suitable for light hydrocarbons as well as polar oxygenates. The sample was introduced using a 1 mL sample loop and used the split injection technique with the helium carrier two gas flow rate of 1.5 mL per minute. The split ratio was set to a value of 50:1. Temperature programming was used to enable separation within a reasonable amount of time.

3.3   Computational specifications

This study compares the results obtained from numerical simulations to the corresponding experimental values. The numerical simulations assume homogeneous finite rate kinetics and use an existing detailed kinetic scheme for methyl decanoate. The kinetic model used in the simulations has been developed by Herbinet et al. [100] and includes 3012 species and 8820 reactions. This mechanism contains both the low and high-temperature chemistry relevant to methyl decanoate. The simulations use the single-zone internal combustion engine model built into the Chemkin Pro® package. This model uses a time-varying cylinder volume, as described in the text by Heywood [78]. It also assumes adiabatic conditions along with the engine parameters provided in Appendix B.

3.4 Results and discussions

3.4.1 Pressure traces

The in-cylinder pressure trace was used to derive global combustion characteristics such as the rate of heat release and the accumulated heat release. These values were obtained as a function of compression ratio using an averaged pressure profile obtained from 300 consecutive motored engine cycles with fuel injection into the air intake. The scatter in the experimental pressure traces at a compression ratio of 6.0 is shown in Figure 3.1. It can be seen from the figure that there is minimal scatter among the recorded cycles and that the average trace adequately captures the general trend for the pressure variations. There is, however, a larger cycle to cycle variation for the cases with a significant second stage heat release (CR≥8.0).
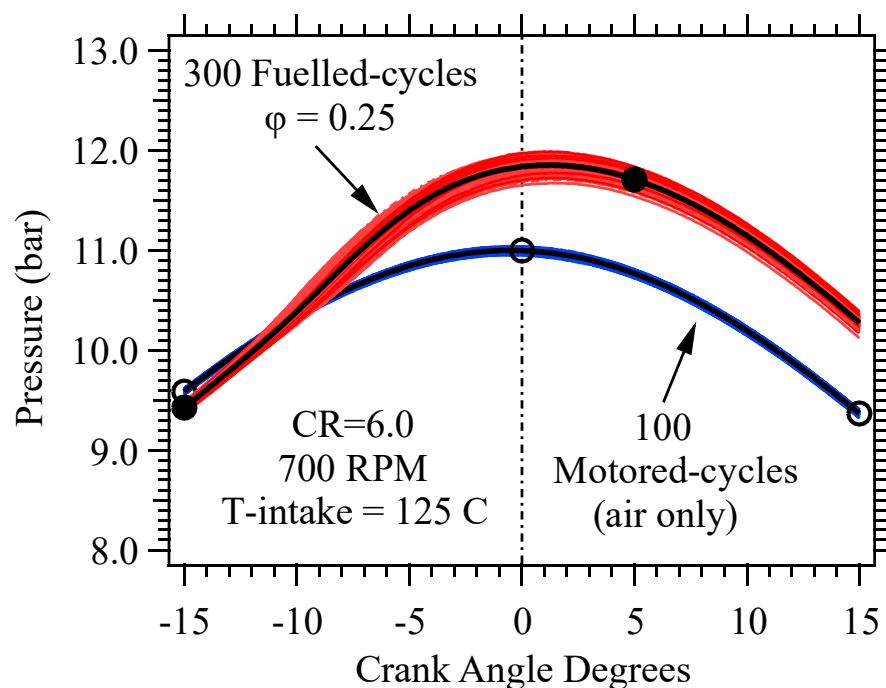
Figure 3.1. The repeatability of the recorded pressure measurements in this work demonstrated by pressure traces of 300 fueled-cycles alongside 100 motored-cycles

The averaged pressure traces for selected compression ratios as a function of the crank angle is shown in Figure 3.2. The averaged pressure traces exhibit a gradual increase with the compression ratio for conditions that have a purely single-stage low-temperature heat release (5.5 ≤ CR≤7.0) followed by relatively sharper subsequent increases as the second stage heat release begins to set in. This transition from a single to a two-stage heat release is visually

apparent due to the change in the curvature of the pressure profiles. The first occurrence of the change in curvature takes place prior to the top dead center, which also corresponds to the first stage heat release. One can also infer the existence of the second stage heat release by observing the shift, to the right, of the location of peak pressure for compression ratios greater than eight. The impact of the low-temperature heat release is to substantially alter the pressure profiles with respect to the crank angle. It is important to be able to predict the global response, such as the pressure time histories that result during the low-temperature oxidation of a fuel. Such a comparison between the experimentally obtained in-cylinder pressure records, and those obtained using computer simulation with the detailed chemical kinetics are shown in Figure 3.2(b).
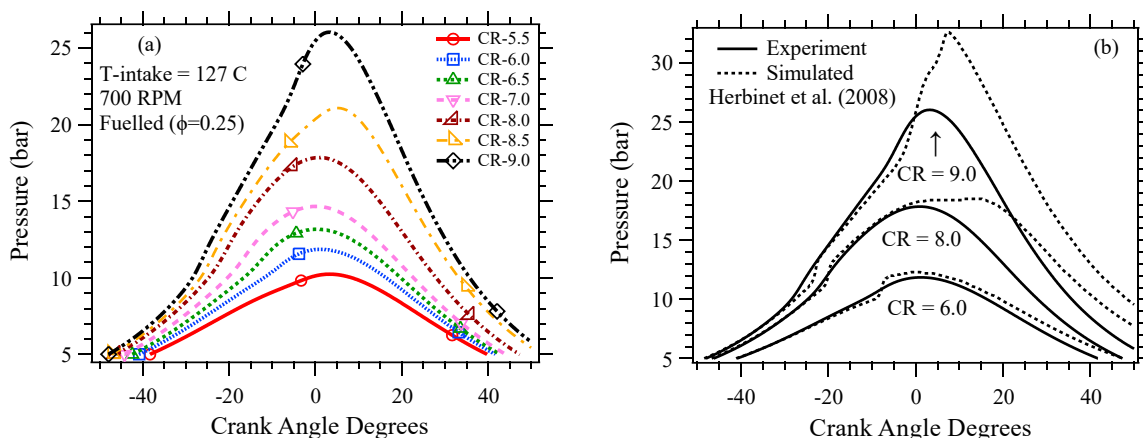
Figure 3.2. Average of 300 fueled experimental pressure traces and (b) comparison of simulated and experimental traces at various compression ratios for $\phi = 0.25$.

There is a reasonably good agreement between the experimental and simulated pressure traces at the lower compression ratios (CR ≤ 6.0). However, the simulations tend to overpredict the pressure rise at higher compression ratios, especially during the power stroke, where the second peak of the low-temperature heat release takes place. This overprediction tends to get enhanced at the higher end of the compression ratios. Furthermore, there are multiple distinct changes in curvature for the simulated results, which points to the existence of multiple peaks in the heat release profile. A detailed analysis of the net heat release trends obtained from these in-cylinder experimental pressure records as discussed in the following section.

3.4.2 Apparent heat release

The apparent heat release trends were obtained following the methodology described by Heywood [78] and are shown in Figure 3.3(a) and (b). There is a clear transition from a

single-stage heat release to a two-stage heat release beyond a compression ratio of 8.0. In the lower compression ratio range (5.5<CR<7.0), the bulk of the low-temperature heat release occurs in a single-window during the compression stroke just before the TDC. A clear two-stage heat release profile is observed at higher compression ratios (CR >8.0) with the first peak occurring much before the top dead center during the compression process and the second peak in the vicinity of or slightly after the TDC. The contribution from the second stage energy release becomes dominant for the two highest values of compression ratios examined in this work, as shown in Figure 3.3(b). The peaks for both the first and second stage heat release in Figure 3.3(a) and (b) shift towards earlier times/crank angles and increase in magnitude with increasing compression ratios. This is expected on account of the different temperature-time history experienced by the compressed gas for each test condition.
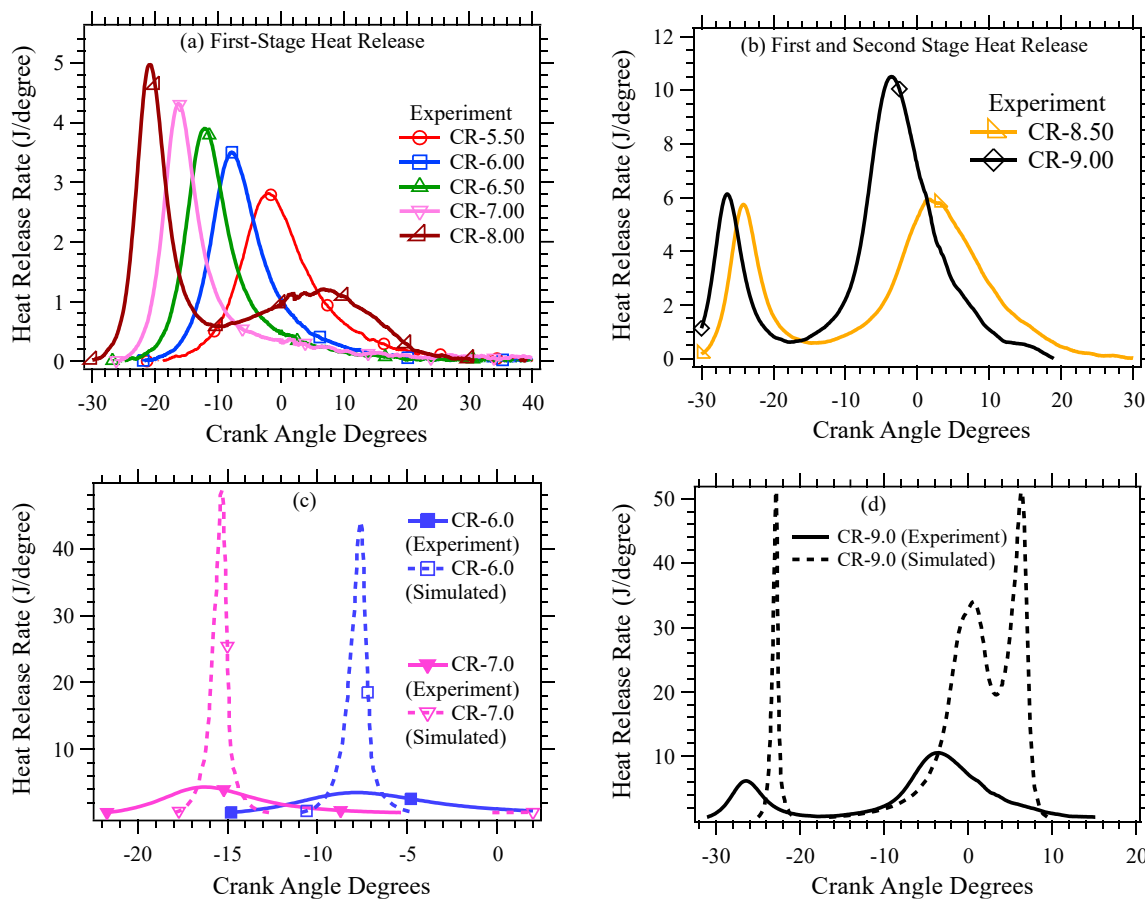
Figure 3.3. Experimental heat release rate profiles at various compression ratios with (a) single first-stage peak (b) dual first and second-stage peaks (c-d) comparison of experimental and simulated heat release rates.

The next set of plots in Figure 3.3(c) and (d) present a comparison between the experimental and simulated heat release rates obtained using the detailed kinetic mechanism

of Herbinet et al. [100] and an appropriate model for the engine experiments [78]. The simulated results for a given compression ratio at the lower end of the experiments show a single-stage heat release similar to what was observed for the experiments. There are, however, significant qualitative differences between the simulated and experimental profiles. The heat release in the simulations is confined to a much narrower region and has a higher maximum value compared to the experiment. Additionally, the simulated results exhibit three heat release peaks at the highest compression ratio, while the experiments under these conditions have at most dual peaks.

A comparison of the relative magnitudes for the peak values for both the first and second stage heat release with the numerical simulations can be seen in Figure 3.4. The first stage heat release is significantly overpredicted in the calculations and is higher by one order of magnitude compared to the experimental values over the entire compression ratio range. Both data sets in Figure 3.4(a), however, are in agreement with respect to the increasing trend over the compression ratio range though the rate of increase is initially much higher in the simulated results. Despite the overprediction, there is some improvement in the ability of the mechanism to reproduce the second stage energy release peak magnitudes, as can be seen in Figure 3.4(b). Note that the experiments and the computed values are in very good agreement about the onset of the second stage heat release at a compression ratio of 7.5.
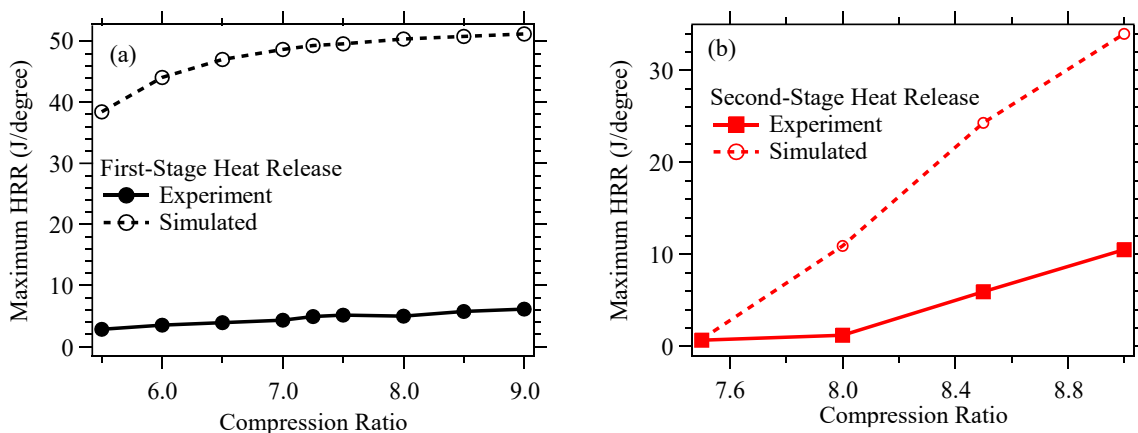
Figure 3.4. Comparison of maximum experimental and simulated values for MD (a) the first stage and (b) second stage heat release as a function of compression ratio.

Another global metric relevant to the heat release process is the location of its peak at different compression ratios. There is an excellent agreement between the experimental data and the computational predictions for the location of the occurrence of the peak value for the first stage heat release as a function of the compression ratio. This agreement in Figure 3.5 is

of significance since it can be treated as a proxy for the ignition delay times measured as a function of temperature using other experimental devices such as rapid compression machines and shock tubes. It is, therefore, reasonable to infer that this mechanism is well optimized concerning its ability to predict ignition delay times with varying temperatures. A closer examination of the experimental curve in Figure 3.5 shows that though the location of peak first stage heat release decreases monotonically over the entire range, there is a region of reduced reactivity in the vicinity of the compression ratio value of 7.25. This reduced reactivity is most likely due to the well-known negative temperature coefficient effect observed in large hydrocarbon oxidation. The computed results however do not show any such feature.
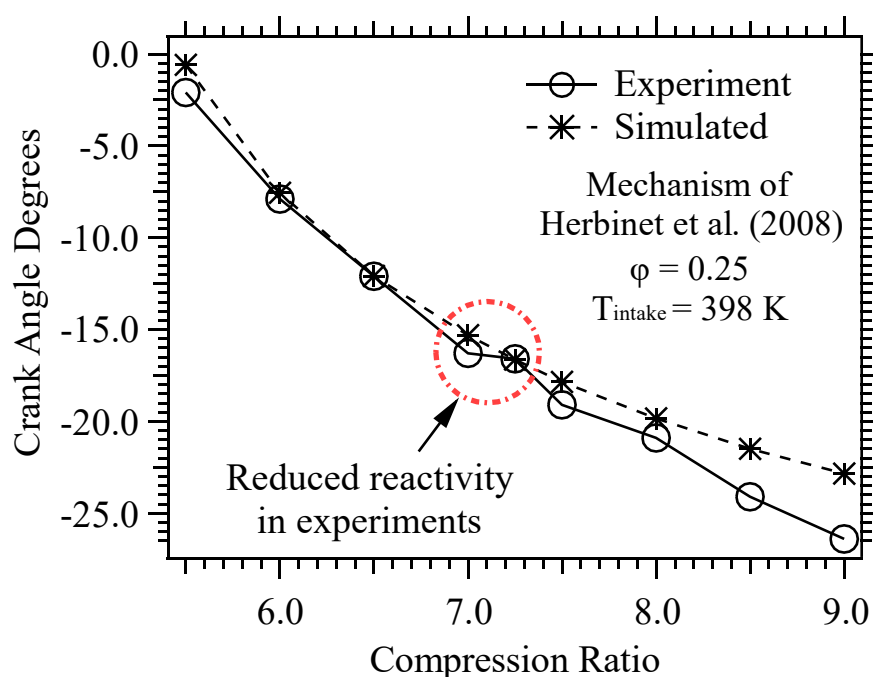
Figure 3.5. Location of peak first-stage heat release as a function of compression ratio

The observation that the experimental heat release rate peaks are shorter and more spread out compared to the simulations leads us to examine the respective areas under the curve for the two under a given compression ratio. This quantity evaluates to the accumulated heat release. The shaded area in Figure 3.6(a) shows an example of the estimation of the experimental accumulated heat release. Note that the left and right cutoffs for carrying out the integration correspond to the first occurrence of the heat release rate value of 0.05 and includes the peak for the second stage heat release if it exists. This integrated value for the experiments is next plotted over the entire compression ratio range and compared to simulated results are shown in Figure 3.6(b). A fair agreement exists between the experimental and simulated values

within the compression ratio range of 5.5 to 7.5, with the simulated values being approximately 1.5 times higher. Both sets of data in Figure 3.4(b) show minimal variations in accumulated heat release with increasing compression ratios in this region (5.5 <CR<7.5). Note that this region of compression ratio is one where only a single-stage heat release is observed. The experimental accumulated heat release remains relatively constant despite the heat release rate curves being qualitatively different (*c.f.* Figure 3.3(a)) as the compression ratio changes (5.5 <CR<7.5). This can be explained by the fact that while the peak height increases with increasing compression ratio, it is also accompanied by a simultaneous reduction in the width of the peak. An increasing compression ratio beyond a value of 7.5 leads to a dramatic increase in the accumulated heat release for the simulations. At the same time, the experiments exhibit a much slower rate of increase.
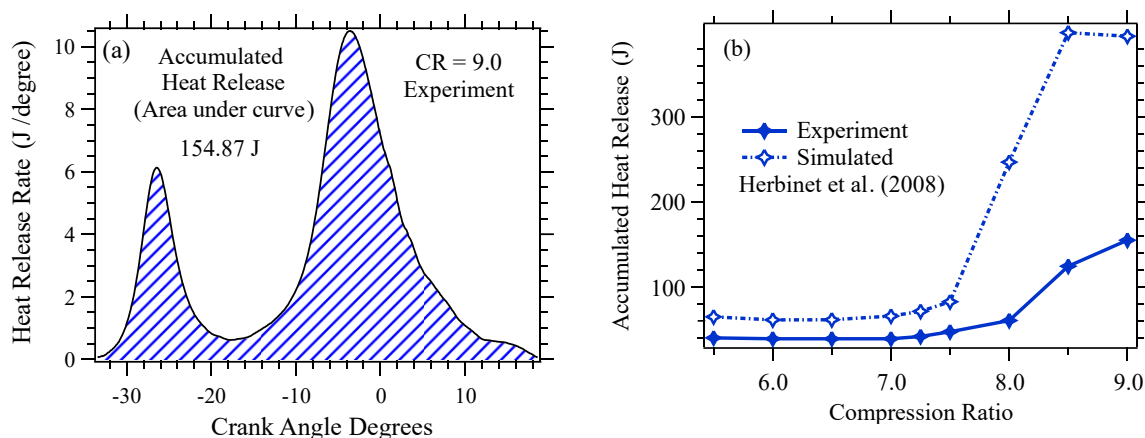
Figure 3.6. (a) Estimation of accumulated heat release (b) comparative variation of accumulated heat release for experiments and simulation with compression ratio

The aforementioned heat release analysis demonstrates the utility of a multi-pronged approach incorporating various global combustion response metrics to compare experiments and simulation. As demonstrated, it is quite possible that a particular measured trend, such as the location of peak pressure, may show an excellent agreement with model predictions while other responses such as peak heat release rates are not adequately captured. It is also important to recognize that an apparently well-predicted response may result from a fortuitous match in integrated quantities (accumulated heat release) even though the underlying profiles (heat release rates) for the experiments and simulations are widely different.

3.4.3 Speciation results

A comprehensive understanding of the oxidation kinetics of fuels is incomplete without having detailed knowledge of reaction product evolution with varying temperatures. An examination of the end products formed during the reaction provides important clues about the reaction pathways. A change in the underlying oxidation mechanism, such as the transition from the low temperature to the high-temperature regime, can be inferred and related to the product distribution. Speciation studies provide detailed information on the actual kinetics of the process than does any single global measurement.

This work follows the end product evolution as a function of the compression ratio using a gas chromatograph-mass spectrometry analysis of the undiluted exhaust gases. A clear variation in the composition of the exhaust gases is apparent with varying compression ratios. The identification of the species was based on the NIST mass spectra library [79]. The Spectral Database for Organic Compounds (SDBS) [80] was also used for identifying a few compounds.

Results for the exhaust analysis for a compression ratio of seven are shown in the form of the total ion chromatogram in Figure 3.7. It shows the peaks for selected light organic compounds (< C7) detected in the products. The peaks are labeled by their retention time within the GC column. Note that the retention time is shown on a logarithmic scale to enable a clear visual presentation. The area under a given peak corresponds to the concentration of the respective compound in the mixture. A total of 66 stable intermediate species were detected and were found to be present in the exhaust products over the entire range of compression ratios. The major classes of compounds detected include alkenes, aldehydes, ketones, dienes, O-heterocycles, alcohols, and methyl esters. The complete list of the detected compounds is presented in Appendix A.

Olefins of chain length between two and nine carbon atoms, including isomeric forms for butene and pentene comprised an important fraction of the oxidation products. The isomeric forms occurred in lower concentrations compared to the straight-chain alkenes. Additionally, compounds such as buta-1,3-diene and penta-1,3-diene were also formed.
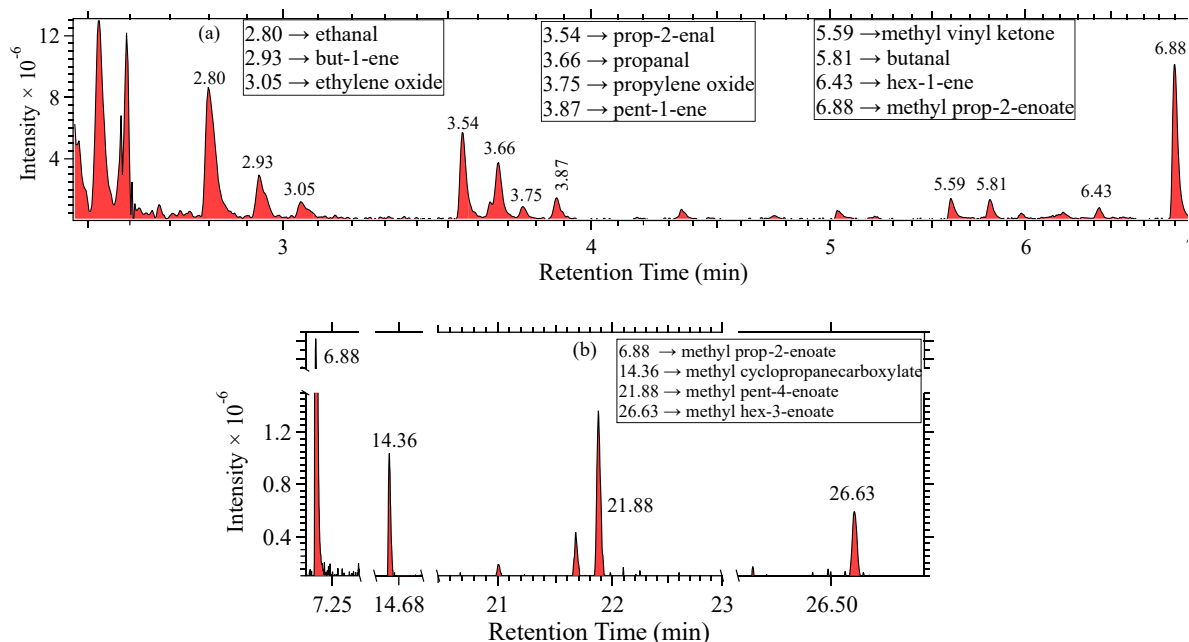
Figure 3.7. (a)Total ion chromatogram (TIC) showing selected intermediates and their retention times (CR=7.0) and (b) sections of the chromatogram showing major methyl esters intermediates.

The major carbonyl compounds detected include straight-chain saturated aldehydes with carbon numbers between two and seven. Ketones (C3: propan-2-one – C7: 4-methylhexan-2-one) were also formed in significant quantities. The unsaturated carbonyl compounds that were identified include prop-2-enal, but-2-enal, pent-2-enal, but-3-en-2-one, and pent-1-en-2-one. Additionally, o-heterocycles with three- and five-membered rings such as oxirane, 2-methyloxirane, and oxolane were also produced. Ethanal and prop-2-enal were the two dominant carbonyl species formed under all compression ratios examined in this work. The product composition evolution over the entire compression ratio for selected species is shown in in Figure 3.8.
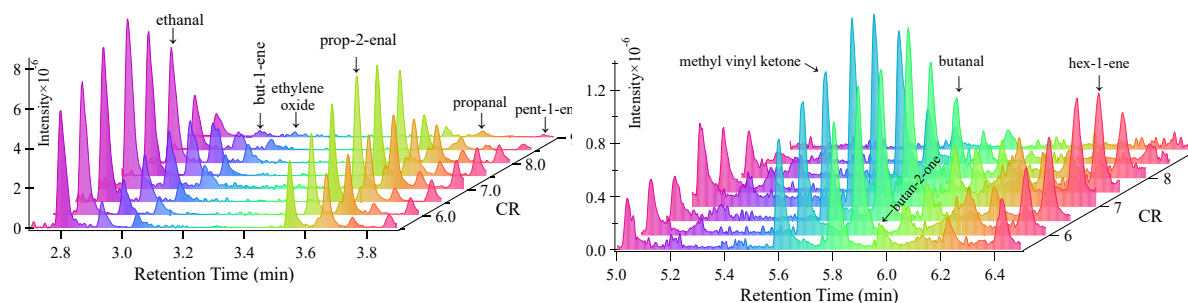
Figure 3.8. Evolution of TIC signal for selected intermediates with variation in compression ratio (CR).

The aforementioned olefinic and carbonyl compounds are very similar to what we observed in a separate study on the oxidation of n-heptane in a motored engine [104]. This

points to strong similarities in the chemistry responsible for the low-temperature heat release, especially the first stage ignition.

However, there are also significant differences between the oxidation chemistry of alkanes as compared to long-chain esters. This is best illustrated by the presence of low carbon number methyl esters shown in Figure 3.7(b) that are exclusively formed in methyl decanoate experiments but were not detected for and heptane studies. Eleven methyl ester intermediates were detected with a good certainty in the products of oxidation of methyl decanoate. There also exist additional isomeric forms of these detected compounds that were not precisely identified yet reported in term of their molecular formulas in Appendix A. Notably, the production of unsaturated methyl esters with one double bond was greater compared to their saturated counterparts. These include methyl esters with carbon numbers between two and seven, including methyl prop-2-enoate through methyl hept-2-enoate. As can be seen in Figure 3.7(b) the most abundant methyl ester intermediates that evolved during the oxidation consist of methyl prop-2-enoate, cyclopropanecarboxlate, methyl pent-4-enoate, and methyl hex-3-enaote. The specie methyl prop-2-enoate in particular is produced in relatively large quantities compared to the other compounds of the same class. This is apparent by its peak height which happens to be nearly one order of magnitude taller than the other methyl esters as well as other compounds. It is, therefore, an important intermediates specie in the low-temperature oxidation of methyl decanoate. Recognizing the importance of these methyl ester intermediate species, it is worth examining their relative variation with respect to the compression ratio and also comparing it to the model predictions.

3.4.4   Qualitative trends for methyl ester formation

The areas under the peaks for the four major methyl ester intermediates are calculated and presented on a common scale in Figure 3.9(a). It can be seen that the peak area for methyl prop-2-enoate is the largest among the four over the entire compression ratio range. The next highest peak areas are those for methyl cyclopropanecarboxylate, which follows a very similar trend to methyl prop-2-enoate. In general, the methyl prop-2-enoate and methyl cyclopropanecarboxylate intermediate production are seen to increase over the compression ratio range of 5.5-7.0, followed by a reduction beyond a compression ratio of 7.5 and higher. This range of compression ratios is associated with a single-stage heat release.
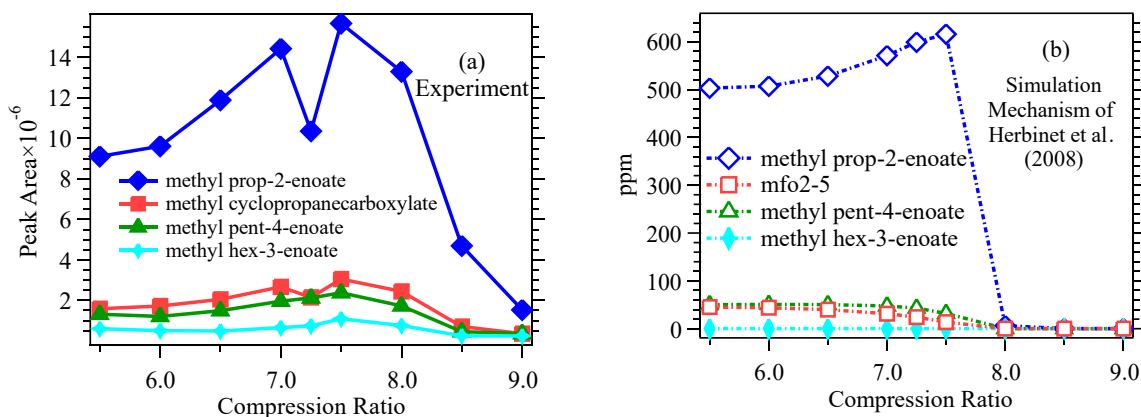
Figure 3.9. Qualitative comparisons methyl ester compounds formed during MD oxidation in (a) experiments and (b) simulations.

A reduction in the peak areas for the two compounds is also evident around the compression ratio of 7.25. This behavior is consistent with previously noted similar observations related to the peak heat release rate as well as the location of its maxima and may be related to the NTC of the reaction rate. On the other hand, methyl pent-4-enoate and methyl-hex-3-enoate show a different trend where the areas initially decrease very slightly from a compression ratio of 5.5 – 6.0, followed by an increase in the range of 6.5 – 7.5, and then again a decrease beyond 7.5.

The simulated results in Figure 3.9(b) show that the mechanism succeeds in predicting methyl prop-2-enoate to be the dominant methyl ester intermediate. The relative trend with the compression ratio is also adequately captured except the dip at a compression ratio of 7.25. The trends and the relative magnitudes for the other three compounds are also very well predicted in the qualitative sense. The model, however, predicts less than 1.0 ppm of methyl hex-3-enoate production, while the area under its GC-MS peak suggests a somewhat higher generation.

3.4.5   Quantitation of selected intermediates with varying compression ratios

Quantitative measurements were carried out for selected intermediates belong to the various chemical classes. Figure 3.10(a) shows the exhaust/end-point quantities of selected alkenes, namely but-1-ene, pent-1-ene, and hex-1-ene. The trends show the selectivity of smaller olefins at all the studied compression ratios. Smaller carbon number alkenes are preferentially generated across the same chemical class for all compression ratios. A similar selectivity was observed among all the other chemical classes. The olefinic species show a

similar variation in concentrations with the compression ratio. In general, for the experiments, the species concentration increases as the compression ratio increases during the first-stage ignition (CR 5.5 – 7.0), followed by a sudden reduction at a compression ratio of 7.25, which suggests an NTC behavior in this region. As we advance into the intermediate-temperature regime (CR 7.5 – 9.0), the experimental olefinic species concentrations start decreasing.

The simulations correctly predict the relative ranking of the olefinic species production but are unable to reproduce the concentration dip at a compression ratio of 7.25. Unlike the experimental observations, the model predicts a significant initial concentration at the lowest compression ratio of 5.5 for the alkenes. There is also an overprediction of the absolute concentrations for the three alkenes up to a compression ratio of 7.5. A rather sharp dropoff (7.5<CR<8.0) followed by a complete cessation of alkene production is predicted by the model, which is not observed in the experiments.
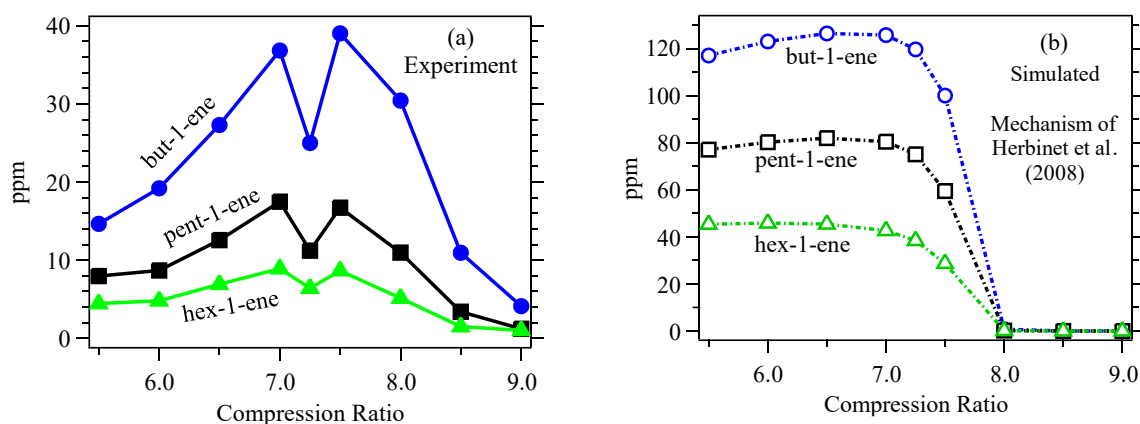
Figure 3.10. (a) Experimental and (b) simulated exhaust/end-point concentration of selected alkene intermediates for varying compression ratios.

An overview of the comparison between the experimental and model results are presented in Figure 3.11 for several major intermediates, as well as CO and CO_2. The alkene, aldehyde, and butan-2-one concentrations are significantly overpredicted up to a compression ratio of 7.5, followed by an underprediction beyond that. There is a somewhat better agreement between the simulated and experimental values for methanol, carbon monoxide, and carbon dioxide though the model fails to account for the presence of CO at compression ratios higher than 8.0. The simulated trend for 2-methyloxirane is very distinctive and does not match the experimental or any other simulated trends. Acetone is the one specie that is consistently underestimated over the entire compression ratio range; on average, its simulated concentration is 26.1 times less than the experimental values.
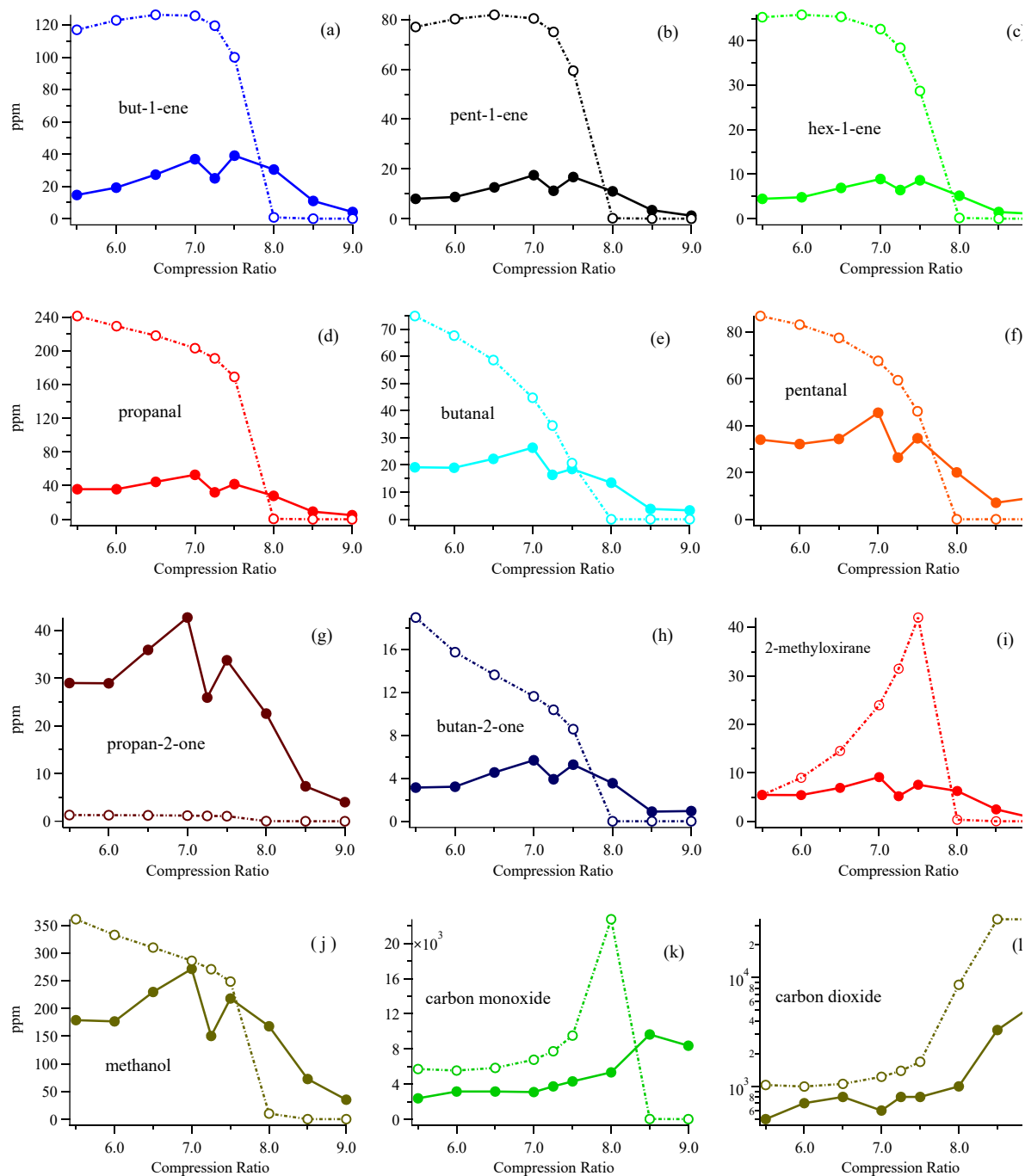
Figure 3.11. Comparisons of experimental (filled symbols) and simulated (empty symbols) exhaust/end-point concentrations of selected intermediates. (a – c) alkenes; (d – f) aldehydes; (g – h) ketones; (i) cyclic ether; (j) alcohol; (k & l) carbon monoxide & carbon dioxide.

3.4.6 Intermediate selectivity within a given chemical class

It is important to develop an understanding of the relative production of species belonging to different chemical classes over the entire oxidation temperature range. Such

information can provide insights into the dominant chemical pathways and also help identify conditions that lead to changes in the controlling chemistry.
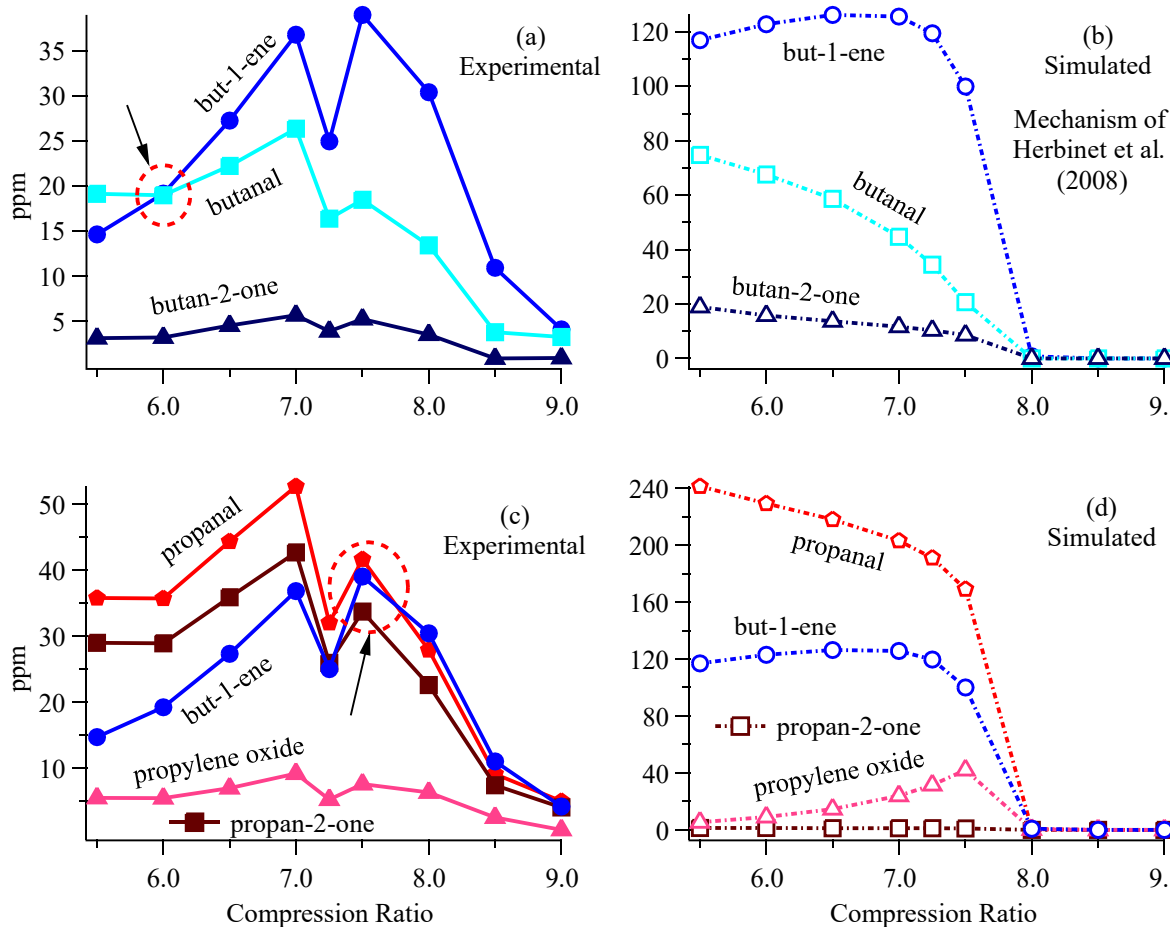
Figure 3.12. Comparison of relative trends for various intermediates

The relative production of an alkene, aldehyde, and a ketone, all having four carbon atoms, is compared in Figure 3.12(a). The experimental results indicate that the aldehyde intermediate, namely butanal, is favored over the olefin but-1-ene under the lowest temperature conditions of the study (5.0 <CR<6.0). The production of the olefinic compounds, however, is much more sensitive to temperature variations over the entire compression ratio range. This increase temperature sensitivity leads to a higher but-1-ene selectivity at elevated temperature conditions in the compression ratio range with a crossover at a compression ratio of 6.0. The alkene and aldehyde production is favored over the ketone specie (butan-2-one) for all test conditions. The corresponding computed results for this set of data are shown in Figure 3.12(b) where the relative rankings for the species concentrations are correctly predicted in the mid-range of compression ratios (6.0<CR<8.0). However, the mechanism does not show a lower

production of but-1-ene followed by a crossover at a compression ratio of 6.0 as when compared to butanal. Another key disagreement relates to the complete lack of production of these three intermediates beyond a compression ratio of 8.0. Thus there appears to be a reason to consider reviewing the intermediate temperature chemistry in the model. Furthermore, the temperature sensitivity for butanal and butanone in the simulations is opposite to what was observed in the experiments under the low-temperature conditions (5.5<CR<7.0).

Figure 3.12(c) once again demonstrates that the aldehyde species (propanal) is produced in larger quantities than the corresponding ketone (propan-2-one) for all the compression ratios. The two carbonyl compounds are also seen to have a higher concentration than the cyclic ether propylene oxide (2-methyloxirane). This figure also illustrates the increasing importance of the olefinic species compared to the carbonyl compounds as the oxidation proceeds to relatively high-temperature conditions. The compound but-1-ene starts to compete with the shorter aldehyde and ketone species (propanal and propan-2-one) at the onset of the second-stage ignition (CR 7.5) and subsequently becomes the most abundant component. The associated computations in Figure 3.12(d) do show a similar ranking for intermediate selectivity at the lower end of the compression ratio except for propanone, which is not generated in the computed results. The model also predicts vanishing concentrations of the intermediates beyond a compression ratio of 8.0, which is at variance with the experiments.

3.4.7   Further observations on the low-temperature heat release

The heat generated during methyl decanoate oxidation is strongly correlated to the CO and CO2 production, as shown in Figure 3.13(a). At lower compression ratios (5.5<CR<7.0), the accumulated heat release is almost constant around 38.5 J, and there is also a relatively small change in the total CO and CO2 concentrations.

The reactions do, however, proceed at a much faster rate, as is evidenced by the rapid heat release over a shorter crank angle duration. The relatively rapid energy release at a compression ratio of 7.0 compared to that for 5.5 is shown in Figure 3.13(b). Note that the heat release profile gets peakier and is confined to a narrower region for the higher compression ratio shown in Figure 3.5. The region corresponding to 80% of the accumulated heat release is spread over 16.7 and 23.4 crank angle degrees for compression ratios of 7.0 and 5.5, respectively. It is also of interest to note that the system temperature in the simulations during the peak first-stage heat release shows a limited variation between 795-820 K. This, in

conjunction with the rapid shift in the location of first-stage peak heat release (c.f. Figure 3.5), suggests a very high sensitivity of the first stage ignition to temperature variations. The speciation analysis also supports the increase in chemical reactivity in this small region where the accumulated heat release appears to remain constant. Nearly all the stable intermediate species quantified in this work exhibit an increase in their respective concentration for compression ratios between 5.5 and 7.0. As noted earlier, CO and CO2 production and oxidation are still constrained and set-off rapidly only at compression ratios beyond 7.5.
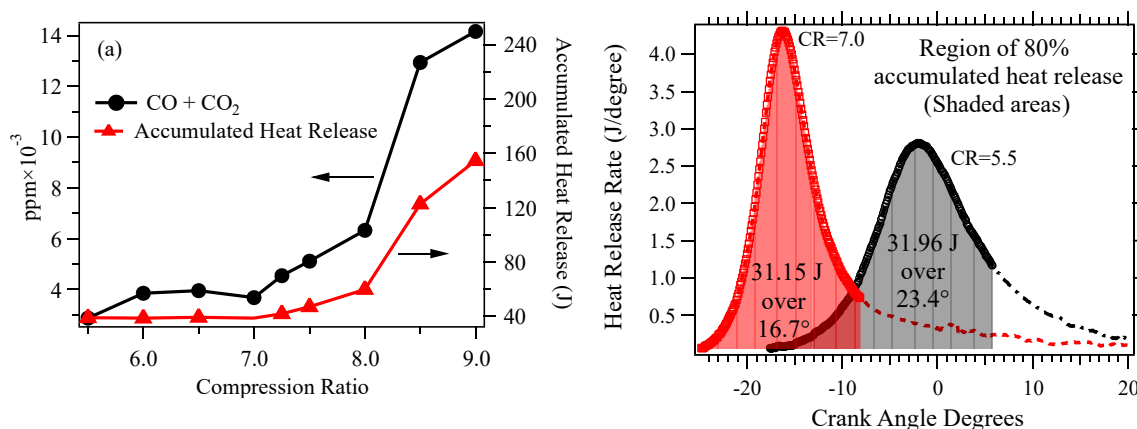
Figure 3.13. (a) Accumulated heat release and the combined CO and CO2 production as a function of compression ratio (b) Variation of heat release rate with the crank angle at compression ratios of 5.5 and 7.0.

The onset of the second-stage heat release is associated with a decrease in most of the stable intermediate concentrations but a sharp increase in the end products of combustion (CO/CO2). This approach to the zone of intermediate/high-temperature oxidation chemistry releases substantially more energy and manifests itself as a larger cycle to cycle variation in the pressure records as well as the heat release profiles, as shown in Figure 3.14. A comparison of the pressure traces in Figure 3.14(a) and (b) shows that the first-stage heat release process is rather stable and associated with a much lower scatter than that for the second-stage.
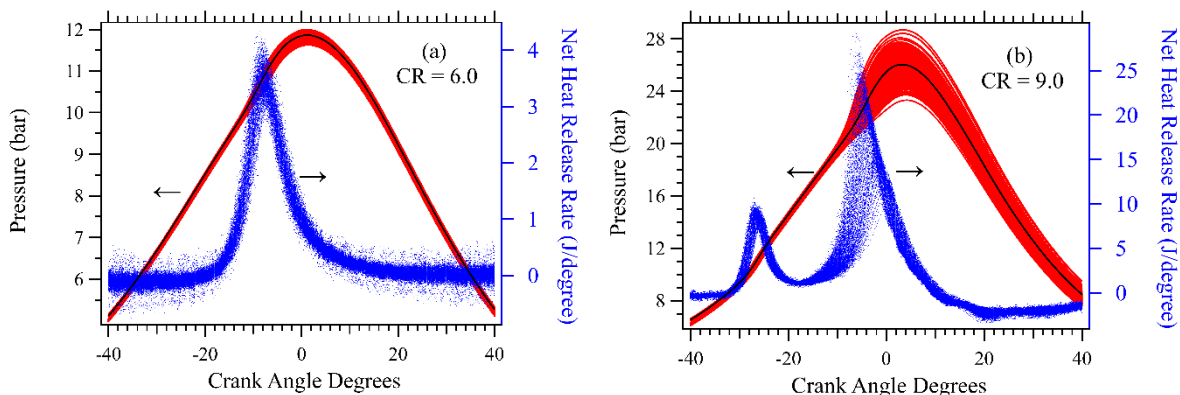
Figure 3.14. Pressure and heat release traces for 300 consecutive cycles at (a) low and (b) high compression ratios

3.4.8   Comparison of methyl decanoate to n-heptane oxidation

The direct comparison between methyl decanoate and n-heptane experimental results is complicated by the fact that the tests were conducted under different intake temperature conditions. A fair comparison would require the reactants to undergo the same temperature-time history. Fortunately, there exist two experimental combinations of compression ratios and the intake temperatures that provide a very similar temperature-time profile for the compression of air within the engine. They correspond to (CR=5.5, T_{in}=398K) and (CR=6.5, T_{in}=383 K). The temperature profile for these combinations is shown in Fig. 15(a). We compare the methyl decanoate results obtained at (CR=5.5, T_{in}=398K) with the n-heptane results at (CR=6.5, T_{in}=383 K).
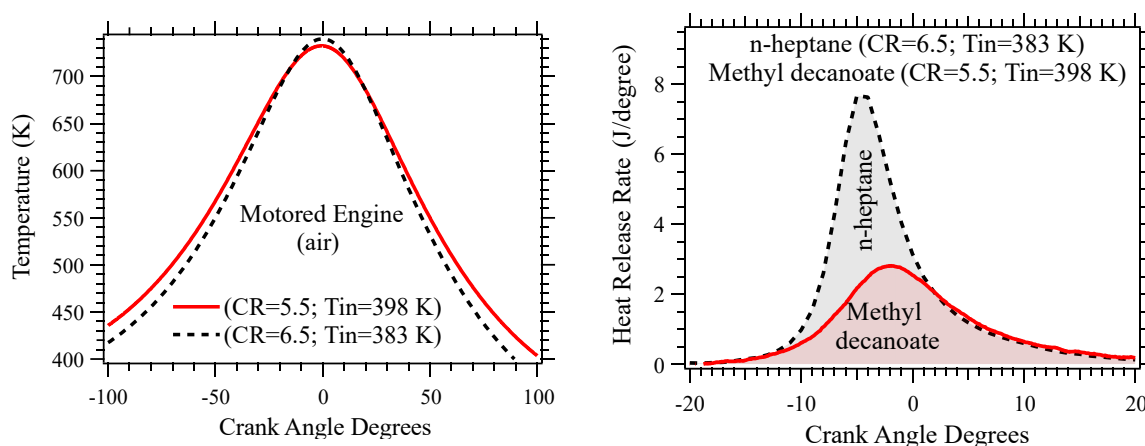
Figure 3.15. Unfueled motored engine experiments that produce similar temperature-crank angle profiles (b) Comparison between the oxidation of n-heptane and methyl decanoate under the compression ratio and intake temperatures as in (a)

The most important similarity in the oxidation characteristic of the two fuels is that they exhibit a similar global feature of a single heat release peak under the given conditions. Furthermore, the heat release occurs over a near-identical range of crank angle degrees with significant overlap in the profile in the tail end. However, the magnitude of the peak and accumulated heat release rates are different, with n-heptane exhibiting a higher value. The earlier sharp rise in the peak heat release rates and the higher energy release for n-heptane is consistent with its higher reactivity in terms of its cetane rating.

Chapter 4: Low-Temperature Oxidation Studies on Canola and Coconut Derived Biodiesel Fuels in a Motored Engine

4.1 Introduction

Understanding combustion kinetics can help the development of more efficient and cleaner, environmentally friendly combustors. For instance, low-temperature combustion engine technologies [105] development depends on comprehending the kinetics of autoignition in the low-temperature regime. Curran et al. established the general kinetic scheme and pertinent elementary reactions to low and high-temperature of hydrocarbon oxidation during the development of detailed chemical kinetic mechanisms for the diesel surrogates n-heptane and iso-octane [11, 12].

Researchers also reported that biodiesel fuels have the potential to significantly reduce greenhouse gas emissions, particulate matter, unburned hydrocarbons, and carbon monoxide when used in internal combustion engines [106-113]. Fisher et al. [89] developed a detailed mechanism of 264 species and 1219 reactions for the combustion of methyl butanoate as a biodiesel surrogate to include the specific features of methyl ester oxidation.

The use of surrogates in combustion kinetic research enabled a fundamental understanding of the nature of ignition, combustion, and emissions while building models of reasonable computational requirements compared to the complex multi-constituent biodiesel fuels. Therefore, extensive research targeted several neat methyl esters that have the potential to represent commercial biodiesel in oxidation modeling [26-28, 30, 31, 48, 52, 84, 92, 98, 114-118]. Researchers have given methyl butanoate [29, 30, 83, 85, 119, 120] and methyl decanoate [28, 91, 93, 97, 99, 118, 121-123] a special place as these compounds first helped to establish a fundamental understanding of the ester group effect on the combustion kinetics. At the same time, methyl decanoate to be a better surrogate at predicting the features of real biodiesel oxidation. Herbinet et al. [100] developed a detailed methyl decanoate oxidation model composes of 8820 reactions and 3012 species.

The most prominent constituents of commercial biodiesels are the fatty acids that contain an unsaturated carbon chain in their structures; few oxidation experiments have targeted surrogates containing C=C carbon bond at different locations of the aliphatic chain [94, 120, 124-126] [127] [35]. These studies reported a reduction in low-temperature reactivity

for the unsaturated methyl esters compared to their saturated counterparts. Westbrook et al. [127] reasoned that the weak allylic radical sites for molecular oxygen that do not support subsequent isomerization reactions lead to reduced low-temperature reactivity. A recent study further introduced, for the first time, experimental jet-stirred reactor investigation of long-chain methyl ester reactivity, specifically those present in commercial biodiesel such as methyl oleate [128].

The continued experimental efforts have established the fundamental knowledge that enabled the construction and validation of biodiesel oxidation models [101, 128, 129]. Review articles document the development of kinetic modeling of oxygenated fuel can be found in the references [9, 25, 130-132]. Herbinet et al. developed a blend surrogates mechanism containing methyl decanoate, methyl-9-decenoate, and n-alkanes [101]. The model was tested against experimental data for rapeseed oil methyl esters in a jet-stirred reactor [33], methyl palmitate/n-decane [133], and motored engine experiments on C9 methyl esters [35].

Most of the aforementioned studies were conducted in laboratory apparatuses such as jet-stirred reactors, rapid compression machines, and shock tubes. Engine experiments targeting the combustion kinetics are quite scarce [35, 65, 68, 69, 71, 134, 135]. These works studied biodiesels/diesel surrogates oxidation. However, none was performed on real biodiesel. The main reason for the lack of experiments investigating the oxidation kinetics of biodiesel is its complex molecular structure that imposes experimental and modeling challenges [25].

Therefore, this work will be among the first to investigate the oxidation kinetics of commercial biodiesel in a motored engine. The oxidation of commercial biodiesel has been reported in jet-stirred reactor studies [33, 133]. In the current work, sixty-four intermediate species were detected in the exhaust gas of canola oil methyl ester combustion via gas chromatogram mass spectrometer (GC-MS). The oxidation experiments were carried out in a pressure range of 9.7 – 19.7 bar and temperature range of 725 – 895 K. Moreover, heat release analysis and end-combustion product quantitation were performed and reported to provide a comprehensive insight into the combustion characteristics of biodiesel and its relation to the evolution of the intermediate at the studied conditions. Such data are crucial for the development and validation of oxidation chemistry models of biodiesel.

Additionally, this work conducted a similar analysis of coconut oil methyl ester. The fuel was chosen for its composition, which is dominated by saturated fatty acids. Coconut

biodiesel oxidation is expected to exhibit features similar and in between to these observed for canola biodiesel and the surrogate methyl decanoate.

4.2   Experimental method

A modified Waukesha Cooperative Fuel Research (CFR), a single-cylinder engine, was used to conduct the experiments as described in the preceding chapters. The engine operates in an HCCI mode where the fuel is injected into the pre-heated intake air. The temperature of the intake air was maintained at 125 °C via an external heater to enable proper fuel evaporation. Accordingly, the fuel was injected to obtain a fuel-lean mixture of 0.25 equivalence ratio. The mixture was combusted by compression at a fixed engine speed of 700 rpm to ensure somewhat similar residence time throughout all the tests. The extent of the combustion was controlled by varying the compression ratio. The cylinder head has a variable compression plug hand-wheel assembly that permits continuous adjustment of compression ratio while the engine is in operation. A compression ratio step of 0.5 in the range of 5.5 – 9.0 was used for the reported experiments.

In-cylinder pressure measurements were acquired by means of a piezoelectric pressure transducer at a resolution of 0.1 crank angle degree. The undiluted combustion exhaust gas was drawn into a clean and vacuumed silonite coated stainless steel canister via an oil-free metal bellows pump. Off-line exhaust analysis was performed separately via a scientific gas chromatogram - mass spectrometer (Finnigan TRACE DSQ GC-MS). The stable intermediate species were detected, identified, and quantified by means of mass fragmentation. The gas chromatograph was equipped with a 50-meter fused silica capillary column having a 0.2 mm ID (Restek Rtx-DHA). The sample was introduced using a 1 mL sample loop and used the split injection technique with the helium carrier two gas flow rate of 1.5 mL per minute. The split ratio was set to a value of 50:1. Temperature programming was used to enable separation within a reasonable amount of time.

4.2.1   Tested fuels

The biodiesel fuels tested in this work, canola oil and coconut oil biodiesel, were manufactured in-house from their feedstock coconut oil and canola oil and tested according to ASTM D6751 standard. Methanol was used in the transesterification reaction in the presence of potassium hydroxide as a catalyst. The precise compositions of the fuels from the various

methyl esters were not determined. However, it is reported that commercial biodiesel feedstock composition, such as soybean and canola, are dominated by unsaturated fatty acids of eighteen carbon chain lengths (C18:1-3). While lighter and saturated compounds, such as lauric (C12:0) and palmitic (C16:0), are the main constituents of potential commercial biodiesel feedstock, such as coconut and palm oil respectively [136]. The compositions of coconut oil and canola oil are shown in Figure 4.1[136]. Saturated biodiesel surrogates oxidation, especially methyl decanoate, are expected to show better agreement with coconut biodiesel oxidation as capric (C10:0) and lauric (C12:0) fatty acids comprise around 50 % of the fuel composition, while unsaturated fatty acids make up less than 10 %. On the other hand, unsaturated fatty acids make up more than 90% of canola biodiesel. Therefore, unsaturated surrogates are expected to result in better agreement with biodiesel fuel such as canola.
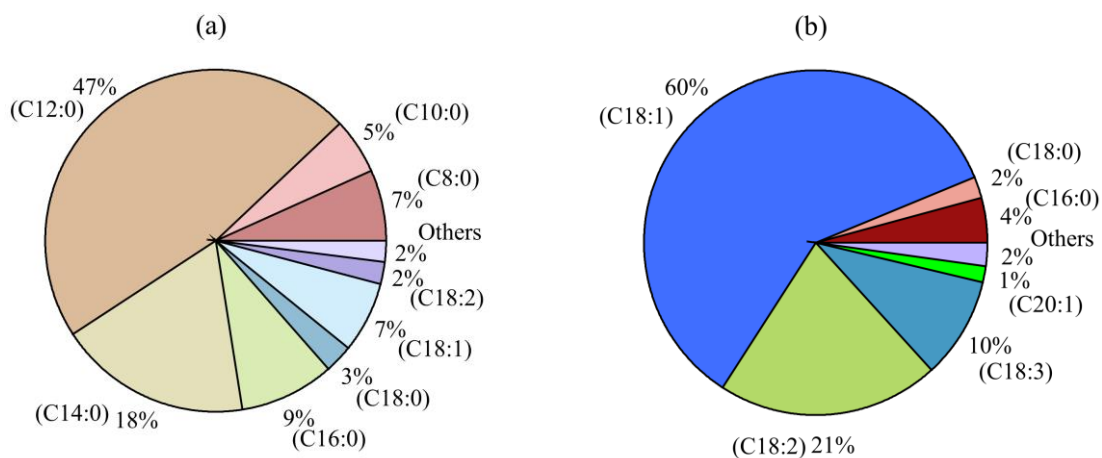
Figure 4.1. Average fatty acid compositional profiles from the feedstocks (a) coconut oil, (b) canola oil of the tested fuels as reported in the literature [136].

4.3   Results

4.3.1   Apparent heat release

4.3.1.1   Coconut oil biodiesel

Pressure measurements of 300 fueled cycles were recorded and averaged during coconut oil biodiesel combustion at each studied compression ratio. The average pressure traces as a function of the crank angle are shown in Figure 4.2(a) near the top-dead-center. The traces are nearly symmetrical around the TDC, with subtle inflection points prior to the TDC. The inflection points are better viewed in Figure 4.2(b), where the fueled traces for selected

compression ratios are posted alongside their corresponding unfueled cycles (air only). The inflection points are evident at the lowest compression ratios and shift to an earlier crank angle as the compression ratio increases. This reveals a low-temperature heat release across the studied range, as shown in Figure 4.2(c). The heat release profiles were computed based on the average pressure traces using the model described in Heywood's text [78].
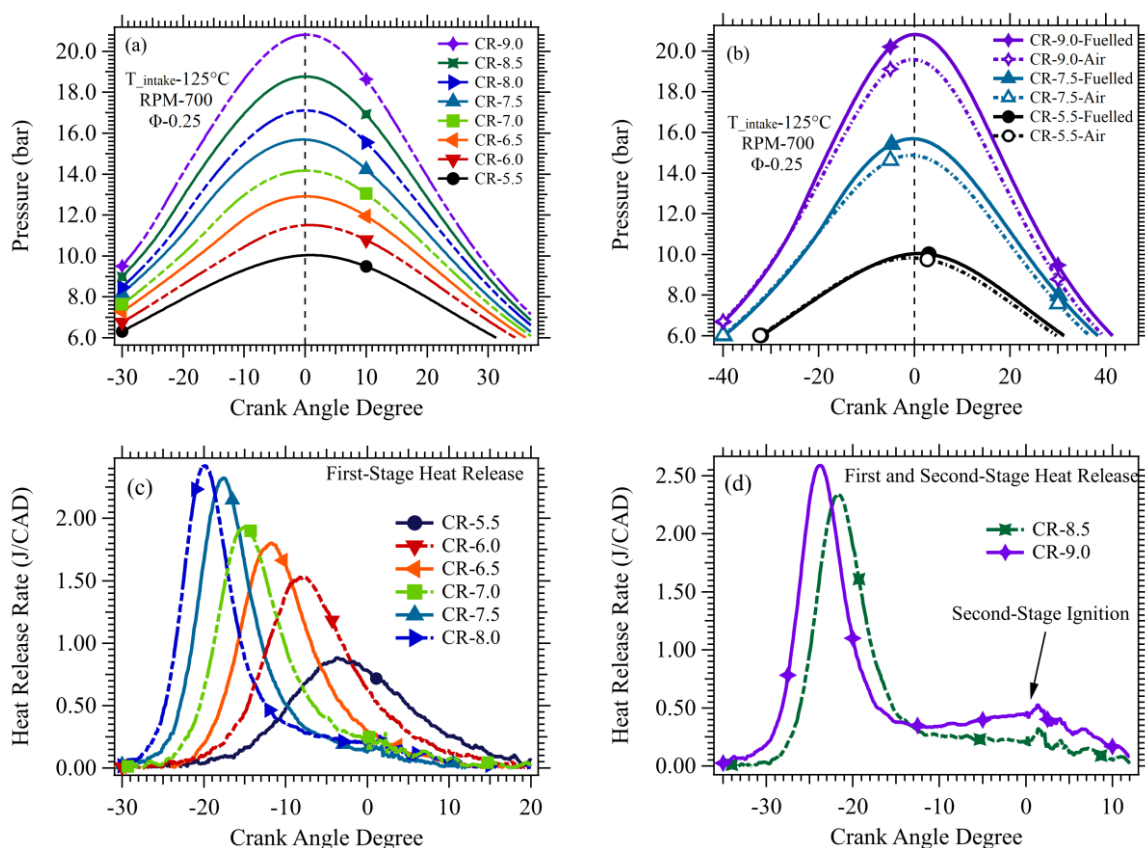
Figure 4.2. Pressure measurements and heat release analysis during coconut oil methyl ester combustion. (a) Average pressure traces during fueled cycles for all studied compression ratios (b) Average pressure traces during fueled cycles compared to unfueled cycles for selected compression ratios (c) low-temperature heat release profiles (d) heat release profiles showing the evolution of a second-stage ignition.

This suggests that coconut oil biodiesel, which is a combination of saturated and unsaturated long fatty acids methyl esters, undergoes low-temperature oxidation chemistry similar to the one observed in classes such as alkane and neat saturated methyl ester. The heat release profiles illustrate a faster heat release rate and earlier ignition at higher compression ratios. The first-stage heat release occurred entirely before the TDC at compression ratios higher than 6.0. As the compression ratio exceeds 8.5 units, the profiles start to develop a second-stage heat release near the TDC, as shown in Figure 4.2(d). Tests at compression ratios higher than 9.0 were not possible due to the engine's specification limit.

4.3.1.2 Canola oil biodiesel

The average pressure profiles of canola oil methyl ester oxidation at the same conditions of coconut oil biodiesel oxidation are shown in Figure 4.3(a). The inflection points are barley seen as the pressure traces exhibit symmetry around the TDC. However, Figure 4.3(b) manifests an obscured deviation in the pressure traces of the fueled cycles compared to the unfueled cycles. For instance, at the compression ratio 9.0, the average maximum pressure during fueled cycles was found to be 19.6 bar compared to 19.2 bar in case of unfueled cycles. Note that these values are averages of three-hundreds cycles, thus reduce experimental uncertainties and cycle to cycle variation.
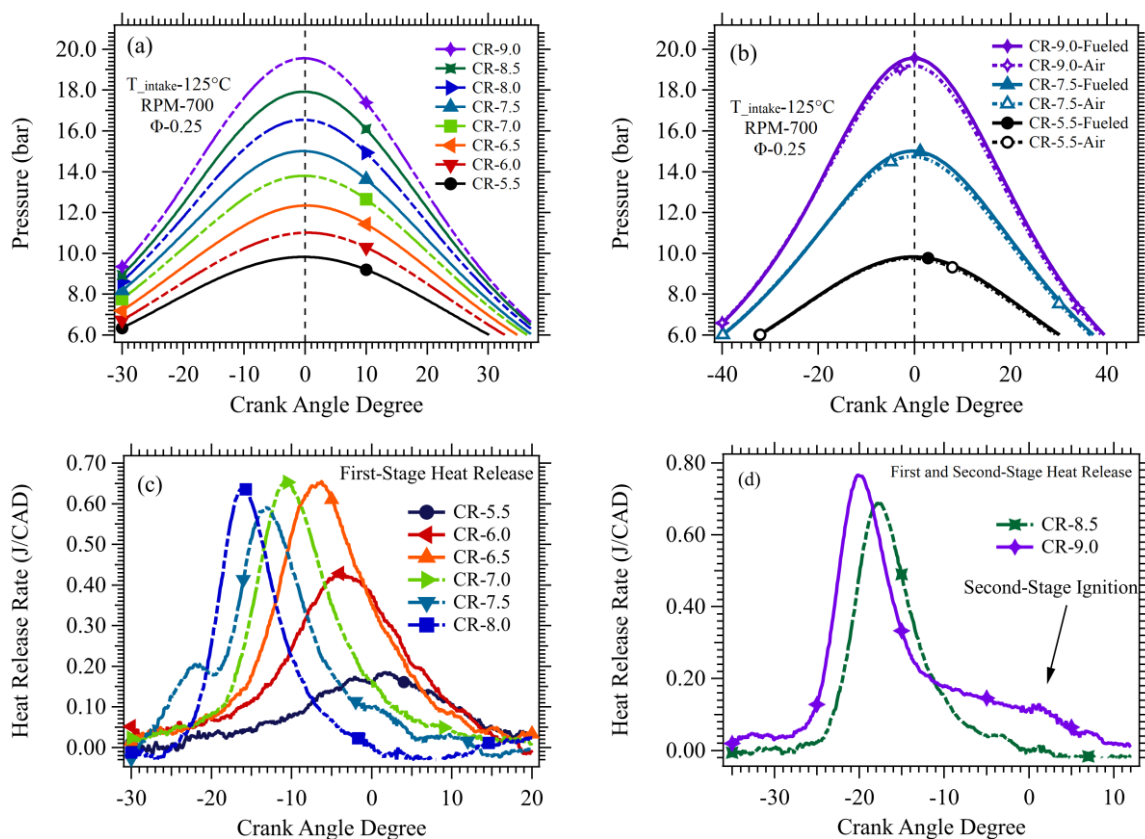
Figure 4.3. Pressure measurements and heat release analysis during canola oil methyl ester combustion. (a) Average pressure traces during fueled cycles for all studied compression ratios (b) Average pressure traces during fueled cycles compared to unfueled cycles for selected compression ratios (c) low-temperature heat release profiles (d) heat release profiles showing the evolution of a second-stage ignition.

Therefore, the deviation must be a consequence of the low-temperature oxidation kinetics and the accompanying heat release. The heat release profiles for the canola oil methyl ester oxidation tests are as depicted in Figure 4.3(c) for the compression ratios 5.5 – 8.0. The profiles demonstrate evident low-temperature heat release characteristics as they shift to earlier

crank angles as the compression ratio increases, with faster rates and earlier ignitions. The heat release at the compression ratio 7.5 exhibits a unique profile where two peaks were observed during the first-stage ignition. This behavior was exhibited repeatedly throughout the three-hundred fueled-cycles. And it is not the second-stage ignition feature known in hydrocarbon oxidation, as the behavior vanished at higher compression ratios, as shown by the single-peak heat release profile at the compression ratio 8.0. Following that, the oxidation exhibits potential transition toward the second-stage ignition feature at the compression ratios 8.5 – 9.0 as shown in Figure 4.3(d). Worth noting that it is the same compression ratio range coconut biodiesel oxidation starts to enter the second stage ignition regime.

4.3.2   Intermediate species formation

4.3.2.1   Coconut oil biodiesel

The exhaust gases of the coconut oil biodiesel combustion were analyzed via GC-MS for each studied compression ratio. Numerous reaction products were detected, which range from light (C1 – C5) to moderately-heavy (C6 – C10) species. Sixty-four intermediates were identified and reported in Appendix A. The detection of species of carbon numbers larger than ten (> C10) was not possible using the applied method. The species belong to the chemical classes methyl esters, alkenes, aldehydes, ketones, alcohols, cyclic ethers, dienes, and aromatics. The identification was accomplished based on the match between the mass spectrum of each peak with the database available by NIST or Spectral database for organic compounds (SDBS). Furthermore, there was no variation in the types of detected species across the studied compression ratio range. In other words, all the intermediates were detected at each studied compression ratio. However, the concentrations of the intermediates varied as the compression ratio varied, as could be inferred from the areas under the chromatograms' peaks.

The total ion chromatogram (TIC) signal intensity from the mass spectrometer during the analysis of the exhaust gases of the compression ratio 7.0 is shown in Figure 4.4(a). Most of the reported species are obscured behind the high intensity of few species. For instance, a closer look at the chromatogram in the retention time range 2.8 – 6.3 mins, as shown in Figure 4.4(b) illustrates several peaks of low intensities.
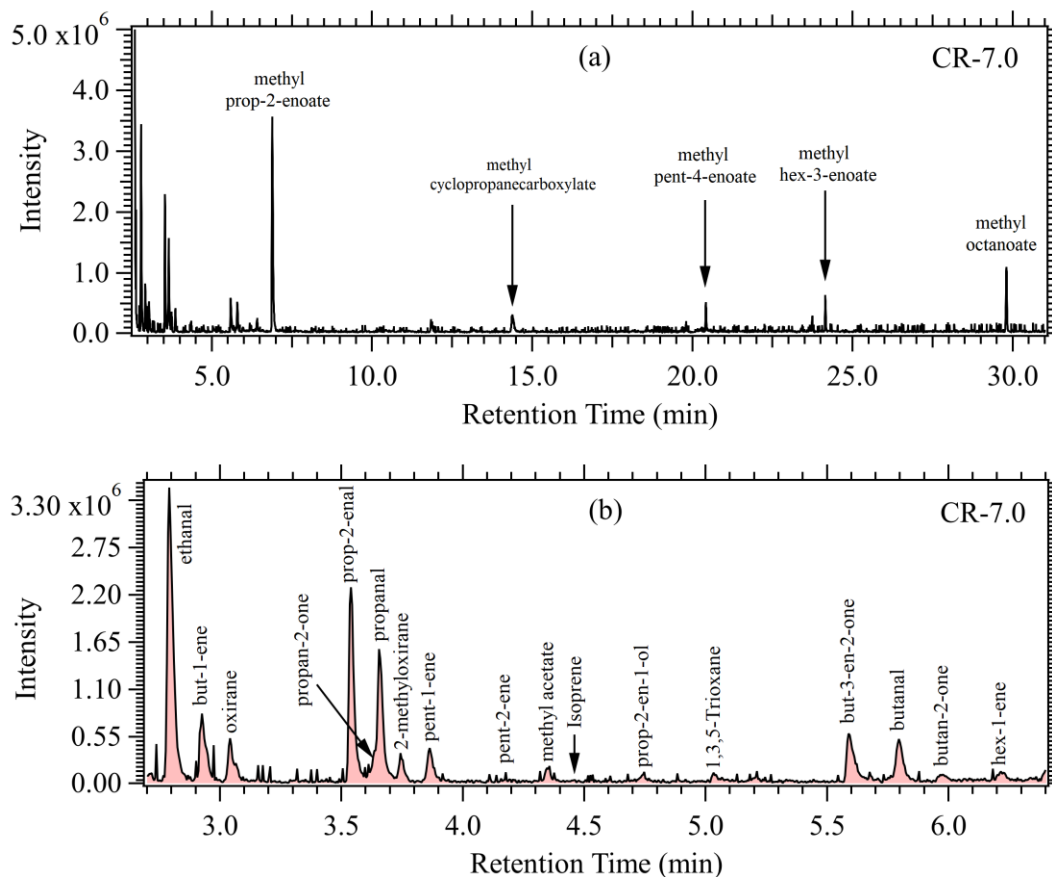
Figure 4.4. (a) Total ion chromatogram of the exhaust gases of coconut biodiesel for the compression ratio 7.0 (b) portion of the chromatogram shows light intermediates belong to various chemical classes

Figure 4.4(a) demonstrates the formation of methyl ester compounds of unsaturated and saturated aliphatic chains. Unsaturated methyl esters of three to seven carbon numbers with single C = C double bond were identified (C3:1 – C7:1). In general, they have higher intensities compared to the other heavy products. Their formations have been reported repeatedly in methyl esters oxidation studies [34, 68, 115, 133]. It is believed that they are formed through the same pathways that generate olefins during alkanes oxidation. Moreover, The peak of the species methyl prop-2-enoate evidence a considerably higher generation than all the other detected products. Similar to what Zhang et al. observed when oxidized C7 esters and reported higher generation of methyl prop-2-enoate compared to the unsaturated ester species [71]. On the other hand, saturated methyl esters formation during methyl esters oxidation has not been reported. In this work, four saturated methyl esters were identified, namely methyl acetate, methyl propanoate, methyl hexanoate, and methyl octanoate. However,

the latter two compounds could be components of the fuel itself due to the presence of fatty acids such as capriotic and caprylic in the feedstock.

The other species detected in this work belong to the chemical classes alkenes (C2 – C9), saturated aldehydes (C1 – C7), saturated ketones (C3 – C7), saturated alcohols mainly methanol and ethanol, cyclic ethers of three and five-membered rings, and dienes such as buta-1,3-diene, cyclopenta-1,3-diene, and 2-methylbuta-1,3-diene. Figure 4.4(b) displays selected light species belong to these classes. Benzene was the only aromatic intermediate detected in the exhaust gases. Unsaturated species belong to the same classes were also formed and reported. In general, the unsaturated species, other than methyl esters, exhibited lower intensities compared to the saturated counterparts. Exceptions for this observation was the higher generation of the aldehyde prop-2-enal and the ketone but-3-en-2-one.

4.3.2.2   Canola oil biodiesel

The intermediates detected during the analysis of canola biodiesel oxidation products were found to be surprisingly identical to those formed during coconut biodiesel oxidation and reported in Appendix A. However, the intensities of their peaks were significantly lower compared to the chromatogram of the coconut biodiesel oxidation products, which led to higher noise to signal ratio as shown in Figure 4.5(a). In other words, the lower generation of the intermediates was experienced during canola biodiesel oxidation. For certain species, the peaks were completely hindered by the noise. Nonetheless, a thorough investigation of the chromatograms revealed fragmentations similar to what was observed in the chromatogram of the coconut biodiesel oxidation products. The speciation method was held constant for the two fuels to enable the comparison.

In brief, the speciation analysis of canola biodiesel oxidation products exhibited similar features to those discussed for coconut biodiesel. These include the evolution of the unsaturated methyl ester intermediates with the species methyl prop-2-enoate being the most abundant methyl ester. Also, the detection of species belong to alkenes, aldehydes, ketones, cyclic ethers, alcohols, dienes, and aromatics is confirmed in the case of canola biodiesel, with lower concentrations compared to coconut biodiesel.
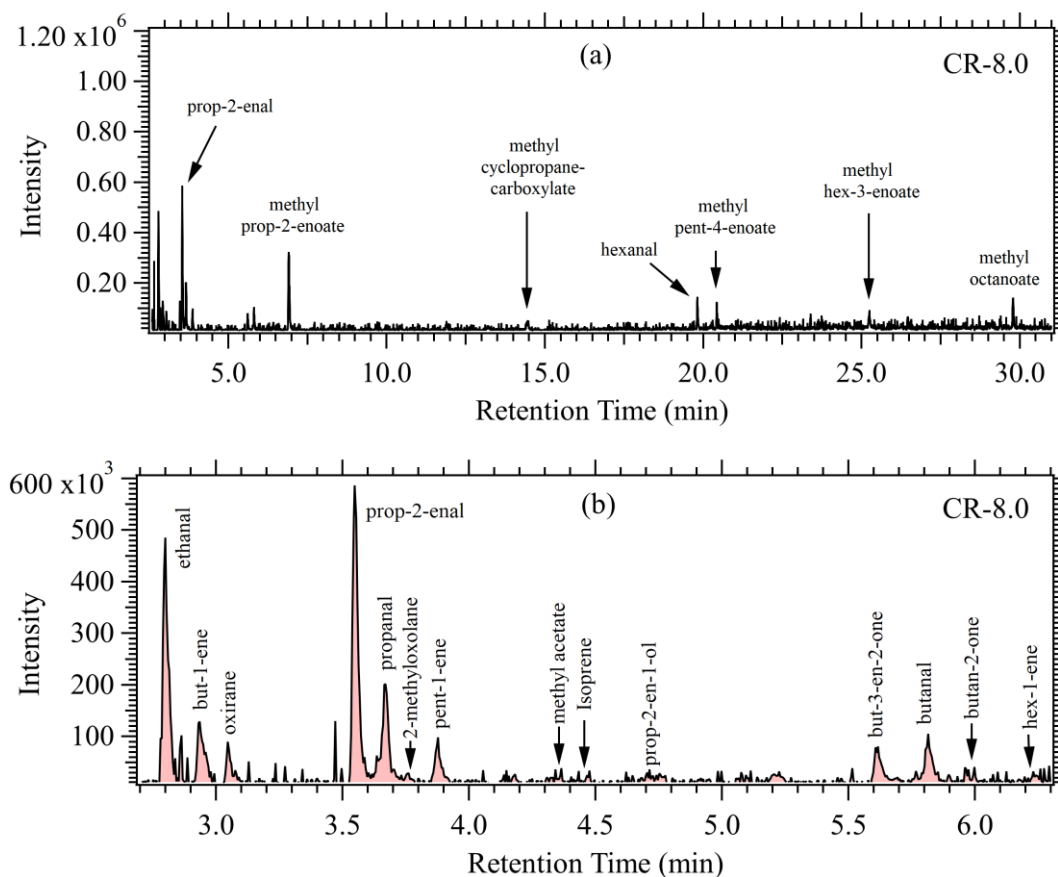
Figure 4.5. (a) Total ion chromatogram of the exhaust gases of canola biodiesel for the compression ratio 8.0 (b) portion of the chromatogram shows light intermediates belong to various chemical classes

On the other hand, minor differences can be deduced from the two chromatograms. The highest intensity signal in the case of canola biodiesel products comes from the unsaturated aldehyde, namely prop-2-enal, as shown in Figure 4.5(a). Moreover, unlike coconut biodiesel, prop-2-enal has higher intensity compared to the shorter aldehyde ethanal, as manifested in Figure 4.5(b). A similar observation can be made on the intensities of the two species butan-2-one and butanal.

4.4   Discussion

The speciation analysis of the exhaust gases of canola biodiesel and coconut biodiesel oxidation revealed the formation of similar intermediates during the combustion of the two fuels. Interestingly, in the previous chapter, combustion products of methyl decanoate under the same experimental conditions were also the same set of intermediate species that evolved in the current work. The thorough inspection of the chromatogram of the canola biodiesel oxidation products proved that nearly all the species detected in the methyl decanoate oxidation

products could be recognized even with the lack of appreciable peaks. Such observations suggest that biodiesel fuels, in this study coconut and canola oil methyl esters, have fundamentally similar low-temperature oxidation chemistry to that observed for saturated methyl esters. Similarly, it is believed that the aliphatic chain of the saturated methyl ester participates in the low-temperature oxidation chemistry similar to the carbon chain in alkanes, while the ester group remains intact [68].

However, the experiments exhibited a higher generation of the combustion intermediates in the ascending order canola biodiesel < coconut biodiesel < methyl decanoate. This is perceived from the areas under the chromatograms' peaks of the oxidation products for the three fuels as shown in Figure 4.6 The lower generation of the intermediate species in canola and coconut biodiesel compared to methyl decanoate was accompanied by corresponding suppression in the low-temperature heat release as shown in Figure 4.7. Where methyl decanoate show a higher peak heat release rate of a factor of 2.23 and 6.58 compared to coconut biodiesel and canola biodiesel respectively at the same experimental conditions.
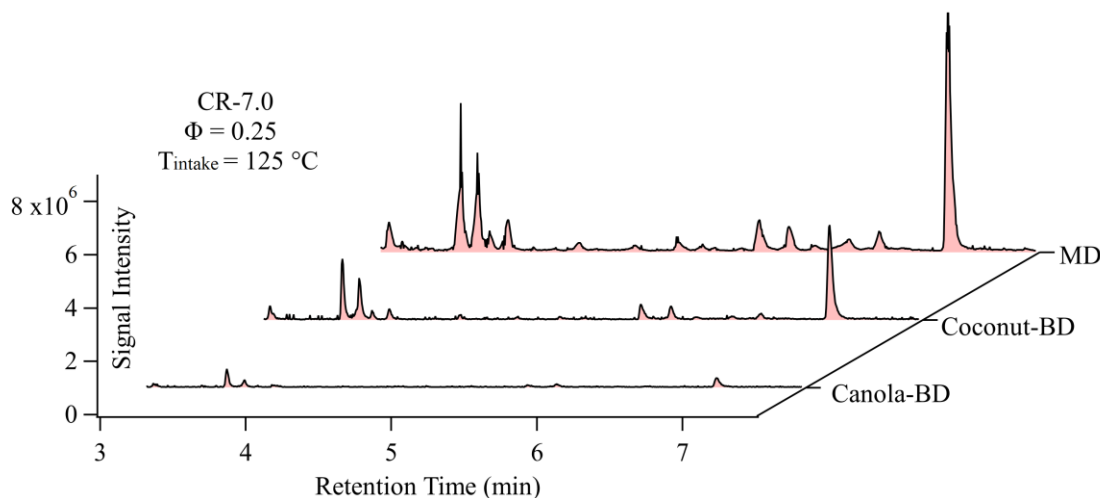
Figure 4.6. The total ion chromatograms of the exhaust gases of biodiesel fuels compared to methyl decanoate when oxidized at the same conditions.

Methyl decanoate is a saturated methyl ester of ten carbon atoms chain. Hence, its aliphatic chain participates in alkane-like low-temperature oxidation chemistry. Saturated methyl esters, however, exhibited suppressed first-stage ignition compared to counterpart alkanes [71]. Coconut biodiesel, as it appears from the composition of its feedstock, is dominated by saturated methyl esters, which make up 90% of its composition, mainly methyl laurate ($C_{13}H_{26}O_2$) and methyl myristate($C_{14}H_{28}O_2$). On average, coconut biodiesel can be

represented as saturated methyl laurate. Therefore, it is expected that the fuel would exhibit a more pronounced low-temperature heat release compared to the shorter methyl decanoate. In contrast, suppressed first-stage ignition is demonstrated by both the concentration of the products and the heat release rate trends of the oxidation process in Figure 4.6 and Figure 4.7, respectively. It is mostly the effect of the 10 % unsaturated methyl esters present in the fuel that led to such suppression. Unsaturation in coconut biodiesel can come in form of methyl oleate $C_{19}H_{36}O_2$ and methyl linoleate $C_{19}H_{34}O_2$.

The effect of the unsaturation on the reactivity of the biodiesel can be emphasized by the large suppression of the low-temperature heat release and intermediates generation in case of canola biodiesel. Which is dominated by unsaturated methyl esters of C18 aliphatic chain of one, two, and three C=C double bonds, namely methyl oleate $C_{19}H_{36}O_2$, methyl linoleate $C_{19}H_{34}O_2$, and methyl linolenate $C_{19}H_{32}O_2$.
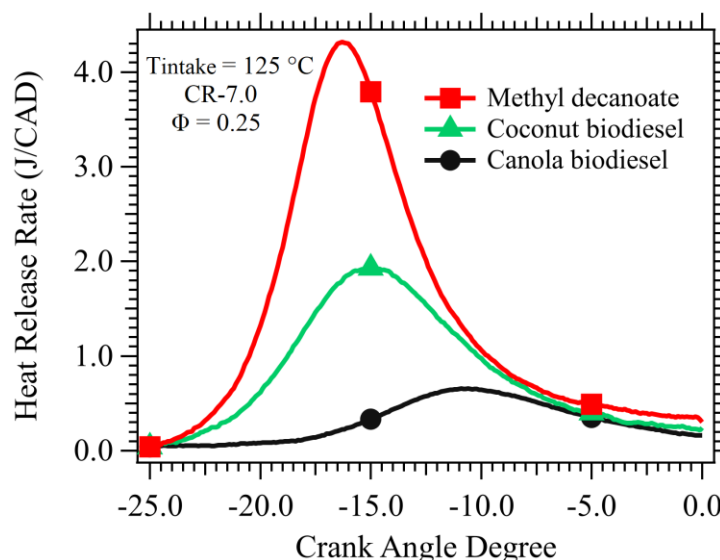
Figure 4.7. Heat release profiles during the oxidation of three different esters oxidized at the same conditions.

Bax et al. [115] studied the oxidation of methyl oleate/n-decane blend (26 mol%/74 mole%) in a jet stirred reactor over the temperature range 550 – 1000 K. Their speciation analysis enabled the detection of both light and large compounds in the oxidation product, including those of C19 carbon chain. As far as species of carbon number less than C10 are concerned, the current work shows a high agreement with their reported intermediates. Moreover, they concluded that the presence of the double bond in methyl oleate have a lower effect on the reactivity of the fuel as it is located in between two large alkylic chains allowing the low-temperature chemistry to proceed. Their conclusion was established based on fuel

conversion measurements. However, the reactivity of methyl oleate may have been overwhelmed by the high reactivity of n-decane. On the other hand, Zhang et al. [35] studied moderately large neat C9 unsaturated methyl esters in a motored engine similar to the setup used in this study. Through heat release analysis, they observed that methyl nonanoate experiences two-stage ignition while the unsaturated esters exhibit only single-stage ignition. The saturated ester also exhibited earlier ignition and a higher heat release rate. They also compared the reactivity of two unsaturated C9 methyl esters with different double bond locations namely methyl 2-nonenoate and 3-nonenoate and found that the latter exhibit lower reactivity with negligible low-temperature heat release, which emphasizes the suppression effect of the C=C double bond on the reactivity of the ester. Similar conclusion has been made by Tanaka et al. [137] when they compared the reactivity of 1-heptene, trans-2-heptene, and trans-3-heptene. While the formers exhibited two-stage ignition, the letter experienced single-stage ignition. The reactivity reduction for the unsaturated compounds in the low-temperature regime was attributed to the reduction of the possible number of six- or seven-membered transition state rings that can be formed during oxidation with the presence of a double bond in the aliphatic chain [127]. The positioning of the double bond toward the center of the aliphatic chain reduces these rings. Similarly, the saturated ester may form more seven-membered rings, consequently, increase low-temperature reactivity.

The heat release analysis of canola biodiesel oxidation in this work seems to have similar characteristics to these observed by Zhang et al. for the ester 3-nonenoate [35]. Where the low-temperature heat release generation is negligible compared to the high-temperature heat release. It is therefore, more accurate to employ unsaturated methyl esters with centered C = C double bond in the oxidation chemistry modeling of biodiesel with high unsaturation content such as canola biodiesel. On the other hand, biodiesel of composition dominated by saturated methyl esters, such as coconut biodiesel, can be fairly represented by saturated methyl ester surrogates. The current results introduce an evident on the method used by Herbinet et al. [101] in building biodiesel mechanism using a combination of saturated and unsaturated methyl esters, namely methyl decanoate and methyl-9-decenoate. They stated that the mechanism could be used for the modeling of biodiesel fuels from various origins by adjusting the mole fractions of the three fuel components, n-heptane, methyl decanoate, and methyl-9-decenoate, in the reactant mixture. However, it is suggested by the canola biodiesel

results that an unsaturated methyl ester with a C = C double bond, such as methy-5-decenoate or methyl-3-noneate, would be better at predicting commercial biodiesel oxidation.

4.5   Conclusion

The current research contributes to the knowledge of biodiesel oxidation kinetics in the low-temperature regime. Coconut oil methyl ester and canola oil methyl ester have been oxidized in a pressure range of 9.7 – 19.7 bar and temperature range of 725 – 895 K via a motored engine. The oxidation exhibits low-temperature heat release for the two esters.

We report sixty-six stable intermediates, have been detected in the exhaust gas of the biodiesel fuels oxidation. The intermediate species belong to the chemical classes alkenes, aldehydes, ketones, cyclic ethers, alcohols, dienes, and methyl esters. The generation was dominated by species of carbon chain length less than five. The most pronounced methyl esters detected in the exhaust gas were methyl prop-2-enoate, cyclopropanecarboxlate, methyl pent-4-enoate, and methyl hex-3-enaote. The biodiesel fuel oxidation products are qualitatively similar to those that evolve during the oxidation of biodiesel surrogates such as methyl decanoate. However, the biodiesel oxidation exhibited suppressed low-temperature heat release compared to the surrogates, accordingly, generating less amount of the intermediate products.

The low-temperature heat release in coconut and canola oil biodiesel correlates with the amount of the saturated methyl esters in their compositions. Coconut biodiesel oxidation illustrated a considerable low-temperature heat release as it is dominated by saturated methyl esters. On the other hand, canola biodiesel oxidation exhibited almost negligible, largely suppressed low-temperature heat release as it is dominated by unsaturated components. Moreover, canola biodiesel oxidation illustrates similar characteristics to the oxidation of unsaturated methyl esters with a centered carbon double bond. Therefore, methyl esters, such as methyl-3-nonenate and methyl-5-decenoate can be more suitable surrogates for the modeling purposes of the oxidation of commercial biodiesel.

Chapter 5: Ignition and Combustion Characteristics of Decanoic Acid derived Alkyl Esters in a Fuel Ignition Tester

Published in Fuel.

"Ignition and combustion characteristics of decanoic acid derived alkyl esters in a fuel ignition tester," Fuel 276 (2020) 117982.

5.1   Abstract

This work investigated the combustion characteristics of decanoic acid-derived alkyl esters in an ASME standard Fuel Ignition Tester (FIT), with special emphasis on the influence of carbon number variation for the alkyl moiety within the alkoxy group on the autoignition delay times. The compounds of interest include methyl, ethyl, propyl, and butyl decanoate. It was found that higher carbon numbers lead to an increase in reactivity in terms of the decreased ignition delay times for methyl through propyl decanoate. However, there was a small reduction in relative reactivity for butyl decanoate. With increasing air temperature, while the ignition delay times showed a monotonic reduction for all the four fuels, the maximum rate of pressure rise exhibited a non-linear variation. Specifically, the maximum rate of pressure rise was found to increase in the temperature range of 700–758 K and then decrease within 758–825 K. The post-combustion peak pressures also exhibited a similar trend. It is hypothesized that this reduction in reactivity with increasing temperature correlates to the negative temperature coefficient behavior. In addition, all the test fuels show a two-stage ignition response at the lowest oxidizer temperatures investigated. Therefore, the current experiments demonstrate the suitability of the FIT as a research tool that can be used to extract information on fuel reactivity other than the widely studied metric of the derived cetane number.

5.2   Introduction

Renewable fuel technologies can help alleviate problems associated with fossil fuel combustion. Biofuels, in particular, can be used to transition from petroleum-derived fuels to cleaner-burning fuels with minimal modifications to existing infrastructure [138]. Biodiesel is the product of a triglyceride-alcohol transesterification reaction in the presence of a catalyst. Consequently, the composition and characteristics of the resulting ester fuel depend on the starting triglyceride and alcohol reactants. Vegetable oils, animal fats, and algal lipids are

among the feedstocks used to extract triglycerides. The fatty acid composition profile of the biodiesel thus obtained can vary both in terms of the carbon chain length as well as the degree of unsaturation. Vegetable oil derived biodiesel primarily consists of alkyl esters of palmitic ($C_{16:0}$), stearic ($C_{18:0}$), oleic ($C_{18:1}$), and linoleic ($C_{18:2}$) acids [129]. Detailed documentation of the variations in the fatty acid compositional profiles for various feedstocks can be found in the review by Hoekman et al. [136]. The fatty acid profile has a pronounced influence on the autoignition tendency of the resulting biodiesel. Fatty Acid Methyl Esters (FAME) are known to exhibit greater reactivity with increasing carbon chain length, thereby leading to a higher cetane rating. On the other hand, the increase in the degree of unsaturation leads to reduced reactivity and, consequently, a lower cetane rating [136].

Biodiesel synthesized from practical feedstocks typically consists of a mixture of alkyl esters of a few different fatty acids which impart its characteristic physical and chemical properties. The description of the detailed oxidation chemistry for large alkyl esters is still under development, as the kinetic models are complex and involve a large number of species and elementary reactions [28, 31]. The complexity and size of the reaction mechanisms currently preclude the possibility of computationally studying realistic biodiesel, which consists of a mixture of several large alkyl esters. Therefore, research attention has been directed toward studying simpler alkyl esters that act as surrogate components for real biodiesel. This approach of studying the oxidation kinetics of individual compounds with a specific functional group follows a hierarchical approach in terms of carbon number. It also builds on existing knowledge for validated kinetic sub-models with the inclusion of new fuel-specific chemical reactions. Previous research efforts on alkyl ester oxidation kinetics have focused on fatty acid methyl esters with short carbon chain length [27, 30, 31, 83, 97, 124, 135, 139-141]. Methyl decanoate, a relatively large carbon number straight-chain methyl ester, has been a compound of particular interest for kinetic modelers and is widely used as a surrogate for biodiesel in the combustion literature [28, 31, 91, 97, 99, 100, 118, 121, 122, 142]. It is also noted that methyl esters are the most common compounds found in biodiesel, because methanol is one of the reactants in the transesterification process. The usage of methanol is due to its inherent cost advantages. Alcohol with a longer carbon chain leads to other alkyl esters. This study aims to examine the ignition and combustion characteristics of four different decanoic acid derived alkyl esters, namely methyl, ethyl, propyl, and butyl decanoate (MD,

ED, PD, and BD, respectively). Figure 5.1 shows the molecular structures for the four test fuels used in this study.
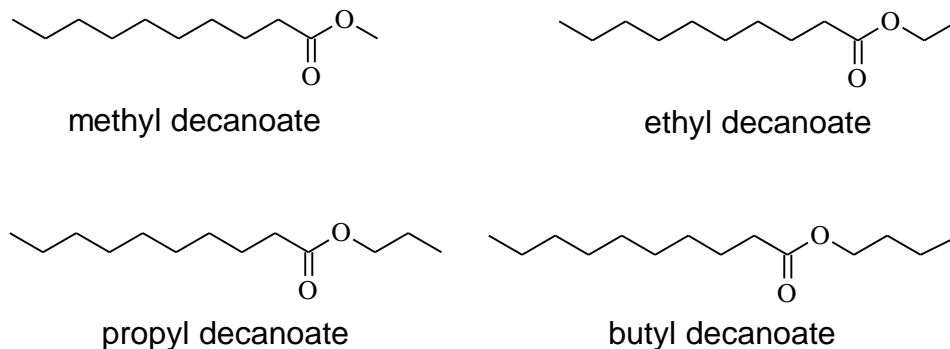
Figure 5.1: Molecular structures of decanoic acid esters investigated in this study.

There are few studies on the ignition characteristics of straight-chain alkyl esters other than those on methyl esters. Prior work on the ignition characteristics of ester compounds has focused mainly on methyl decanoate. The ignition characteristics of methyl decanoate have been studied using various laboratory apparatuses such as shock tube [91, 143], constant volume combustion chamber [94], and flow reactor [122]. Additionally, there also exists chemical kinetic models for the oxidation of methyl decanoate [28, 144]. However, the influence of carbon number variation for the alkyl moiety within the alkoxy group on ignition delay times is not well understood [136]. Thus, this work seeks to fill in this fundamental gap. Accurate quantification of the effect of the carbon number variation on ignition delay times requires a well-controlled and repeatable experiment facility with minimal fluid dynamic and other extraneous influences. A constant volume combustion chamber with a fuel injector and a quiescent pre-heated oxidizer provides an ideal platform for such experiments.

5.3 Experimental Apparatus and Methods

The experimental apparatus used in this study is a constant volume combustion chamber with provisions for fuel injection. It operates under elevated pressure and temperature conditions and is the standard apparatus for obtaining the Derived Cetane Number (DCN) of fuels following the ASTM D7170 standard, known as a Fuel Ignition Tester (FIT). Fuel is injected into preheated and compressed air within a cylindrical combustion chamber of 0.60±0.03 liters. The initial pressure of the system is 24 bar. The temperature of the oxidizer is adjusted to obtain a specified ignition delay time for a calibration fuel. A single test consists of 2 preliminary injections to stabilize the operating conditions, followed by 25 recorded

injection events. The chamber is evacuated after each injection event and filled with fresh oxidizer. During each injection, the combustion pressure rise is recorded using a pressure sensor and used to infer the ignition delay time. The ignition delay time is defined as the time from the start of the fuel injection to a point where the chamber pressure is 0.2 bar above the initial static charge pressure. An empirical equation, DCN=171/ID, is used to convert the mean ignition delay time (ID) in millisecond to a DCN value. n-Heptane (OmniSolv 99%) was the calibration fuel. The accepted reference ignition delay time value of 3.15±0.04 ms was met three times for the calibration fuel before conducting the FIT experiments on the fuels under test. Figure 5.2 shows the pressure traces of the 25 injections of n-heptane during a calibration test, as well as plots an averaged pressure trace for the 25 individual injections alongside the rate of pressure rise for the averaged trace.
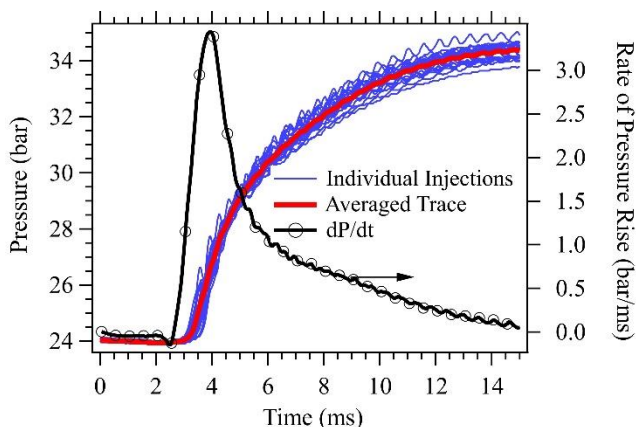
Figure 5.2. Pressure traces from a calibration run of the FIT using n-heptane as a fuel.

In addition to the DCN determination for each of the four alkyl esters, a different set of experiments was carried out to obtain the temperature dependence of ignition delay time, the rate of pressure rise, and the peak post-combustion pressure. The test fuels had a minimum purity of 98%, obtained from Tokyo Chemical Industries (TCI), Acros, and Alfa Aesar (cf. Table 5.1. Experimental conditions used to study the influence of temperature variation). In addition, the initial pressure for these tests was 24 bar, and the oxidizer temperature varied in the range of 691–825 K. A total of 10 separate fuel injections were carried out for each test temperature. An analysis of the exhaust gas composition provided an estimate of the global equivalence ratios for the tests, as done in [145]. In particular, non-dispersive infrared analyzers were used to measure the CO, CO2, and unburned hydrocarbons in the burnt gases. Table 5.1. Experimental conditions used to study the influence of temperature variation lists

the experimental conditions used in the second set of experiments for examining the influence of temperature on the ignition and combustion characteristics.

Table 5.1. Experimental conditions used to study the influence of temperature variation	
Initial pressure	24.0±0.2 bar
Air temperature	691–825 K
Fuel temperature	308.0±2.0 K
Injector coolant temperature	303.0±0.5 K
Average injection period	5.00±0.04 ms
Global equivalence ratio	MD(0.115),ED(0.114),PD(0.115),BD(0.113)
Methyl Decanoate	Source: TCI;　　　Purity: 98% (All tests)
Ethyl Decanoate	Source: TCI;　　　Purity: 98% (DCN tests)
Ethyl Decanoate	Source: Acros; Purity: 99% (T variation test)
Propyl Decanoate	Source: Alfa Aesar;　Purity: 98% (All tests)
Butyl Decanoate	Source: TCI;　　　Purity: 98% (All tests)

5.4 Results and Discussion

5.4.1 Influence of the Alcohol Moiety on Cetane Rating

Figure 3 summarizes the DCN results for the twenty-five sets of injections for each of the test fuels. Again, the DCN estimate is obtained using the median value for the twenty-five runs. The results show that DCN increases with increasing carbon number for the alkyl moiety in the alkoxy group for the first three decanoic acid-derived esters, i.e. MD, ED, and PD. However, the derived cetane number for butyl decanoate was found to be 6.7 units lower compared to propyl decanoate. The relative reactivity in the order of increasing DCN for the four test fuels is as PD ($C_{13}H_{26}O_2$) > ED ($C_{12}H_{24}O_2$) > BD ($C_{14}H_{28}O_2$) > MD ($C_{11}H_{22}O_2$). In Figure 5.3, the box plot shows that the DCN values for methyl decanoate lie between the range of 46.3–52.1 units. The next higher alkyl ester, ethyl decanoate, has a spread of DCN values between 53.8 and 61.7. A comparison of the DCN results for ED and PD shows a significant overlap in the DCN values over the twenty-five experimental runs. The DCN values for propyl decanoate are in the range of 54.6–62.4 and exhibit a slightly higher scatter compared to all the other datasets. Butyl decanoate shows a small reduction in the DCN value even despite an increase in carbon number. Furthermore, the DCN value for butyl decanoate is lower than those of both propyl decanoate and ethyl decanoate, but still higher compared to methyl decanoate.
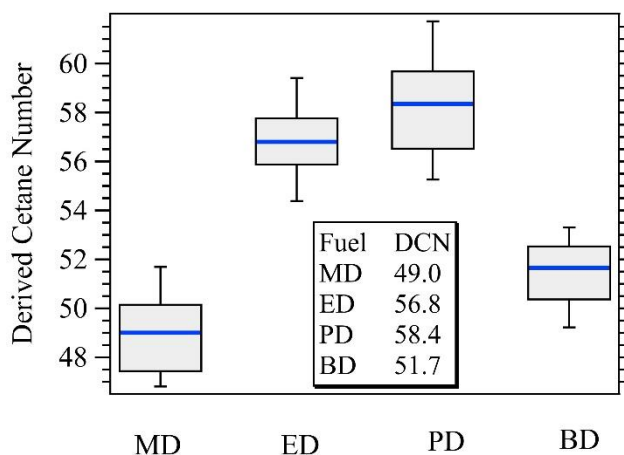
Figure 5.3. Derived cetane numbers determined in the FIT for the four test fuels. Plots also show the variability for the 25 repeated runs used to obtain each DCN value.

A comparison of the DCN values obtained using the current FIT and the cetane number (CN) values obtained using a single-cylinder, variable compression ratio, direct-injected engine by Klopfenstein [146] is shown in Figure 5.4(a). The plot in Figure 5.4(a) shows that the current DCN results are higher compared to the CN results obtained using a single-cylinder engine for methyl through propyl decanoate but lower for butyl decanoate. Although the current DCN result for butyl decanoate does not follow the increasing CN trend with increasing carbon number. The literature data [146-148] suggest that for a given straight-chain saturated fatty acid, the esters resulting from alcohols of varying chain lengths tend to show an increase in the cetane number with increasing carbon number. This trend is illustrated for various esters derived from four different fatty acids in Figure 5.4(b). Based on Figure 5.4(b), it can be inferred that the hexanoic acid esters show a much more significant variation in cetane number as the alkyl chain length within the alkoxy group increases when compared to the tetradecanoic acid esters. However, none of the acids derived esters show a decrease with increasing alkyl chain length expect for butyl decanoate in the present work. This trend of anomalous reactivity with increasing carbon number has been previously reported for methyl esters. A comparative study of the autoignition delay times of methyl ethanoate through butanoate found that methyl ethanoate was more reactive than methyl propanoate in the low-to-intermediate temperature regime [84]. This trend was also confirmed using simulations with detailed kinetic models for these compounds. Computed results in [84] showed that methyl ethanoate had shorter ignition delay times (more reactive) than methyl propanoate despite having a smaller carbon number. There is a need for further experimental and numerical work to confirm and explain the origins

of this decreased reactivity observed with increasing carbon number for both the fatty acid as well as the alkyl moiety within the alkoxy group.
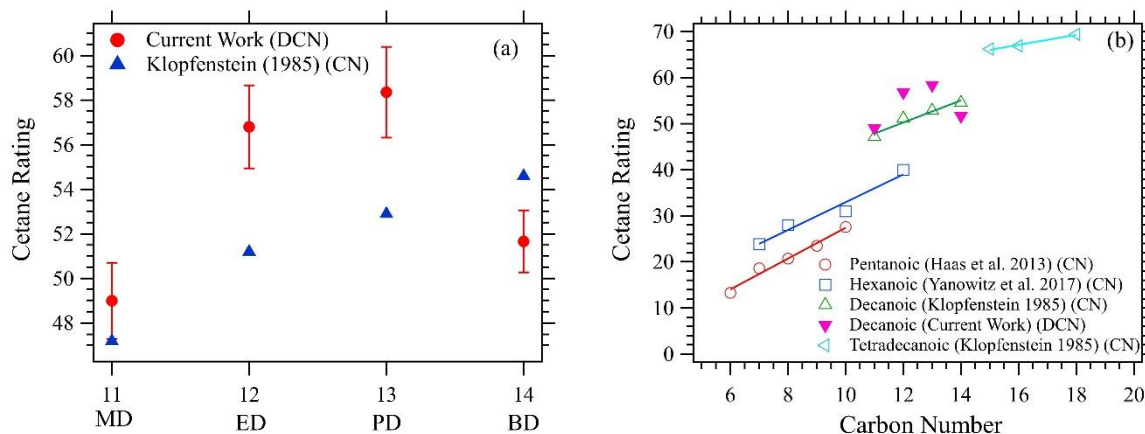
Figure 5.4. (a) Comparison of current DCN data with literature CN data. (b) Trends for cetane number with increasing carbon number for various saturated straight-chain fatty acid esters.

5.4.2   Influence of Alkyl Moiety on Combustion Quality

5.4.2.1   Absolute pressure rise

We next examine and compare the combustion characteristics of the four test fuels through analysis of the experimental pressure traces. Figure 5.5 shows the averaged pressure traces for twenty-five ignition events for each of the four fuels. The averaged pressure trace provides a useful and consistent metric for comparison across fuels and eliminates the effects of variations observed within multiple runs for the same fuel. The ignition delay time, as inferred from the pressure trace, shows the same trend as the DCN. Propyl decanoate is the most reactive, followed by ethyl, butyl, and methyl decanoate. The pressure traces in Figure 5.5 also demonstrate that methyl decanoate achieves a slightly higher post-combustion peak pressure (33.7 bar) compared to the other three fuels, exhibiting very similar peak pressure values (33.1–33.2 bar). After all the fuels have ignited, the pressure traces exhibit a cross-over at around 4.9 ms due to the different relative rates of pressure rise. Methyl decanoate, which has the longest ignition delay time, shows the most significant rate of pressure rise and exceeds the pressure rise of all other three fuels after 4.9 ms. Interestingly, the relative ranking in ascending order of the pressure values after 4.9 ms is just the reverse of the DCN trends.
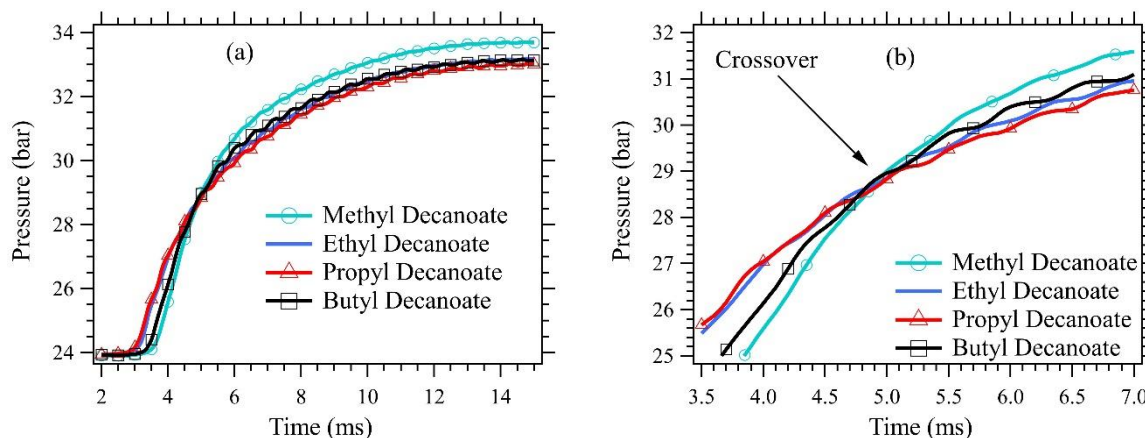
Figure 5.5. Averaged pressure traces of twenty-five combustion events at the DCN conditions for the four decanoic acid esters

5.4.2.2 Rate of Pressure rise

The rate of pressure rise trends for the four fuels are similar except for the peak values and the locations of the peak. It is seen from Figure 5.6 that the location of the peak for the rate of pressure rise correlates well with increasing DCN values. The most reactive fuel with the highest DCN exhibits peak at a relatively earlier time. In addition, the maximum values for the rates of pressure rise for the four fuels show a significant difference. The maximum values for the rates of pressure rise obtained in this study at the DCN conditions can be ranked as MD (3.87 bar/ms) > BD (3.52 bar/ms) > ED (3.15 bar/ms) > PD (3.04 bar/ms). This ranking order demonstrates that the fuel with the lower DCN tends to show a higher peak value for the rate of pressure rise.

Figure 5.6 also shows that the combustion energy release is complete in approximately 15 ms after the start of ignition, and the pressure traces for the four fuels display a negligible rate of pressure rise after this time. As the area under the rate-of-pressure rise curve is a measure of the total heat released, this measure is found to be remarkably consistent for ethyl, propyl, and butyl decanoate (~9.3 units). Methyl decanoate shows a slightly higher energy release compared to the other three fuels. The shaded area shown in Figure 5.6 lies between the two zero-crossings of the dp/dt curve with the x-axis. Hence, the difference between methyl decanoate and the other three fuels could be on account of complete combustion for MD due to the relatively higher fuel bound oxygen content compared to the other three fuels.
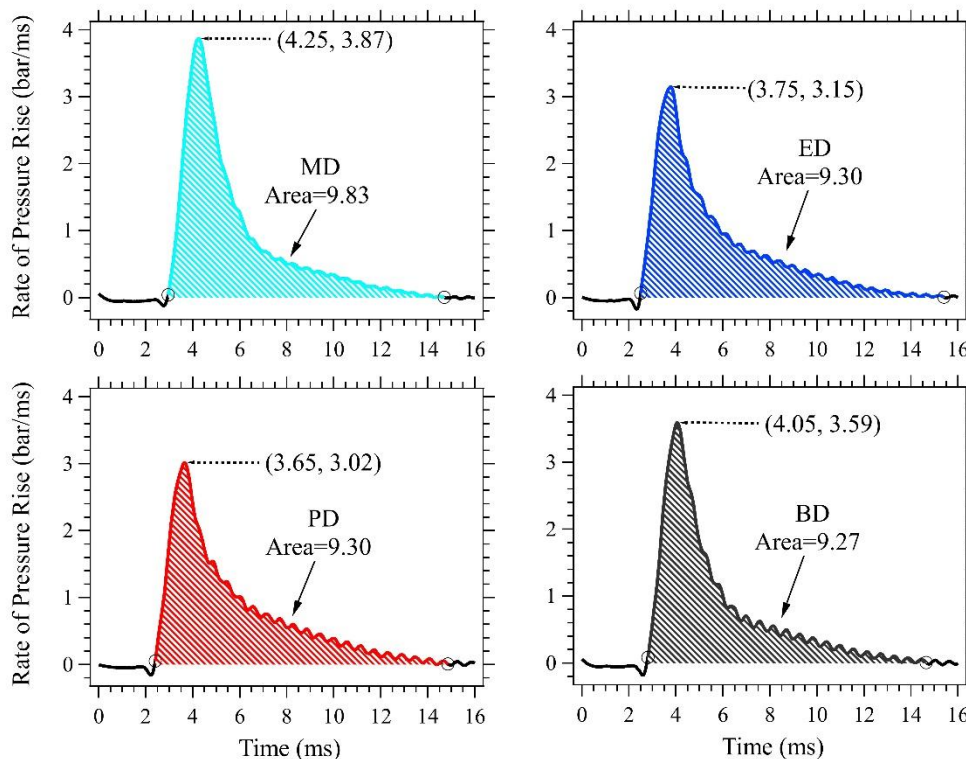
Figure 5.6. Rates of pressure rise based on the averaged pressure traces.

5.4.3   Temperature Dependence of Ignition Delay Time

Each of the four alkyl esters was also studied to understand the influence of the oxidizer temperature on their respective ignition delay times. The temperature variation was in the range of 691–825 K for a fixed initial pressure of 24 bar and an injection period of 5.0 ms. Note that fixing the injection time while changing the oxidizer temperature is likely to cause a change in the global equivalence ratio. However, previous studies have shown that this effect is not very pronounced and no more than ±0.02 in terms of the equivalence ratio variation [145]. Therefore, based on the emissions analysis, we can assign a global equivalence ratio of approximately $\varphi=0.12\pm0.02$ for these tests (cf. Table 1).

Figure 5.7 demonstrates the ability of the FIT to carry out tests with varying oxidizer temperatures, showing the pressure traces for the largest carbon number fuel (BD) close to the lower end and the mid-range of the temperatures investigated in this work. A comparison of the two plots in Figure 5.7 shows that while the scatter in pressure-time traces for the individual injections is relatively higher at the lower temperature (699 K), the ignition delay times are grouped tightly together with very little spread under both the temperature conditions. This

observation leads to a high degree of confidence in the ignition delay times reported for this set of tests. The plots in Figure 5.7 also include the averaged pressure trace, as shown by the solid red line. For each oxidizer temperature, a total of ten experimental pressure traces, shown as dashed lines, are used in the averaging. It should be noted that the onset of ignition and the 0.2 bar pressure rise criterion used to estimate the DCN is highly reproducible under both the low- and high-temperature conditions shown in Fig. 7. Furthermore, the set of low-temperature tests shown in Fig. 7 indicates a two-stage ignition characteristic as seen from the pressure traces. As noted previously, the onset of the first-stage ignition is highly repeatable but there is a variation in the post-combustion peak pressure of approximately 10% of the initial oxidizer pressure. Moreover, the first-stage pressure rise is observed between 16–24 milliseconds and represents the low-temperature heat release (LTHR) for the fuel. The second-stage ignition follows this and is slightly weaker in terms of the rate of pressure rise. Additionally, the individual traces are seen to have significant scatter in the second-stage ignition region. It is, therefore, much more straightforward and accurate to discuss the autoignition trends in terms of various operating parameters and fuels in terms of an averaged pressure trace constructed out of multiple repeated tests under identical conditions.
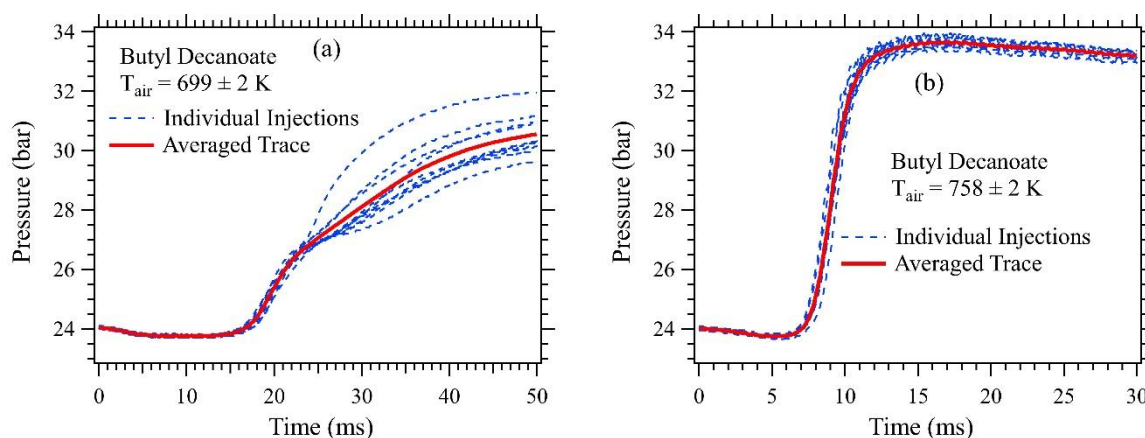
Figure 5.7. Pressure traces at (a) low (699 K) and (b) mid-range (758 K) oxidizer temperatures for butyl decanoate.

Figure 5.8(a)-(d) show these averaged pressure traces for each of the four fuels under conditions of varying oxidizer temperatures. The experiments were conducted at five different initial oxidizer temperatures, approximately 30 K apart, to understand the influence of initial oxidizer temperature on the ignition delay time and combustion characteristics. Each pressure trace in Figure 5.8 is an average of ten individual combustion events. The averaged pressure traces show that the ignition delay times decrease with increasing oxidizer temperature. The

reduction in ignition delay time is much greater at the lower temperature conditions when progressing through the temperature increments and a relatively small decrease is observed as one progresses toward the high-temperature conditions. This feature is common for all the four fuels though the absolute magnitudes and the gap in ignition delay times are different for each fuel. An interesting feature observed from the experimental traces is that the peak pressure tends to get reduced as the oxidizer temperature is increased above 758 K. This temperature corresponds closely to the onset of the negative temperature coefficient (NTC) window of the reaction rate for long-chain n-alkanes. The reduction in peak pressures above 758 K for all the four decanoic esters points to the possible existence of an NTC trend for this class of fuels in the studied carbon number range.
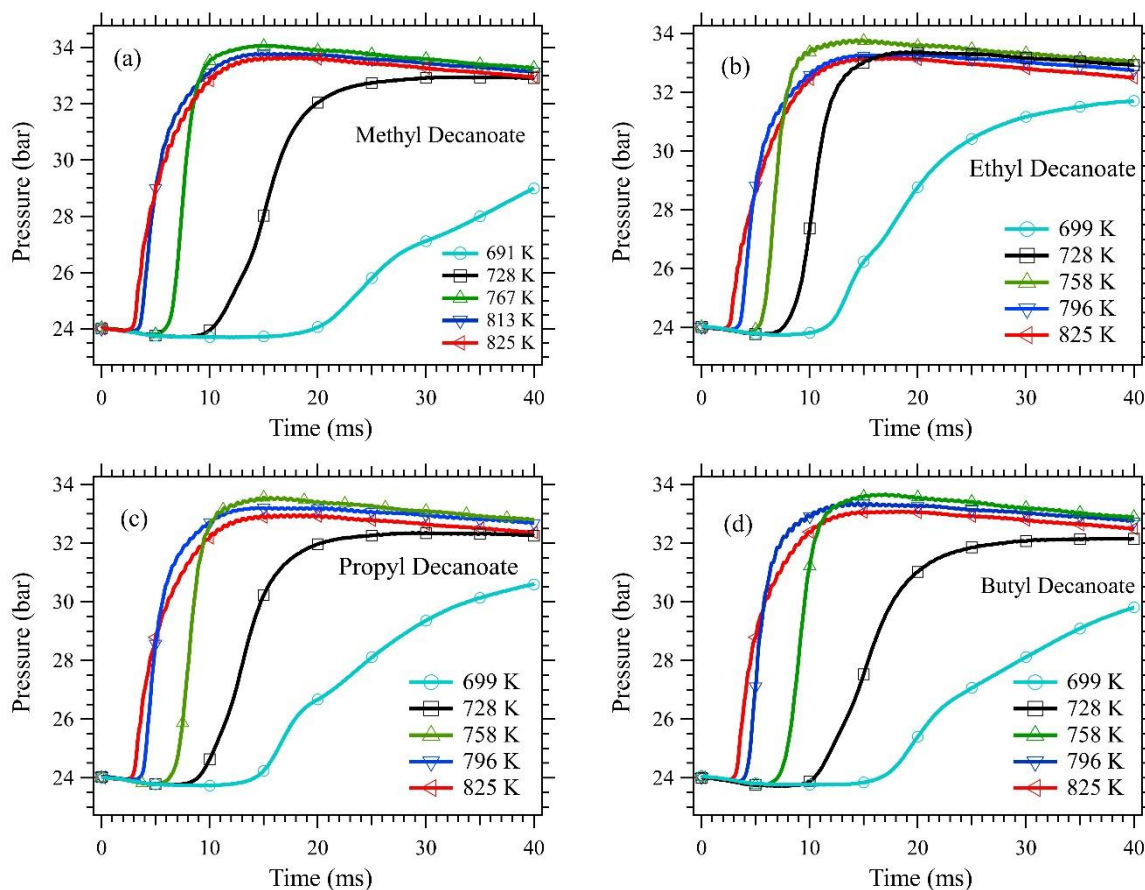
Figure 5.8. Pressure traces (average of 10 injections) showing the evolution of autoignition for various oxidizer temperatures at a fixed injection duration of 5.0 ms and an initial pressure of 24 bar.

This reduction in peak pressure at temperatures above 758 K was observed over multiple injections and is not merely a manifestation of experimental scatter. The conclusion about the existence of NTC behavior in decanoic acid esters is further supported by the

presence of a two-stage ignition trend at 699 K which slowly transitions to a single-stage ignition event at higher temperatures as shown in Fig. 8. It is further noted that the current experiments have just approached the onset of NTC but not traversed through it over its entire temperature range.

Figure 5.9(a) illustrates that the experimental ignition delay times for the four fuels show the typical Arrhenius trend with respect to the temperature. The trend is monotonic with temperature and does not show the apparent increase in ignition delay time at temperatures above 758 K. Since the ignition delay times for the current FIT experiments were based on the 0.2 bar pressure rise criterion, the expected NTC-like trend could not be readily captured, and hence other markers need to be used to confirm its existence. Verification of the existence of NTC was carried out for methyl decanoate through computations using the detailed kinetic model of Herbinet et al. [100]; the results of which are shown in Figure 5.9(b). The computations assume constant volume and adiabatic conditions and use a temperature rise of 15 K to define the onset of ignition. Note that this homogenous constant volume simulation under identical initial pressure and for a similar global equivalence ratio shows a very distinct NTC in the temperature range of 870–940 K. The experimental data points shown in Figure 5.9(b) do not include temperatures higher than 825 K due to the limitations of the FIT apparatus.
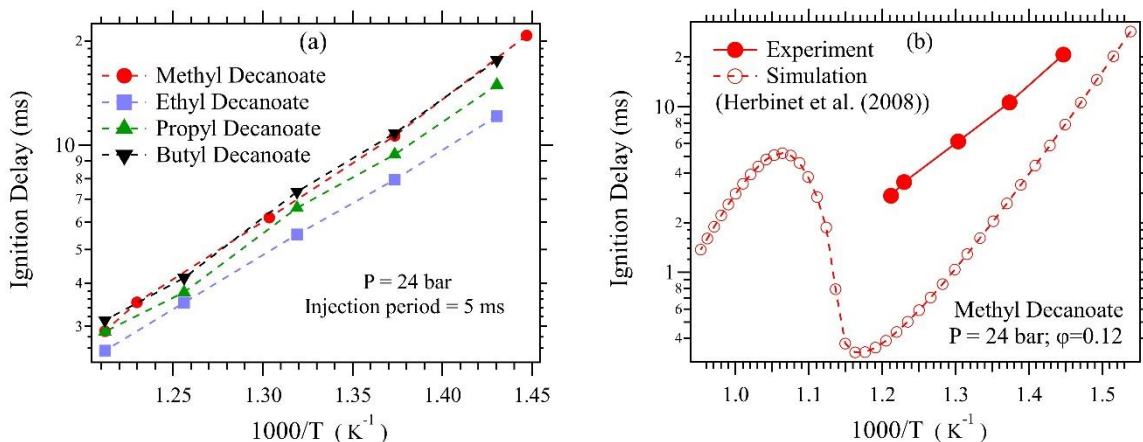
Figure 5.9. Temperature dependence of ignition delay times for (a) the four decanoic acid esters in the current experiments and (b) the simulation of methyl decanoate autoignition in air using the chemical kinetic model of [100].

A lack of apparent NTC in the ignition delay times was observed for n-heptane in a study using an Ignition Quality Tester (IQT) by Bogin et al. [149], in which the authors attributed this to spray physics effects during ignition times less than 20 ms. Note that the

ignition delay times in the current temperature dependence study is less than 20.73 ms. Hence, spray and vaporization characteristics are likely to influence the ignition delay times. This should lead to longer ignition delay times than the corresponding homogeneous cases. The difference between the FIT spray ignition delay times and the simulated homogeneous autoignition under similar conditions is shown in Fig. 9(b) where the current experiments indeed exhibit longer ignition delay times compared to the model of Herbinet et al. [100]. The kinetic model of Herbinet et al. [100] was shown to have good agreement with n-decane shock-tube ignition delay time data over the low-to-intermediate temperature conditions and for pressures of 12 and 50 atmospheres.

5.4.4   Effect of Temperature on the Rate of Pressure Rise

An alternative approach to probe the possible existence of NTC from the FIT results is to examine the rate of pressure rise as a function of oxidizer temperature. This average rate of pressure rise for various oxidizer temperatures is shown in Figure 5.10, demonstrating a twin-peak response in the rate of pressure rise with time for all the four fuels. It can also be seen that the maximum rate of pressure rise for methyl and ethyl decanoate is obtained at 767 K while that for propyl and butyl decanoate the same occurs at approximately 796 K. Above these temperatures, there is a clear reduction in the rate of pressure rise for each of the fuels. This reduction may be an indicator of the occurrence of NTC for the respective fuels above those temperatures. As mentioned previously, the reduced reactivity, as seen through the rate of pressure rise, does not necessarily reflect as a longer ignition delay time due to the complex nature of physicochemical interactions inherent in the FIT apparatus.

The reduction in the peak rates of pressure rise was further confirmed in the simulations using a detailed chemical kinetic model for methyl decanoate taken from [16]. The simulations are based on the assumption of homogeneous gas-phase chemistry under constant volume condition with no heat loss. We recognize that such simulations cannot capture the complex multi-phase/heterogeneous ignition/combustion phenomena present in the FIT experiment. However, they still provide useful insights in terms of the relative trend as observed with the experiments and among the simulated cases.

Results for experimental and simulated results shown in Figure 5.11 illustrate that while the peak rate of pressure rise first increases up to a specific temperature and then begins to show a reduction for both the experiments as well as the computations. The decrease in the

peak value starts at 813 K in the simulation while the same occurs at 767 K for the FIT data. The absolute values of the rates of pressure rise are also comparable between the two, with the homogeneous adiabatic simulation predicting higher values as expected. Note that this comparison between experiments and simulation was limited to methyl decanoate because it is the only ester, among the esters of interest, that has an existing detailed kinetic model reported in the literature. Simulations using similar conditions but with a fuel that does not show an NTC behavior (e.g., methane [150]) showed a monotonic increase in the peak values of the rate of pressure rise for temperatures of 758−825 K.
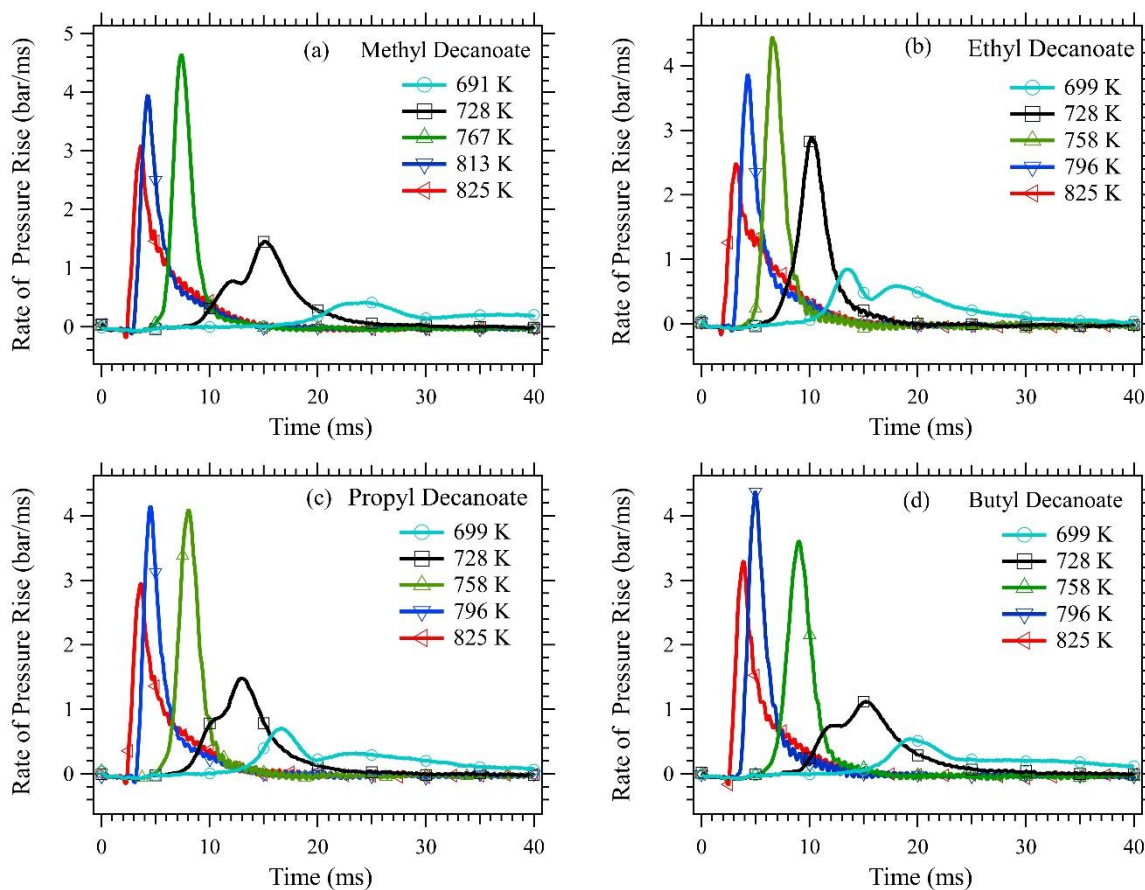
Figure 5.10. Representative rate of pressure rise at five different oxidizer temperatures for the four decanoic acid esters.
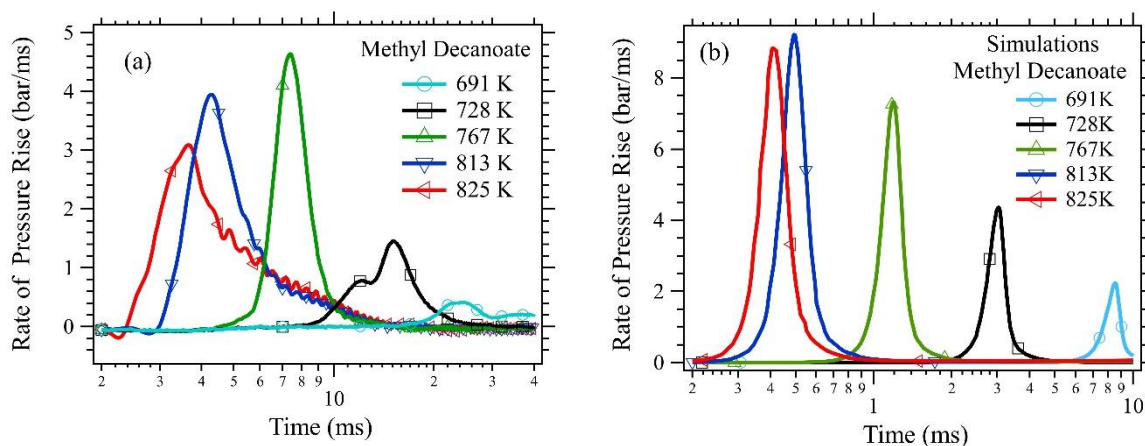
Figure 5.11. Experimental and simulated rates of pressure rise for methyl decanoate. Simulations use the chemical kinetic model of Herbinet et al. [100].

Figure 12(a) plots the variation in the maximum rate of pressure rise as a function of temperature. The most important feature of this plot is that all four decanoic acid esters show a non-monotonic trend for the variation in their respective maximum rates of pressure rise. It first increases with increasing temperature, followed by a decrease as the temperature is further increased. However, the onset of this reduction occurs at slightly different temperatures for each. The more reactive fuels, propyl and ethyl decanoate, show an earlier NTC behavior compared to the less reactive fuels, butyl and methyl decanoate.
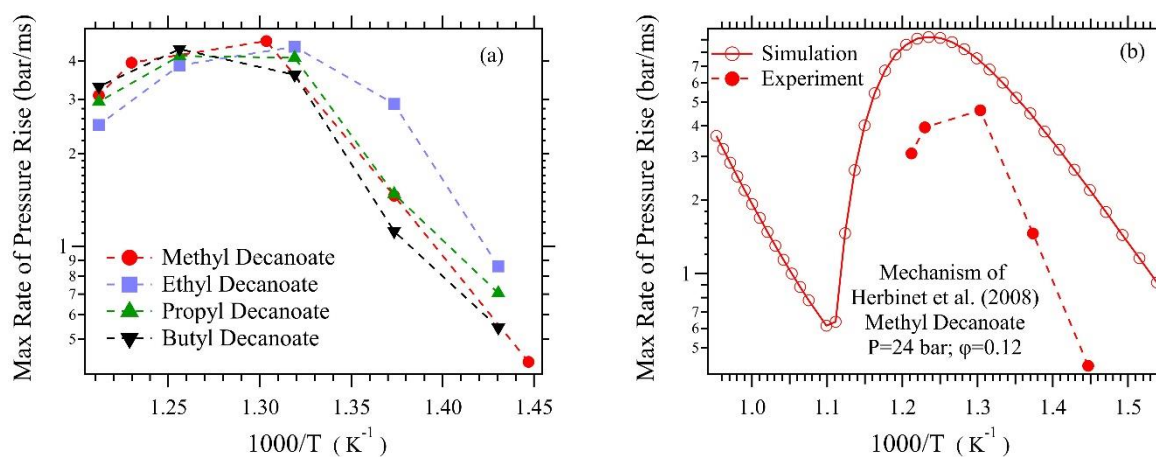
Figure 5.12: Maximum rates of pressure rise with varying oxidizer temperatures for (a) four decanoic acid esters in FIT experiments and (b) comparing experimental and simulated results of methyl decanoate.

Figure 5.12(b) displays the experimental and simulated maximum rates of pressure rise for methyl decanoate. The computed values, based on the chemical kinetic model of Herbinet et al. [100], show agreement with the experimental data in the studied temperature range. Furthermore, the trends for both show an increase in the combustion rate (maximum rate of

pressure rise) as the temperature increases, followed by a reduction as the temperature approaches the NTC regime.

5.5 Conclusions

The ignition and combustion characteristics of four decanoic acid-based esters, namely methyl, ethyl, propyl, and butyl decanoate, were investigated using an ASME standard fuel ignition tester to understand the effect of alcohol moiety on the derived ester autoignition. It was observed that increasing alcohol chain length increased the fuel reactivity. However, this enhancement diminishes as the carbon number exceeds a certain value, eventually leading to a negative impact on the ester reactivity. The derived cetane numbers of the four fuels can be ranked as methyl decanoate (49.0) < butyl decanoate (51.4) < ethyl decanoate (56.9) < propyl decanoate (58.3). Furthermore, the peak post-combustion pressure, as well as the maximum combustion rate, exhibited an opposite trend to that observed for the cetane rating, where the least reactive fuel, methyl decanoate, demonstrated the highest pressure rise rate, followed by butyl, ethyl, and propyl decanoate. In addition, the four test fuels had a similar accumulated rate of heat release with a slight excess for methyl decanoate.

Further, the rates of pressure rise of the four fuels exhibited a two-stage ignition behavior, which transited to a single-stage ignition phenomenon as the temperature increases. The ignition delay times exhibited a high degree of repeatability at both low and high temperatures and showed an Arrhenius behavior in the studied temperature range. This lack of NTC behavior in the experimental ignition delay times is likely attributable to the spray physics effects. However, the maximum combustion rates at the test conditions suggest that the four fuels enter the NTC regime in the temperature range of 758–796 K. Numerical simulations with detailed chemistry conducted for methyl decanoate supported the experimental observation of the onset of the NTC regime in this temperature range via both maximum rate of pressure rise as well as ignition delay time. Therefore, using the pressure rise rate in conjunction with the overall ignition delay times can provide additional insight into fuel combustion chemistry in the low-to-intermediate temperature regime.

Chapter 6: Conclusions and Future Work

In this work, the oxidation of n-heptane, methyl decanoate, coconut oil methyl ester, and canola oil methyl ester was studied in the low-to-intermediate temperature regime via motored engine experiments. Speciation analysis of the oxidation products was conducted using a GC-MS and an FTIR. Additionally, the autoignition of four decanoic acid derived alkyl esters, namely, methyl, ethyl, propyl, and butyl decanoate were studied in a fuel ignition tester.

Fifty-six stable intermediate species across a wide range of chemical classes such as alkenes, aldehydes, ketones, ethers, alcohols, and acids were identified in the oxidation products of n-heptane. Heat release analysis illustrated a transition from a first-stage ignition to second-stage ignition at higher temperatures. A comparison between the experimental and computed results showed an excellent agreement for the accumulated heat release, although the profiles for the heat release themselves were not in agreement. The results for the temperature sensitivity of the system indicate that parent-fuel specific reactions are important for the first-stage heat release.

The analysis of methyl decanoate oxidation products revealed a total of sixty-six intermediate species. Unsaturated methyl esters were an additional class of compounds detected in considerable amounts when compared to the products of n-heptane oxidation. The low-temperature oxidation chemistry of saturated methyl esters is similar to that of paraffins as deduced from the common products of combustion across both types of fuels. However, the heat release analysis and intermediate species quantitation showed that methyl decanoate underwent a relatively suppressed low-temperature oxidation compared to n-heptane.

The biodiesel fuel oxidation products are qualitatively similar to those that evolve during the oxidation of the biodiesel surrogate methyl decanoate. However, the biodiesel had a diminished low-temperature heat release compared to the surrogate, accordingly, generating lower concentrations of similar stable intermediate species. The low-temperature heat release in coconut and canola oil biodiesel correlates well with the amount of the saturated methyl esters in their respective compositions. Coconut biodiesel oxidation showed a considerable low-temperature heat release when compared to canola as it is dominated by saturated methyl esters. On the other hand, canola biodiesel oxidation exhibited negligible, largely suppressed

low-temperature heat release as unsaturated components dominate its makeup. Moreover, canola biodiesel oxidation had characteristics similar to the oxidation of unsaturated methyl esters with a centered carbon double bond. Therefore, methyl esters, such as methyl-3-nonenate and methyl-5-decenoate may be more suitable surrogates for modeling biodiesel combustion.

Autoignition experiments showed that increasing alcohol chain length in alkyl esters enhances fuel reactivity. However, this enhancement diminishes as the carbon number exceeds a certain value, eventually leading to a negative impact on the ester reactivity.

6.1 Future Work

Autoignition studies on biodiesel fuels, coconut oil methyl ester and canola oil methyl ester, using the fuel ignition tester apparatus, can help develop a better understanding of their combustion characteristics.

Engine experiments on blends of the studied fuels, especially within the various saturated and unsaturated esters, will help quantify the role of saturated methyl esters components in observed combustion trends for real biodiesels.

References

[1] Annual Energy Outlook 2020 with projections to 2050, U.S. Energy Information Administration, Washington, DC, 2020.

[2] P. F. Nelson, Effects of vehicle type and fuel quality on the exposure risk of toxic emissions from diesel vehicles, Environmental Chemistry 6 (3) (2009) 260-267.

[3] E. Zervas, X. Montagne, J. Lahaye, C1−C5 Organic Acid Emissions from an SI Engine: Influence of Fuel and Air/Fuel Equivalence Ratio, Environmental Science & Technology 35 (13) (2001) 2746-2751.

[4] E. Zervas, X. Montagne, J. Lahaye, Emission of Alcohols and Carbonyl Compounds from a Spark Ignition Engine. Influence of Fuel and Air/Fuel Equivalence Ratio, Environmental Science & Technology 36 (11) (2002) 2414-2421.

[5] A. K. Agarwal, Biofuels (alcohols and biodiesel) applications as fuels for internal combustion engines, Progress in Energy and Combustion Science 33 (3) (2007) 233-271.

[6] S. Gan, H. K. Ng, K. M. Pang, Homogeneous Charge Compression Ignition (HCCI) combustion: Implementation and effects on pollutants in direct injection diesel engines, Applied Energy 88 (3) (2011) 559-567.

[7] R. H. Stanglmaier, C. E. Roberts, Homogeneous Charge Compression Ignition (HCCI): Benefits, Compromises, and Future Engine Applications, SAE Transactions 108 (1999) 2138-2145.

[8] H. Bendu, S. Murugan, Homogeneous charge compression ignition (HCCI) combustion: Mixture preparation and control strategies in diesel engines, Renewable and Sustainable Energy Reviews 38 (2014) 732-746.

[9] F. Battin-Leclerc, E. Blurock, R. Bounaceur, R. Fournet, P.-A. Glaude, O. Herbinet, B. Sirjean, V. Warth, Towards cleaner combustion engines through groundbreaking detailed chemical kinetic models, Chemical Society Reviews 40 (9) (2011) 4762-4782.

[10] J. Bugler, K. P. Somers, E. J. Silke, H. J. Curran, Revisiting the Kinetics and Thermodynamics of the Low-Temperature Oxidation Pathways of Alkanes: A Case Study of the Three Pentane Isomers, The Journal of Physical Chemistry A 119 (28) (2015) 7510-7527.

[11] H. J. Curran, P. Gaffuri, W. J. Pitz, C. K. Westbrook, A Comprehensive Modeling Study of n-Heptane Oxidation, Combustion and Flame 114 (1) (1998) 149-177.

[12] H. J. Curran, P. Gaffuri, W. J. Pitz, C. K. Westbrook, A comprehensive modeling study of iso-octane oxidation, Combustion and Flame 129 (3) (2002) 253-280.

[13] I. M. R. Fattah, C. Ming, Q. N. Chan, A. Wehrfritz, P. X. Pham, W. Yang, S. Kook, P. R. Medwell, G. H. Yeoh, E. R. Hawkes, A. R. Masri, Spray and Combustion Investigation of Post Injections under Low-Temperature Combustion Conditions with Biodiesel, Energy & Fuels 32 (8) (2018) 8727-8742.

[14] X. Fu, S. K. Aggarwal, Two-stage ignition and NTC phenomenon in diesel engines, Fuel 144 (2015) 188-196.

[15] S. S. Goldsborough, S. Hochgreb, G. Vanhove, M. S. Wooldridge, H. J. Curran, C.-J. Sung, Advances in rapid compression machine studies of low- and intermediate-temperature autoignition phenomena, Progress in Energy and Combustion Science 63 (2017) 1-78.

[16] H. Tao, K. C. Lin, Pathways, kinetics and thermochemistry of methyl-ester peroxy radical decomposition in the low-temperature oxidation of methyl butanoate: A computational study of a biodiesel fuel surrogate, Combustion and Flame 161 (9) (2014) 2270-2287.

[17] S. M. Villano, H.-H. Carstensen, A. M. Dean, Rate Rules, Branching Ratios, and Pressure Dependence of the HO2 + Olefin Addition Channels, The Journal of Physical Chemistry A 117 (30) (2013) 6458-6473.

[18] S. M. Villano, L. K. Huynh, H.-H. Carstensen, A. M. Dean, High-Pressure Rate Rules for Alkyl + O2 Reactions. 1. The Dissociation, Concerted Elimination, and Isomerization Channels of the Alkyl Peroxy Radical, The Journal of Physical Chemistry A 115 (46) (2011) 13425-13442.

[19] S. M. Villano, L. K. Huynh, H.-H. Carstensen, A. M. Dean, High-Pressure Rate Rules for Alkyl + O2 Reactions. 2. The Isomerization, Cyclic Ether Formation, and β-Scission Reactions of Hydroperoxy Alkyl Radicals, The Journal of Physical Chemistry A 116 (21) (2012) 5068-5089.

[20] Z. Wang, O. Herbinet, N. Hansen, F. Battin-Leclerc, Exploring hydroperoxides in combustion: History, recent advances and perspectives, Progress in Energy and Combustion Science 73 (2019) 132-181.

[21] Z. Wang, L. Zhang, K. Moshammer, D. M. Popolan-Vaida, V. S. B. Shankar, A. Lucassen, C. Hemken, C. A. Taatjes, S. R. Leone, K. Kohse-Höinghaus, N. Hansen, P. Dagaut, S. M. Sarathy, Additional chain-branching pathways in the low-temperature oxidation of branched alkanes, Combustion and Flame 164 (2016) 386-396.

[22] J. Zou, X. Zhang, Y. Li, L. Ye, L. Xing, W. Li, C. Cao, Y. Zhai, F. Qi, J. Yang, Experimental and kinetic modeling investigation on ethylcyclohexane low-temperature oxidation in a jet-stirred reactor, Combustion and Flame 214 (2020) 211-223.

[23] C. Morley, M. J. Pilling, in: Low-Temperature Combustion and Autoignition, M. J. Pilling, (Ed.) Elsevier: 1997; Vol. 35, p XV.

[24] E. Blurock, F. Battin-Leclerc, in: Cleaner Combustion, F. Battin-Leclerc; J. M. Simmie; E. Blurock, (Eds.) Springer: London, 2013; p 27.

[25] L. Coniglio, H. Bennadji, P. A. Glaude, O. Herbinet, F. Billaud, Combustion chemical kinetics of biodiesel and related compounds (methyl and ethyl esters): Experiments and modeling – Advances and future refinements, Progress in Energy and Combustion Science 39 (4) (2013) 340-382.

[26] G. Dayma, S. Gaïl, P. Dagaut, Experimental and Kinetic Modeling Study of the Oxidation of Methyl Hexanoate, Energy & Fuels 22 (3) (2008) 1469-1479.

[27] G. Dayma, S. M. Sarathy, C. Togbé, C. Yeung, M. J. Thomson, P. Dagaut, Experimental and kinetic modeling of methyl octanoate oxidation in an opposed-flow diffusion flame and a jet-stirred reactor, Proceedings of the Combustion Institute 33 (1) (2011) 1037-1043.

[28] P. Diévart, S. H. Won, S. Dooley, F. L. Dryer, Y. Ju, A kinetic model for methyl decanoate combustion, Combustion and Flame 159 (5) (2012) 1793-1805.

[29] A. Farooq, D. F. Davidson, R. K. Hanson, L. K. Huynh, A. Violi, An experimental and computational study of methyl ester decomposition pathways using shock tubes, Proceedings of the Combustion Institute 32 (1) (2009) 247-253.

[30] S. Gaïl, M. J. Thomson, S. M. Sarathy, S. A. Syed, P. Dagaut, P. Diévart, A. J. Marchese, F. L. Dryer, A wide-ranging kinetic modeling study of methyl butanoate combustion, Proceedings of the Combustion Institute 31 (1) (2007) 305-311.

[31] P. A. Glaude, O. Herbinet, S. Bax, J. Biet, V. Warth, F. Battin-Leclerc, Modeling of the oxidation of methyl esters—Validation for methyl hexanoate, methyl heptanoate, and methyl decanoate in a jet-stirred reactor, Combustion and Flame 157 (11) (2010) 2035-2050.

[32] C. J. Hayes, D. R. Burgess, Exploring the oxidative decompositions of methyl esters: Methyl butanoate and methyl pentanoate as model compounds for biodiesel, Proceedings of the Combustion Institute 32 (1) (2009) 263-270.

[33] P. Dagaut, S. Gaı̈l, M. Sahasrabudhe, Rapeseed oil methyl ester oxidation over extended ranges of pressure, temperature, and equivalence ratio: Experimental and modeling kinetic study, Proceedings of the Combustion Institute 31 (2) (2007) 2955-2961.

[34] P. Dagaut, S. Gaïl, Chemical Kinetic Study of the Effect of a Biofuel Additive on Jet-A1 Combustion, The Journal of Physical Chemistry A 111 (19) (2007) 3992-4000.

[35] Y. Zhang, Y. Yang, A. L. Boehman, Premixed ignition behavior of C9 fatty acid esters: A motored engine study, Combustion and Flame 156 (6) (2009) 1202-1213.

[36] A. M. El-Nahas, M. V. Navarro, J. M. Simmie, J. W. Bozzelli, H. J. Curran, S. Dooley, W. Metcalfe, Enthalpies of Formation, Bond Dissociation Energies and Reaction Paths for the Decomposition of Model Biofuels: Ethyl Propanoate and Methyl Butanoate, The Journal of Physical Chemistry A 111 (19) (2007) 3727-3739.

[37] Y. R. Luo, Comprehensive Handbook of Chemical Bond Energies, Taylor and Francis Group, Boca Raton: CRC Press, 2007

[38] J. M. Simmie, G. Black, H. J. Curran, J. P. Hinde, Enthalpies of Formation and Bond Dissociation Energies of Lower Alkyl Hydroperoxides and Related Hydroperoxy and Alkoxy Radicals, The Journal of Physical Chemistry A 112 (22) (2008) 5010-5016.

[39] Y. Xu, S. Xi, F. Wang, X. Li, Theoretical Study on Reactions of Alkylperoxy Radicals, The Journal of Physical Chemistry A 123 (18) (2019) 3949-3958.

[40] C. W. Gao, J. W. Allen, W. H. Green, R. H. West, Reaction Mechanism Generator: Automatic construction of chemical kinetic mechanisms, Computer Physics Communications 203 (2016) 212-225.

[41] V. V. Warth, F. Battin-Leclerc, R. Fournet, P. A. Glaude, G. M. Come, G. Scacchi, Computer based generation of reaction mechanisms for gas-phase oxidation, Computers & chemistry 24 (5) (2000) 541-60.

[42] F. Battin-Leclerc, O. Herbinet, P.-A. Glaude, R. Fournet, Z. Zhou, L. Deng, H. Guo, M. Xie, F. Qi, Experimental Confirmation of the Low-Temperature Oxidation Scheme of Alkanes, Angewandte Chemie International Edition 49 (18) (2010) 3169-3172.

[43] J. Biet, M. H. Hakka, V. Warth, P.-A. Glaude, F. Battin-Leclerc, Experimental and Modeling Study of the Low-Temperature Oxidation of Large Alkanes, Energy & Fuels 22 (4) (2008) 2258-2269.

[44] A. Chakir, M. Bellimam, J. C. Boettner, M. Cathonnet, Kinetic study of n-heptane oxidation, International Journal of Chemical Kinetics 24 (4) (1992) 385-410.

[45] O. Herbinet, F. Battin-Leclerc, S. Bax, H. L. Gall, P.-A. Glaude, R. Fournet, Z. Zhou, L. Deng, H. Guo, M. Xie, F. Qi, Detailed product analysis during the low temperature oxidation of n-butane, Physical Chemistry Chemical Physics 13 (1) (2011) 296-308.

[46] R. K. Jensen, S. Korcek, L. R. Mahoney, M. Zinbo, Liquid-phase autoxidation of organic compounds at elevated temperatures. 1. The stirred flow reactor technique and analysis of primary products from n-hexadecane autoxidation at 120-180.degree.C, Journal of the American Chemical Society 101 (25) (1979) 7574-7584.

[47] K. Kumar, G. Mittal, C.-J. Sung, Autoignition of n-decane under elevated pressure and low-to-intermediate temperature conditions, Combustion and Flame 156 (6) (2009) 1278-1288.

[48] K. Kumar, C.-J. Sung, Autoignition of methyl butanoate under engine relevant conditions, Combustion and Flame 171 (2016) 1-14.

[49] C.-J. Sung, H. J. Curran, Using rapid compression machines for chemical kinetics studies, Progress in Energy and Combustion Science 44 (2014) 1-18.

[50] G. Vanhove, G. Petit, R. Minetti, Experimental study of the kinetic interactions in the low-temperature autoignition of hydrocarbon binary mixtures and a surrogate fuel, Combustion and Flame 145 (3) (2006) 521-532.

[51] K. Zhang, C. Banyon, C. Togbé, P. Dagaut, J. Bugler, H. J. Curran, An experimental and kinetic modeling study of n-hexane oxidation, Combustion and Flame 162 (11) (2015) 4194-4207.

[52] B. Akih-Kumgeh, J. M. Bergthorson, Shock Tube Study of Methyl Formate Ignition, Energy & Fuels 24 (1) (2010) 396-403.

[53] D. F. Davidson, Z. Hong, G. L. Pilla, A. Farooq, R. D. Cook, R. K. Hanson, Multi-species time-history measurements during n-heptane oxidation behind reflected shock waves, Combustion and Flame 157 (10) (2010) 1899-1905.

[54] B. M. Gauthier, D. F. Davidson, R. K. Hanson, Shock tube determination of ignition delay times in full-blend and surrogate fuel mixtures, Combustion and Flame 139 (4) (2004) 300-311.

[55] Y. Li, C.-W. Zhou, K. P. Somers, K. Zhang, H. J. Curran, The oxidation of 2-butene: A high pressure ignition delay, kinetic modeling study and reactivity comparison with isobutene and 1-butene, Proceedings of the Combustion Institute 36 (1) (2017) 403-411.

[56] K. E. Noorani, B. Akih-Kumgeh, J. M. Bergthorson, Comparative High Temperature Shock Tube Ignition of C1−C4 Primary Alcohols, Energy & Fuels 24 (11) (2010) 5834-5843.

[57] P. Dagaut, M. Reuillon, M. Cathonnet, Experimental study of the oxidation of n-heptane in a jet stirred reactor from low to high temperature and pressures up to 40 atm, Combustion and Flame 101 (1) (1995) 132-140.

[58] J. F. Griffiths, P. A. Halford-Maw, D. J. Rose, Fundamental features of hydrocarbon autoignition in a rapid compression machine, Combustion and Flame 95 (3) (1993) 291-306.

[59] O. Herbinet, B. Husson, Z. Serinyel, M. Cord, V. Warth, R. Fournet, P.-A. Glaude, B. Sirjean, F. Battin-Leclerc, Z. Wang, M. Xie, Z. Cheng, F. Qi, Experimental and modeling investigation of the low-temperature oxidation of n-heptane, Combustion and Flame 159 (12) (2012) 3455-3471.

[60] R. Minetti, M. Carlier, M. Ribaucour, E. Therssen, L. R. Sochet, A rapid compression machine investigation of oxidation and auto-ignition of n-Heptane: Measurements and modeling, Combustion and Flame 102 (3) (1995) 298-309.

[61] E. Ranzi, P. Gaffuri, T. Faravelli, P. Dagaut, A wide-range modeling study of n-heptane oxidation, Combustion and Flame 103 (1) (1995) 91-106.

[62] R. Seiser, H. Pitsch, K. Seshadri, W. J. Pitz, H. J. Gurran, Extinction and autoignition of n-heptane in counterflow configuration, Proceedings of the Combustion Institute 28 (2) (2000) 2029-2037.

[63] E. J. Silke, H. J. Curran, J. M. Simmie, The influence of fuel structure on combustion as demonstrated by the isomers of heptane: a rapid compression machine study, Proceedings of the Combustion Institute 30 (2) (2005) 2639-2647.

[64] C. Yao, C. Cheng, S. Liu, Z. Tian, J. Wang, Identification of intermediates in an n-heptane/oxygen/argon low-pressure premixed laminar flame using synchrotron radiation, Fuel 88 (9) (2009) 1752-1757.

[65] J. R. Agudelo, M. Lapuerta, O. Moyer, A. L. Boehman, Autoignition of Alcohol/C7-Esters/n-Heptane Blends in a Motored Engine under HCCI Conditions, Energy & Fuels 31 (3) (2017) 2985-2995.

[66] D. B. Lenhert, D. L. Miller, N. P. Cernansky, K. G. Owens, The oxidation of a gasoline surrogate in the negative temperature coefficient region, Combustion and Flame 156 (3) (2009) 549-564.

[67] H. Liu, K. H. Yoo, A. L. Boehman, Z. Zheng, Experimental Study of Autoignition Characteristics of the Ethanol Effect on Biodiesel/n-Heptane Blend in a Motored Engine and a Constant-Volume Combustion Chamber, Energy & Fuels 32 (2) (2018) 1884-1892.

[68] J. P. Szybist, A. L. Boehman, D. C. Haworth, H. Koga, Premixed ignition behavior of alternative diesel fuel-relevant compounds in a motored engine experiment, Combustion and Flame 149 (1) (2007) 112-128.

[69] Z. Wang, B. Chen, K. Moshammer, D. M. Popolan-Vaida, S. Sioud, V. S. B. Shankar, D. Vuilleumier, T. Tao, L. Ruwe, E. Bräuer, N. Hansen, P. Dagaut, K. Kohse-Höinghaus, M. A. Raji, S. M. Sarathy, n-Heptane cool flame chemistry: Unraveling intermediate species measured in a stirred reactor and motored engine, Combustion and Flame 187 (2018) 199-216.

[70] Y. Zhang, A. L. Boehman, Oxidation of 1-butanol and a mixture of n-heptane/1-butanol in a motored engine, Combustion and Flame 157 (10) (2010) 1816-1824.

[71] Y. Zhang, A. L. Boehman, Autoignition of binary fuel blends of n-heptane and C7 esters in a motored engine, Combustion and Flame 159 (4) (2012) 1619-1630.

[72] G. M. Côme, V. Warth, P. A. Glaude, R. Fournet, F. Battin-Leclerc, G. Scacchi, Computer-aided design of gas-phase oxidation mechanisms—Application to the modeling of n-heptane and iso-octane oxidation, Symposium (International) on Combustion 26 (1) (1996) 755-762.

[73] C. K. Westbrook, W. J. Pitz, J. E. Boercker, H. J. Curran, J. F. Griffiths, C. Mohamed, M. Ribaucour, Detailed chemical kinetic reaction mechanisms for autoignition of isomers of heptane under rapid compression, Proceedings of the Combustion Institute 29 (1) (2002) 1311-1318.

[74] K. Zhang, C. Banyon, J. Bugler, H. J. Curran, A. Rodriguez, O. Herbinet, F. Battin-Leclerc, C. B'Chir, K. A. Heufer, An updated experimental and kinetic modeling study of n-heptane oxidation, Combustion and Flame 172 (2016) 116-135.

[75] M. Mehl, W. J. Pitz, M. Sjöberg, J. E. Dec, Detailed Kinetic Modeling of Low-Temperature Heat Release for PRF Fuels in an HCCI Engine, SAE International, 2009-01-1806, 2009.

[76] M. Mehl, W. J. Pitz, C. K. Westbrook, H. J. Curran, Kinetic modeling of gasoline surrogate components and mixtures under engine conditions, Proceedings of the Combustion Institute 33 (1) (2011) 193-200.

[77] CHEMKIN-PRO, Reaction Design: San Diego, 2011

[78] J. B. Heywood, Internal Combustion Engine Fundamentals, McGraw-Hill, New York, 1988

[79] S. E. Stein, W. Wallace, NIST/EPA/NIH Mass Spectral Library (NIST 17) and NIST Mass Spectral Search Program (Version 2.3)

[80] SDBSWeb : https://sdbs.db.aist.go.jp, National Institute of Advanced Industrial Science and Technology. (June, 2020)

[81] N. Blin-Simiand, F. Jorand, K. Keller, M. Fiderer, K. Sahetchian, Ketohydroperoxides and ignition delay in internal combustion engines, Combustion and Flame 112 (1) (1998) 278-282.

[82] R. W. Walker, C. Morley, in: Low-Temperature Combustion and Autoignition M. J. Pilling, (Ed.) Elsevier: 1997; Vol. 35, pp 108-119.

[83] S. Dooley, H. J. Curran, J. M. Simmie, Autoignition measurements and a validated kinetic model for the biodiesel surrogate, methyl butanoate, Combustion and Flame 153 (1) (2008) 2-32.

[84] K. Kumar, C.-J. Sung, B. W. Weber, J. A. Bunnell, Autoignition of methyl propanoate and its comparisons with methyl ethanoate and methyl butanoate, Combustion and Flame 188 (2018) 116-128.

[85] S. M. Walton, D. M. Karwat, P. D. Teini, A. M. Gorny, M. S. Wooldridge, Speciation studies of methyl butanoate ignition, Fuel 90 (5) (2011) 1796-1804.

[86] Y. Wang, Z. Yang, X. Yang, D. Han, Z. Huang, X. Lu, Experimental and Modeling Studies on Ignition Delay Times of Methyl Hexanoate/n-Butanol Blend Fuels at Elevated Pressures, Energy & Fuels 28 (8) (2014) 5515-5522.

[87] B. W. Weber, J. A. Bunnell, K. Kumar, C.-J. Sung, Experiments and modeling of the autoignition of methyl pentanoate at low to intermediate temperatures and elevated pressures in a rapid compression machine, Fuel 212 (2018) 479-486.

[88] S. Dooley, M. P. Burke, M. Chaos, Y. Stein, F. L. Dryer, V. P. Zhukov, O. Finch, J. M. Simmie, H. J. Curran, Methyl formate oxidation: Speciation data, laminar burning velocities, ignition delay times, and a validated chemical kinetic model, International Journal of Chemical Kinetics 42 (9) (2010) 527-549.

[89] E. M. Fisher, W. J. Pitz, H. J. Curran, C. K. Westbrook, Detailed chemical kinetic mechanisms for combustion of oxygenated fuels, Proceedings of the Combustion Institute 28 (2) (2000) 1579-1586.

[90] T. Vaughn, M. Hammill, M. Harris, A. J. Marchese, Ignition Delay of Bio-Ester Fuel Droplets, SAE International, 2006.

[91] W. Wang, M. A. Oehlschlaeger, A shock tube study of methyl decanoate autoignition at elevated pressures, Combustion and Flame 159 (2) (2012) 476-481.

[92] M. F. Campbell, D. F. Davidson, R. K. Hanson, Ignition delay times of very-low-vapor-pressure biodiesel surrogates behind reflected shock waves, Fuel 126 (2014) 271-281.

[93] W. Wang, L. Yu, Y. Feng, Y. Qian, D. Ju, X. Lu, Autoignition study of methyl decanoate using a rapid compression machine, Fuel 266 (2020) 117060.

[94] C. Hotard, A. Tekawade, M. A. Oehlschlaeger, Constant volume spray ignition of C9-C10 biodiesel surrogates: Methyl decanoate, ethyl nonanoate, and methyl decenoates, Fuel 224 (2018) 219-225.

[95] E. Al-Gharibeh, R. Leathers, K. Kumar, C.-J. Sung, Ignition and combustion characteristics of decanoic acid derived alkyl esters in a fuel ignition tester, Fuel 276 (2020) 117982.

[96] Y. L. Wang, Q. Feng, F. N. Egolfopoulos, T. T. Tsotsis, Studies of C4 and C10 methyl ester flames, Combustion and Flame 158 (8) (2011) 1507-1519.

[97] R. Grana, A. Frassoldati, C. Saggese, T. Faravelli, E. Ranzi, A wide range kinetic modeling study of pyrolysis and oxidation of methyl butanoate and methyl decanoate – Note II: Lumped kinetic model of decomposition and combustion of methyl esters up to methyl decanoate, Combustion and Flame 159 (7) (2012) 2280-2294.

[98] O. Herbinet, J. Biet, M. H. Hakka, V. Warth, P.-A. Glaude, A. Nicolle, F. Battin-Leclerc, Modeling study of the low-temperature oxidation of large methyl esters from C11 to C19, Proceedings of the Combustion Institute 33 (1) (2011) 391-398.

[99] O. Herbinet, P.-A. Glaude, V. Warth, F. Battin-Leclerc, Experimental and modeling study of the thermal decomposition of methyl decanoate, Combustion and Flame 158 (7) (2011) 1288-1300.

[100] O. Herbinet, W. J. Pitz, C. K. Westbrook, Detailed chemical kinetic oxidation mechanism for a biodiesel surrogate, Combustion and Flame 154 (3) (2008) 507-528.

[101] O. Herbinet, W. J. Pitz, C. K. Westbrook, Detailed chemical kinetic mechanism for the oxidation of biodiesel fuels blend surrogate, Combustion and Flame 157 (5) (2010) 893-908.

[102] A. S. Cheng, C. E. Dumitrescu, C. J. Mueller, Investigation of Methyl Decanoate Combustion in an Optical Direct-Injection Diesel Engine, Energy & Fuels 28 (12) (2014) 7689-7700.

[103] M. K. Le, R. L. Zhang, L. Z. Rao, S. Kook, E. R. Hawkes, The development of hydroxyl and soot in a methyl decanoate-fuelled automotive-size optical diesel engine, Fuel 166 (2016) 320-332.

[104] E. Al-Gharibeh, K. Kumar, Speciation Studies during Low-to-Intermediate Temperature Oxidation of n-heptane in a Motored Engine, 11th U. S. National Combustion Meeting, Pasadena, California, 2019.

[105] M. Krishnamoorthi, R. Malayalamurthi, Z. He, S. Kandasamy, A review on low temperature combustion engines: Performance, combustion and emission characteristics, Renewable and Sustainable Energy Reviews 116 (2019) 109404.

[106] S. A. Basha, K. R. Gopal, S. Jebaraj, A review on biodiesel production, combustion, emissions and performance, Renewable and Sustainable Energy Reviews 13 (6) (2009) 1628-1634.

[107] E. Dobrzyńska, M. Szewczyńska, M. Pośniak, A. Szczotka, B. Puchałka, J. Woodburn, Exhaust emissions from diesel engines fueled by different blends with the addition of nanomodifiers and hydrotreated vegetable oil HVO, Environmental Pollution 259 (2020) 113772.

[108] C. C. Enweremadu, H. L. Rutto, Combustion, emission and engine performance characteristics of used cooking oil biodiesel—A review, Renewable and Sustainable Energy Reviews 14 (9) (2010) 2863-2873.

[109] A. K. Hossain, P. A. Davies, Plant oils as fuels for compression ignition engines: A technical review and life-cycle analysis, Renewable Energy 35 (1) (2010) 1-13.

[110] M. Lapuerta, O. Armas, J. Rodríguez-Fernández, Effect of biodiesel fuels on diesel engine emissions, Progress in Energy and Combustion Science 34 (2) (2008) 198-223.

[111] K. Muralidharan, D. Vasudevan, Performance, emission and combustion characteristics of a variable compression ratio engine using methyl esters of waste cooking oil and diesel blends, Applied Energy 88 (11) (2011) 3959-3968.

[112] A. Murugesan, C. Umarani, R. Subramanian, N. Nedunchezhian, Bio-diesel as an alternative fuel for diesel engines—A review, Renewable and Sustainable Energy Reviews 13 (3) (2009) 653-662.

[113] A. N. Ozsezen, M. Canakci, Determination of performance and combustion characteristics of a diesel engine fueled with canola and waste palm oil methyl esters, Energy Conversion and Management 52 (1) (2011) 108-116.

[114] B. Akih-Kumgeh, J. M. Bergthorson, Comparative Study of Methyl Butanoate and n-Heptane High Temperature Autoignition, Energy & Fuels 24 (4) (2010) 2439-2448.

[115] S. Bax, M. H. Hakka, P.-A. Glaude, O. Herbinet, F. Battin-Leclerc, Experimental study of the oxidation of methyl oleate in a jet-stirred reactor, Combustion and Flame 157 (6) (2010) 1220-1229.

[116] M. F. Campbell, D. F. Davidson, R. K. Hanson, C. K. Westbrook, Ignition delay times of methyl oleate and methyl linoleate behind reflected shock waves, Proceedings of the Combustion Institute 34 (1) (2013) 419-425.

[117] W. K. Metcalfe, S. Dooley, H. J. Curran, J. M. Simmie, A. M. El-Nahas, M. V. Navarro, Experimental and Modeling Study of C5H10O2 Ethyl and Methyl Esters, The Journal of Physical Chemistry A 111 (19) (2007) 4001-4014.

[118] S. M. Sarathy, M. J. Thomson, W. J. Pitz, T. Lu, An experimental and kinetic modeling study of methyl decanoate combustion, Proceedings of the Combustion Institute 33 (1) (2011) 399-405.

[119] K. HadjAli, M. Crochet, G. Vanhove, M. Ribaucour, R. Minetti, A study of the low temperature autoignition of methyl esters, Proceedings of the Combustion Institute 32 (1) (2009) 239-246.

[120] B. Yang, C. K. Westbrook, T. A. Cool, N. Hansen, K. Kohse-Höinghaus, Fuel-specific influences on the composition of reaction intermediates in premixed flames of three C5H10O2 ester isomers, Physical Chemistry Chemical Physics 13 (15) (2011) 6901-6913.

[121] S. P. Pyl, K. M. Van Geem, P. Puimège, M. K. Sabbe, M.-F. Reyniers, G. B. Marin, A comprehensive study of methyl decanoate pyrolysis, Energy 43 (1) (2012) 146-160.

[122] K. Seshadri, T. Lu, O. Herbinet, S. Humer, U. Niemann, W. J. Pitz, R. Seiser, C. K. Law, Experimental and kinetic modeling study of extinction and ignition of methyl decanoate in laminar non-premixed flows, Proceedings of the Combustion Institute 32 (1) (2009) 1067-1074.

[123] Y. Zhai, C. Ao, B. Feng, Q. Meng, Y. Zhang, B. Mei, J. Yang, F. Liu, L. Zhang, Experimental and kinetic modeling investigation on methyl decanoate pyrolysis at low and atmospheric pressures, Fuel 232 (2018) 333-340.

[124] S. Gaïl, S. M. Sarathy, M. J. Thomson, P. Diévart, P. Dagaut, Experimental and chemical kinetic modeling study of small methyl esters oxidation: Methyl (E)-2-butenoate and methyl butanoate, Combustion and Flame 155 (4) (2008) 635-650.

[125] S. M. Walton, M. S. Wooldridge, C. K. Westbrook, An experimental investigation of structural effects on the auto-ignition properties of two C5 esters, Proceedings of the Combustion Institute 32 (1) (2009) 255-262.

[126] W. Wang, S. Gowdagiri, M. A. Oehlschlaeger, Comparative Study of the Autoignition of Methyl Decenoates, Unsaturated Biodiesel Fuel Surrogates, Energy & Fuels 27 (9) (2013) 5527-5532.

[127] C. K. Westbrook, W. J. Pitz, S. M. Sarathy, M. Mehl, Detailed chemical kinetic modeling of the effects of CC double bonds on the ignition of biodiesel fuels, Proceedings of the Combustion Institute 34 (2) (2013) 3049-3056.

[128] A. Rodriguez, O. Herbinet, F. Battin-Leclerc, A. Frassoldati, T. Faravelli, E. Ranzi, Experimental and modeling investigation of the effect of the unsaturation degree on the gas-phase oxidation of fatty acid methyl esters found in biodiesel fuels, Combustion and Flame 164 (2016) 346-362.

[129] C. K. Westbrook, C. V. Naik, O. Herbinet, W. J. Pitz, M. Mehl, S. M. Sarathy, H. J. Curran, Detailed chemical kinetic reaction mechanisms for soy and rapeseed biodiesel fuels, Combustion and Flame 158 (4) (2011) 742-755.

[130] F. Battin-Leclerc, Detailed chemical kinetic models for the low-temperature combustion of hydrocarbons with application to gasoline and diesel fuel surrogates, Progress in Energy and Combustion Science 34 (4) (2008) 440-498.

[131] J. Y. W. Lai, K. C. Lin, A. Violi, Biodiesel combustion: Advances in chemical kinetic modeling, Progress in Energy and Combustion Science 37 (1) (2011) 1-14.

[132] L. S. Tran, B. Sirjean, P.-A. Glaude, R. Fournet, F. Battin-Leclerc, Progress in detailed kinetic modeling of the combustion of oxygenated components of biofuels, Energy 43 (1) (2012) 4-18.

[133] M. H. Hakka, P.-A. Glaude, O. Herbinet, F. Battin-Leclerc, Experimental study of the oxidation of large surrogates for diesel and biodiesel fuels, Combustion and Flame 156 (11) (2009) 2129-2144.

[134] K. A. Sahetchian, R. Rigny, S. Circan, Identification of the hydroperoxide formed by isomerization reactions during the oxidation of n-heptane in a reactor and CFR engine, Combustion and Flame 85 (3) (1991) 511-514.

[135] Y. Zhang, A. L. Boehman, Experimental study of the autoignition of C8H16O2 ethyl and methyl esters in a motored engine, Combustion and Flame 157 (3) (2010) 546-555.

[136] S. K. Hoekman, A. Broch, C. Robbins, E. Ceniceros, M. Natarajan, Review of biodiesel composition, properties, and specifications, Renewable and Sustainable Energy Reviews 16 (1) (2012) 143-169.

[137] S. Tanaka, F. Ayala, J. C. Keck, J. B. Heywood, Two-stage ignition in HCCI combustion and HCCI control by fuels and additives, Combustion and Flame 132 (1) (2003) 219-239.

[138] S. C. Bhatia, in: Advanced Renewable Energy Systems, S. C. Bhatia, (Ed.) Woodhead Publishing India: 2014; pp 403-425.

[139] P. Diévart, S. H. Won, J. Gong, S. Dooley, Y. Ju, A comparative study of the chemical kinetic characteristics of small methyl esters in diffusion flame extinction, Proceedings of the Combustion Institute 34 (1) (2013) 821-829.

[140] W. K. Metcalfe, C. Togbé, P. Dagaut, H. J. Curran, J. M. Simmie, A jet-stirred reactor and kinetic modeling study of ethyl propanoate oxidation, Combustion and Flame 156 (1) (2009) 250-260.

[141] L. Sahraoui, K. Khimeche, A. Dahmani, I. Mokbel, J. Jose, Experimental vapor pressures (from 1Pa to 100kPa) of six saturated Fatty Acid Methyl Esters (FAMEs): Methyl hexanoate, methyl octanoate, methyl decanoate, methyl dodecanoate, methyl tetradecanoate and methyl hexadecanoate, The Journal of Chemical Thermodynamics 102 (2016) 270-275.

[142] S. R. Hoffman, J. Abraham, A comparative study of n-heptane, methyl decanoate, and dimethyl ether combustion characteristics under homogeneous-charge compression–ignition engine conditions, Fuel 88 (6) (2009) 1099-1108.

[143] Z. Li, W. Wang, Z. Huang, M. A. Oehlschlaeger, Autoignition of Methyl Decanoate, a Biodiesel Surrogate, under High-Pressure Exhaust Gas Recirculation Conditions, Energy & Fuels 26 (8) (2012) 4887-4895.

[144] R. Grana, A. Frassoldati, A. Cuoci, T. Faravelli, E. Ranzi, A wide range kinetic modeling study of pyrolysis and oxidation of methyl butanoate and methyl decanoate. Note I: Lumped kinetic model of methyl butanoate and small methyl esters, Energy 43 (1) (2012) 124-139.

[145] Q. Xu, R. Leathers, D. Savage, K. Kumar, C.-J. Sung, Influence of Blendingn-Butanol with Isooctane andn-Heptane on Ignition Delay Times in a Fuel Ignition Tester, Energy & Fuels 32 (5) (2018) 6239-6251.

[146] W. E. Klopfenstein, Effect of molecular weights of fatty acid esters on cetane numbers as diesel fuels, J Am Oil Chem Soc 62 (6) (1985) 1029–1031.

[147] F. M. Haas, F. L. Dryer, Prediction of Biofuel Ignition Quality using a DCN↔RON Interconversion Tool, Fall Technical Meeting of the Eastern States Section of the Combustion Institute, Clemson, SC, 2013.

[148] J. Yanowitz, M. A. Ratcliff, R. L. McCormick, J. D. Taylor, M. J. Murphy, Compendium of Experimental Cetane Numbers, National Renewable Energy Laboratory, 2017.

[149] G. E. Bogin, E. Osecky, M. A. Ratcliff, J. Luecke, X. He, B. T. Zigler, A. M. Dean, Ignition Quality Tester (IQT) Investigation of the Negative Temperature Coefficient Region of Alkane Autoignition, Energy & Fuels 27 (3) (2013) 1632-1642.

[150] M. Frenklach, C. T. Bowman, G. P. Smith, GRI-Mech 3.0. http://combustion.berkeley.edu/gri-mech/releases.html (Accessed 2/19/2020)

[151] R. S. Figliola, D. E. Beasley, Theory and Design for Mechanical Measurements, ohn Wiley & Sons, 2015.

Appendix A. Species detected in the oxidation products of n-heptane, methyl decanoate, coconut oil biodiesel and canola oil biodiesel

Table A.1 Species identified in the GC-MS analysis of n-heptane oxidation products.

#	IUPAC Name (Common Name)	Formula	Chemical Class
1	ethene	C_2H_4	olefin
2	prop-1-ene	C_3H_6	
3	but-1-ene	C_4H_8	
4	but-2-ene		
5	pent-1-ene	C_5H_{10}	
6	pent-2-ene		
7	hex-1-ene	C_6H_{12}	
8	hept-1-ene	C_7H_{14}	
9	hept-3-ene		
10	hept-2-ene		
11	methanal (formaldehyde)	CH_2O	aldehyde
12	ethanal (acetaldehyde)	C_2H_4O	
13	propanal	C_3H_6O	
14	butanal	C_4H_8O	
15	pentanal (valeraldehyde)	$C_5H_{10}O$	
16	heptanal	$C_7H_{14}O$	
17	prop-2-enal	C_3H_4O	aldehyde-unsaturated
18	but-2-enal	C_4H_6O	
19	pent-2-enal	C_5H_8O	
20	propan-2-one (Acetone)	C_3H_6O	ketone
21	butan-2-one	C_4H_8O	
22	pentan-2-one	$C_5H_{10}O$	
23	heptan-3-one	$C_7H_{14}O$	
24	heptan-2-one		
25	but-3-en-2-one	C_4H_6O	ketone-unsaturated
26	pent-1-en-3-one	C_5H_8O	
27	methanol	CH_4O	alcohol
28	ethanol	C_2H_6O	
29	hexan-1-ol	$C_6H_{14}O$	
30	prop-2-en-1-ol	C_3H_6O	alcohol-unsaturated
31	3-methylhex-1-yn-3-ol	$C_7H_{12}O$	alcohol
32	methoxymethane (dimethyl ether)	C_2H_6O	ether
33	methoxyethene (methyl vinyl ether)	C_3H_6O	
34	1-ethenoxybutane	$C_6H_{12}O$	ether-unsaturated
35	oxirane (ethylene oxide)	C_2H_4O	three-membered ring
36	2-methyloxirane (propylene oxide)	C_3H_6O	
37	2-ethyloxirane (1-butene oxide)	C_4H_8O	
38	oxolane (tetrahydrofuran)	C_4H_8O	five-membered ring
39	2-methyloxolane	$C_5H_{10}O$	
40	2-methylfuran	C_5H_6O	five-member ring
41	2-ethyl-5-methylfuran	$C_7H_{10}O$	
42	(5-methyloxolan-2-yl) methanol	$C_6H_{12}O_2$	five-membered ring
43	oxolan-2-ylmethanol	$C_5H_{10}O_2$	

#	IUPAC Name (Common Name)	Formula	Chemical Class
44	oxolane-2,4-dione	$C_4H_4O_3$	five-membered ring
45	2-methyloxane	$C_6H_{12}O$	six-membered ring
46	oxan-2-ylmethanol	$C_6H_{12}O_2$	six-member ring
47	3,4-dihydro-2H-pyran-2-carbaldehyde	$C_6H_8O_2$	unsaturated six-membered ring
48	buta-1,3-diene	C_4H_6	diene
49	2-methylbuta-1,3-diene (Isoprene)	C_5H_8	
50	penta-1,3-diene	C_5H_8	
51	hexa-1,4-diene	C_6H_{10}	
52	acetic acid	$C_2H_4O_2$	carboxylic acid
53	pentyl acetate	$C_7H_{14}O_2$	
54	prop-2-enyl acetate	$C_5H_7O_2$	
55	prop-1-en-2-yl acetate	$C_5H_8O_2$	
56	1,3,5-Trioxane	$C_3H_6O_3$	

Table A.2 Species identified in the GC-MS analysis of methyl decanoate oxidation products.

#	IUPAC Name (Common Name)	Formula	Chemical class
1	ethene	C2H4	
2	prop-1-ene	C3H6	
3	but-1-ene	C4H8	
4	but-2-ene		
5	pent-1-ene	C5H10	
6	pent-2-ene		alkene
7	hex-1-ene	C6H12	
8	hept-1-ene	C7H14	
9	oct-1-ene	C8H16	
10	non-1-ene	C9H18	
11	methanal	CH2O	
12	ethanal	C2H4O	
13	propanal	C3H6O	
14	butanal	C4H8O	aldehyde
15	pentanal	C5H10O	
16	hexanal	C6H12O	
17	heptanal	C7H14O	
18	prop-2-enal	C3H4O	
19	but-2-enal	C4H6O	aldehyde-unsaturated
20	pent-2-enal	C5H8O	
21	propan-2-one	C3H6O	
22	butan-2-one	C4H8O	
23	pentan-2-one	C5H10O	ketone
24	hexan-2-one	C6H12O	
25	4-methylhexan-2-one	C7H14O	
26	but-3-en-2-one	C4H6O	
27	pent-1-en-3-one	C5H8O	ketone-unsaturated
28	hex-5-en-2-one	C6H10O	
29	methanol	CH4O	
30	ethanol	C2H6O	alcohol
31	prop-2-en-1-ol	C3H6O	
32	hex-1-yn-3-ol	C6H10O	alcohol-unsaturated
33	methoxyethene	C3H6O	ether-unsaturated

#	IUPAC Name (Common Name)	Formula	Chemical class
34	oxirane	C2H4O	cyclic ether - three-membered ring
35	2-methyloxirane	C3H6O	
36	2-ethyloxirane	C4H8O	
37	oxolane	C4H8O	cyclic ether - five-membered-ring
38	2-methyloxolane	C5H10O	
39	oxolan-2-ylmethanol	C5H10O2	cyclic ether - five-membered ring + C-OH
40	buta-1,3-diene	C4H6	diene
41	cyclopenta-1,3-diene	C5H6	
42	2-methylbuta-1,3-diene	C5H8	
43	penta-1,3-diene	C5H8	
44	hexa-1,4-diene	C6H10	
45	acetic acid	C2H4O2	carboxylic acid
46	methyl acetate	C3H6O2	ester
47	methyl propanoate	C4H8O2	
48	methyl hexanoate	C7H12O2	
49	methyl prop-2-enoate	C4H6O2	Unsaturated Ester
50	prop-2-enyl acetate	C5H8O2	
51	methyl cyclopropanecarboxylate		
52	methyl but-2-enoate		
53	methyl pent-4-enoate	C6H10O2	
54	methyl 3-methylbut-2-enoate		
55	methyl hex-3-enoate	C7H12O2	
56	methyl hept-2-enoate	C8H14O2	
57	benzene	C6H6	Aromatic
58	1,3,5-Trioxane	C3H6O3	Trimer
59	-	C6H12O	unidentified
60	-	C5H8O2	
61	-	C6H8O2	
62	-	C6H8O2	
63	-	C6H10O2	
64	-	C6H10O2	
65	-	C6H10O2	
66	-	C8H14O2	

Table A.3 Species identified in the GC-MS analysis of coconut oil biodiesel and canola oil biodiesel oxidation products.

#	IUPAC Name (Common Name)	Formula	Chemical class
1	ethene	C2H4	alkene
2	prop-1-ene	C3H6	
3	but-1-ene	C4H8	
4	but-2-ene		
5	pent-1-ene	C5H10	
6	pent-2-ene		
7	hex-1-ene	C6H12	
8	hept-1-ene	C7H14	
9	oct-1-ene	C8H16	
10	non-1-ene	C9H18	
11	methanal	CH2O	aldehyde
12	ethanal	C2H4O	
13	propanal	C3H6O	
14	Butanal	C4H8O	
15	pentanal	C5H10O	
16	hexanal	C6H12O	
17	heptanal	C7H14O	
18	prop-2-enal	C3H4O	aldehyde-unsaturated
19	but-2-enal	C4H6O	
20	pent-2-enal	C5H8O	
21	propan-2-one	C3H6O	ketone
22	butan-2-one	C4H8O	
23	pentan-2-one	C5H10O	
24	hexan-2-one	C6H12O	
25	4-methylhexan-2-one	C7H14O	
26	but-3-en-2-one	C4H6O	ketone-unsaturated
27	pent-1-en-3-one	C5H8O	
28	methanol	CH4O	alcohol
29	ethanol	C2H6O	
30	prop-2-en-1-ol	C3H6O	alcohol-unsaturated
31	hex-1-yn-3-ol	C6H10O	
32	methoxyethene	C3H6O	ether-unsaturated
#	**IUPAC Name (Common Name)**	**Formula**	**Chemical class**

33	oxirane	C2H4O	
34	2-methyloxirane	C3H6O	cyclic ether - three-membered ring
35	2-ethyloxirane	C4H8O	
36	oxolane	C4H8O	
37	2-methyloxolane	C5H10O	cyclic ether - five-membered-ring
38	oxolan-2-ylmethanol	C5H10O2	cyclic ether - five-membered ring + C-OH
39	buta-1,3-diene	C4H6	
40	cyclopenta-1,3-diene	C5H6	
41	2-methylbuta-1,3-diene	C5H8	diene
42	penta-1,3-diene		
43	hexa-1,4-diene	C6H10	
44	methyl acetate	C3H6O2	
45	methyl propanoate	C4H8O2	
46	methyl hexanoate	C7H12O2	ester
47	methyl octanoate	C9H18O2	
48	decanoic acid, methyl ester	C11H22O2	
49	methyl prop-2-enoate	C4H6O2	
50	prop-2-enyl acetate	C5H8O2	
51	methyl cyclopropanecarboxylate		
52	methyl (E)-but-2-enoate		unsaturated Ester
53	methyl pent-4-enoate	C6H10O2	
54	methyl 3-methylbut-2-enoate		
55	methyl hex-3-enoate	C7H12O2	
56	methyl hept-2-enoate	C8H14O2	
57	benzene	C6H6	aromatics
58	1,3,5-Trioxane	C3H6O3	heterocyclic
59	-	C6H12O	
60	-	C6H8O2	
61	-	C6H8O2	unidentified
62	-	C6H10O2	
63	-	C6H10O2	
64	-	C6H10O2	

Appendix B. Experiments conditions and simulations parameters

Table B.1 Experiment and simulation parameters used for n-Heptane Tests

Experiment conditions	
Engine Speed	700 ± 10 RPM
Intake Temp	110 ± 5 °C
Intake Pressure	0.94 ± 0.1 bar
Coolant Temp	38 ± 2 °C
Oil Temp	38 ± 2 °C
Compression ratio	$5.5 - 9.0$
Phi	0.25 ± 0.02
Fuel Pressure	50 ± 2 psi
Simulation settings	
Model	Chemkin (0-D, single zone HCCI engine simulator)
Mechanism	LLNL detailed Mehl et al. (2011)
Start CA	-146 (°ATDC)
End CA	140 (°ATDC)
Engine Speed	700 RPM
Bore	8.225 cm
Stroke	11.430 cm
Connecting rod length	25.375 cm
Compression ratio	$5.5 - 9.0$
Temperature	107 °C
Pressure	0.9997 bar
Phi	0.25

Table B.2 Experimental conditions for methyl decanoate, coconut oil biodiesel, canola oil biodiesel Tests.

Experiment conditions	
Engine Speed	700 ± 10 RPM
Intake Temp	125 ± 5 °C
Intake Pressure	0.94 ± 0.1 bar
Coolant Temp	38 ± 2 °C
Oil Temp	38 ± 2 °C
Compression ratio	$5.5 - 9.0$
Phi	0.25 ± 0.02
Fuel Pressure	B ± 2 psi

Table B.3 Parameters used in methyl decanoate simulations.

Simulation settings	
Model	Chemkin (0-D, single zone HCCI engine simulator)
Mechanism	LLNL detailed Herbinet et al. (2008)
Start CA	-146 (°ATDC)
End CA	140 (°ATDC)
Engine Speed	700 RPM
Bore	8.225 cm
Stroke	11.430 cm
Connecting rod length	25.375 cm
Compression ratio	$5.5 - 9.0$
Temperature	121 °C
Pressure	1.0 bar
Phi	0.25

Appendix C. Letters of permission to include the published work.

As the author of this Elsevier article, "Ignition and combustion characteristics of decanoic acid derived alkyl esters in a fuel ignition tester, Fuel 276 (2020) 117982", you retain the right to include it in a thesis or dissertation, provided it is not published commercially. Permission is not required, but please ensure that you reference the journal as the original source.

Appendix D. Uncertainty Analysis

Uncertainty in species concentrations:

Evaluation of uncertainty in the measured quantities provides information on the quality of results obtained in experimental work. One source of error propagation in the measurements is a systematic error, such as the bias during data collection as a result of a device or human error. The other component of error is the random variation of repeated measurements of the same quantity. The latter is unavoidable but can be minimized when proper control over the experiment environment is achieved. This section discusses the uncertainty in the reported experiment and provides statistical and sensitivity analysis.

An uncertainty analysis was performed on the reported concentrations of the intermediates in the exhaust gases. The repeatability of the signal intensity of the GC-MS over time was tracked through a test on a specific quantity of hexane gas. The test was conducted on the same dates of the experiments for the various tested fuels. The areas under the GC-MS signal for 500 ppm hexane gas for a sample of ten tests is shown in Figure D. 1 The standard deviation of the areas suggests a 10 % uncertainty for the reported concentrations. The concentration of most of the quantified intermediates in this work was found to be less than 20 ppm. Therefore, the uncertainty of the concentrations of the reported species does not exceed ±2 ppm.
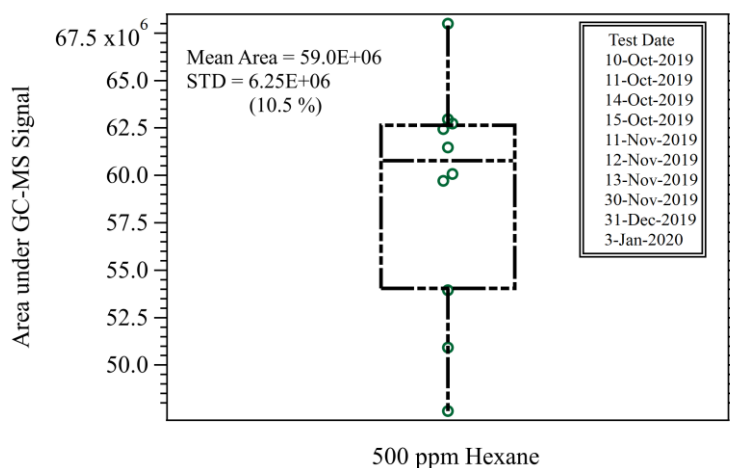
Figure D. 1. Area under GC-MS signal of 500 ppm hexane at various dates throughout the time of the experiments and their standard deviation.

Furthermore, the calibration curves were established for the intermediate species as presented in Table D.1. Linear regression analysis was applied to all the species with forced origin intersection. The slopes of the fits for all the species indicate that an increment of around 10^5 - 10^6 in the value of the area under the signal results in 1.0 ppm increment in the concentration. This suggests a negligible effect of the small fluctuations of the signal intensity on the concentration values. Moreover, the quality of the regression equations used in the quantitation part of the dissertation is demonstrated by the regression parameters in Table D.1.

Table D. 1. Uncertainty analysis of the regression equations used in the quantitation of the intermediate species in the exhaust gases.

	Slope	*Standard Error*	*t Stat*	*P-value*	*Lower 95%*	*Upper 95%*
Methanol	7.09649E-05	6.7508E-07	105.1208	4.91E-08	6.90906E-05	7.28393E-05
Ethanol	2.52859E-05	1.83936E-06	13.7471	0.00525	1.73718E-05	3.32001E-05
Propanal	1.3308E-05	3.05639E-07	43.5417	1.66E-06	1.24594E-05	1.41566E-05
Butanal	1.11282E-05	8.68742E-08	128.0954	5.5E-10	1.09049E-05	1.13515E-05
Pentanal	3.11391E-05	7.29156E-07	42.7057	1.33E-07	2.92647E-05	3.30135E-05
Propylene-Oxide	8.98408E-06	1.30883E-07	68.64189	6.81E-06	8.56755E-06	9.40061E-06
Acetone	3.7319E-05	5.12627E-07	72.79947	9.26E-09	3.60012E-05	3.86367E-05
MEK	1.14472E-05	1.13898E-07	100.5044	1.85E-09	1.11544E-05	1.174E-05
Butene	8.8035E-06	1.52888E-07	57.58136	2.99E-08	8.41049E-06	9.19651E-06
Pentene	7.34232E-06	1.0477E-07	70.08006	1.12E-08	7.07299E-06	7.61164E-06
Hexene	6.28952E-06	4.81733E-08	130.5604	5E-10	6.16569E-06	6.41336E-06

Variations in peak cylinder pressure:

Combustion in engine experiments includes numerous cycle-to-cycle variations due to the interaction and complexity of the physical and chemical aspects of the process. The engine setup used in this work was introduced in Figure 2.1. Slight variations in the operating conditions are unavoidable. For instance, the intake temperature of the fuel-air mixture varies between $T_i \pm 5$ °C, and the equivalence ratio fluctuates between the values $\phi = 0.25 \pm 0.02$. This variation in addition to the error in the measurements, led to a scatter in the in-cylinder pressure values. A suitable approach to account for the contributions of the various errors and variations is to find the amount of dispersion of pressure values for several cycles.

The cycle-to-cycle variation of the peak in-cylinder pressure reported in this dissertation is measured for 300 fueled cycles. These variations are shown at various

compression ratios during the combustion of methyl decanoate in Figure D. 2 It can be seen that the standard deviations of the 300 cycles do not exceed 1.0 % at compression ratios lower than 8.0. At higher compression ratios, the scatter increases due to the irregular nature of the second-stage heat release with a standard deviation of 2.97 %.
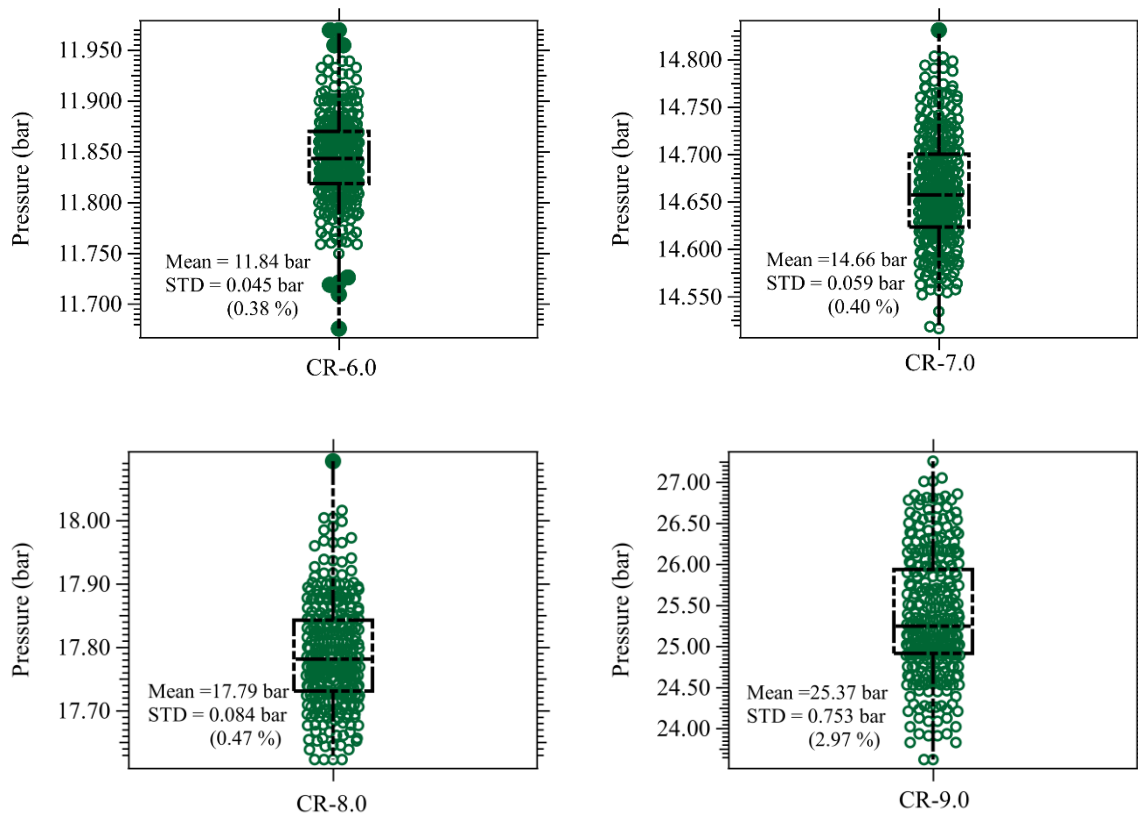
Figure D. 2. Variations for in-cylinder peak pressure for 300 fueled cycles.